AD NUMBER

AD861625

NEW LIMITATION CHANGE

TO

Approved for public release, distribution unlimited

FROM

Distribution authorized to U.S. Gov't. agencies only; Administrative/Operational Use; Oct 1969. Other requests shall be referred to Armed Services Explosives Safty Board, Washington, DC 20315.

AUTHORITY

DDESB ltr, 24 May 1977

AD 861625

Best Available Copy

14 KEY WORDS	LINK A		LINK B		LINK C	
	ROLE	WT	ROLE	WT	ROLE	WT
Adhesive, texturing, Air Force, hydraulic fluid, wearability, freshly laid asphalt						

Engineering Mechanics Division
IIT Research Institute
10 West 35th Street
Chicago, Illinois 60616

Final Technical Report, Project J6166
(Period: October 1968 to July 1969)

Prepared by
T. A. Zaker

Under Contract DAHC-04-69-C-0020

BLAST PRESSURES FROM SEQUENTIAL EXPLOSIONS

October 1969

FOREWORD

Under Contract No. DAHC-04-69-C-0020 between IIT Research Institute and the U. S. Army Research Office-Durham, IITRI has performed a study of the air blast produced by sequentially detonated high explosive charges. This is the final report on the study, conducted during the period October 18, 1968 to July 18, 1969.

The study was performed for the Armed Services Explosives Safety Board under the supervision of Col. B. B. Abrams, Chairman, and Mr. R. G. Perkins, Safety Engineer. Several IITRI staff members in addition to the author contributed significantly to this work. T. V. Eichler and C. A. Kot devised the numerical methods and performed the computer programming. Mrs. H. S. Napadensky designed the test series and assisted in interpretation of the experimental data. D. J. Hrdina, J. E. Daley, and R. P. Joyce carried out the tests.

Respectfully submitted,
IIT RESEARCH INSTITUTE

T. A. Zaker, Science Advisor
Engineering Mechanics Division

ABSTRACT

This report describes a study of the air blast produced by sequentially detonated high explosive charges. Criteria are established relating the coalescence of successive blast waves to explosion time delay, charge weight, and distance from the explosion site.

A finite-difference technique based on the method of characteristics was used to determine numerically the pressure fields produced by spherical charges with various time delays between successive detonations. Small-scale experiments were conducted with hemispherical explosive charges totaling 2 lb in weight detonated on a rigid surface. Transient pressures were observed at six stations on each of two gage lines.

Comparisons are made between the peak pressures and pulse separations predicted numerically and those obtained experimentally. The results are useful in developing recommendations for siting of structures adjacent to multiple-unit explosive stores.

TABLE OF CONTENTS

LIST OF ILLUSTRATIONS

LIST OF ILLUSTRATIONS (CONT)

LIST OF ILLUSTRATIONS (CONT)

BLAST PRESSURES FROM SEQUENTIAL EXPLOSIONS

1. INTRODUCTION

Regulations governing separation distances between multiple-unit explosive stores and other structures such as inhabited buildings or explosive processing facilities currently permit the designer to base the separation distance on the quantity of explosive in a single bay of the multiple-unit store. This is permitted as long as the storage units (or bays in the case of a multiple-unit processing facility) are separated by dividing walls that are considered substantial within the definition of the regulations.[1]*

This practice does not require that the dividing wall prevent explosion propagation from one storage unit or bay to another. It presumes, however, that propagation is delayed sufficiently long so that the blast and missile hazard from explosion of the contents of a single bay controls the placement of adjacent structures. In other words, sequential explosions, if they occur, are assumed to be spaced sufficiently far apart timewise that adjacent buildings are subjected at worst to the effects of the individual explosions successively, and that these effects do not mutually reinforce.

1.1 Problem Background

It is well known that secondary shock waves following an initial shock in air tend to overtake the initial shock. This has been observed experimentally in simple systems such as shock tubes, and the reasons for the overtaking phenomenon are rather well understood in a qualitative sense. Briefly, a shock of finite amplitude will heat the gas through which it passes because the gas is compressed adiabatically, that is, without heat transfer during shock passage. The shock also sets in motion the initially undisturbed gas. The sound speed in gases is an increasing function of the temperature, so that signals following a shock of finite amplitude are propagating in a moving, more dense medium of higher signal speed than the undisturbed gas. Therefore such signals will overtake and reinforce the initial shock. It is only in the case of waves of infinitesimal amplitude (acoustic waves) that this nonlinear effect is absent.

The shock wave formed by any single mass of high explosive in free air becomes well defined and perfectly spherical at some distance (a few charge radii) from the explosive. The homogeneity of the material and the details of the initiation

*Superscript numerals designate appended references.

become unimportant at these distances because of the tendency of secondary shocks and other blast pulse irregularities to overtake the front of the pulse and form a clean shock followed by a relatively smooth expansion or pressure decay.

This means that, for some range of delay time between two adjacent sequential explosions, the effect at a distance from the explosions will be substantially the same as that from a single detonation of the total mass of explosive involved in the two explosions. It is also clear that there will exist some sufficiently long time delay between explosions such that coalescence of the successive blasts does not occur, but this will depend on the distance of the observation point from the site of the explosions.

It has been found in small-scale experiments[2] and in full-scale tests[3] that at inhabited-building distances, blast-wave coalescence occurs for delay times well in excess of that normally associated with explosion propagation between adjacent stores (by fragment initiation, for example). Structural damage sustained from two 5000-lb charges with a 20-msec time delay, at the inhabited-building distance for a barricaded 10,000-lb charge (865 ft), was not significantly different from that resulting from a single explosion of 10,000 lb.

Existing quantity-distance regulations are therefore unconservative with regard to the consideration of sequential explosions of adjacent stores. The goal of the present work is to provide the facilities designer with a tehnically sound basis for deciding when credit can be taken for the nonsimultaneous explosion of more than one explosive store, and when it cannot.

1.2 Study Objectives

The present study consists of a program of numerical analysis of sequential explosions designed to determine quantitatively the time separation of blast pulses from successive explosions as a function of distance from the explosion site, time delay between detonations, and charge weights of the explosions. The results of small-scale experiments with sequentially detonated explosive charges used to support and verify theoretical predictions of the blast-wave coalescence phenomenon.

The specific objectives of the study are to:

1. Determine for sequential spherical explosions the time separation of successive blast pulses as a function of range, charge weights, and time delay between detonations.

2. Investigate the early-time details of explosion product gas expansion to determine an appropriate model for the initial formation of the air shock.

3. Conduct supporting small-scale experiments to validate the numerically determined coalescence criteria for spherical explosions.

4. Make recommendations for supplementing existing quantity-distance regulations to account adequately for the effects of sequential explosions in the design of explosive storage and processing facilities.

In the following sections of this report we summarize the theory of unsteady compressible flow with explosion-produced shocks and we describe numerical methods for solution of these problems. Pressure and velocity fields in the detonation product gases are obtained at early times after central point initiation of a solid explosive sphere. The results of computations of the far-field air blast from successive spherical explosions are presented. The results of experiments with sequential explosions of hemispherical charges totaling 2 lb in weight detonated in free air on a level ground surface are given. Recommendations are made for criteria to supplement existing regulations in regard to multiple explosive stores.

2. EXPLOSION GASDYNAMICS

The flow of compressible fluids is governed by partial differential equations which express the conservation of mass, momentum, and energy, with an equation of state relating the thermodynamic variables. These equations, together with the necessary initial values and boundary conditions, determine the solution and in principle may be integrated to give the flow at later times. Because of the nonlinearity of the equations discontinuities (i.e., shock waves) may develop in an initially continuous flow. In gas flows set up by the sudden energy release of an explosion, a shock wave is in fact present initially. Analytic solution of such problems is possible in only a very few elementary cases, and one must resort to numerical techniques to obtain results in these problems.

2.1 Theoretical Background

We will consider spatially coincident, sequentially detonated spherical explosions. The idealization represented by assuming spatial coincidence of spherical explosions is permissible because the initial separation distance between sequentially detonated charges will generally be quite small compared with distances at which coalescence phenomena are of interest. For example, in recently reported simultaneity tests[3] the 24.5-ft center-to-center distance between two 5000-lb charges is less than three percent of the inhabited building distance ($40\ W^{1/3}$) for barricaded stores based on W = 10,000 lb. With this idealization, the number of independent spatial variables is reduced to one.

In this section, we summarize the governing equations and properties of one-dimensional inviscid compressible flows with plane, cylindrical, or spherical symmetry. The so-called characteristic form of the equations leads to the formulation of a numerical solution method for these problems.

2.1.1 Governing Equations

The equations of compressible fluid motion express the conservation of mass, momentum and energy. Transport effects such as viscosity and heat conduction are neglected; that is, the fluid is assumed to be frictionless and nonconducting. With these assumptions, the entropy of each element of the fluid remains constant until it is traversed by a shock wave. Such flows are termed adiabatic. If the entropy of all fluid elements is the same the flow is termed isentropic. Explosion-induced flows can be treated as adiabatic. They are generally

nonisentropic, however, since shocks will vary in strength in traversing fluid elements as time progresses.

We consider flows with plane, cylindrical, or spherical symmetry, which depend on only one space coordinate r and on the time t. The continuity equation is

$$\frac{\partial \rho}{\partial t} + u \frac{\partial \rho}{\partial r} + \rho \frac{\partial u}{\partial r} + \nu \frac{\rho u}{r} = 0 \tag{2.1}$$

where ρ and u are the density and particle velocity, and the divergence factor ν has the values 0, 1, or 2 for plane, cylindrical, or spherical flow. The momentum equation is

$$\frac{\partial u}{\partial t} + u \frac{\partial u}{\partial r} + \frac{1}{\rho} \frac{\partial p}{\partial r} = 0 \tag{2.2}$$

in all cases, where p is the pressure. Along particle paths given by dr/dt = u, isentropic conditions hold and the energy equation takes the form

$$\frac{\partial e}{\partial t} + u \frac{\partial e}{\partial r} + p \left[\frac{\partial}{\partial t} \left(\frac{1}{\rho} \right) + u \frac{\partial}{\partial r} \left(\frac{1}{\rho} \right) \right] = 0 \tag{2.3}$$

where e is internal energy per unit mass. The pressure, density, and internal energy are related through an equation of state which can be put in the form

$$p = f(\rho, e) \tag{2.4}$$

Finally, the sound speed c is obtained from its definition

$$c^2 = \left(\frac{\partial p}{\partial \rho} \right)_s = \left(\frac{\partial p}{\partial \rho} \right)_e + \frac{p}{\rho^2} \left(\frac{\partial p}{\partial e} \right)_\rho \tag{2.5}$$

where s is the entropy. The sound speed can always be calculated from the right member of Equation (2.5) when the equation of state is in the form of Equation (2.4).

Solution of the foregoing equations in any particular case depends on suitable initial and boundary data prescribed on lines in the plane of independent variables r and t. On

an initial data line values of p, e, and u are prescribed. Regions of the solution in the r, t plane may be separated by interfaces between different fluids (e.g., detonation products and air) or by shock waves. At an interface p and u are continuous. At a shock, the jump conditions which express conservation of mass, momentum, and energy across the discontinuity are applicable. Let subscripts o and s denote the states to either side of a shock moving with velocity U. A suitable form of the jump conditions for our purposes is

$$(u_s-u_o)^2 = (p_s-p_o)\left(\frac{1}{\rho_o} - \frac{1}{\rho_s}\right) \tag{2.6}$$

$$U = \frac{\rho_s u_s - \rho_o u_o}{\rho_s - \rho_o} \tag{2.7}$$

$$e_s-e_o = \frac{1}{2}(p_s+p_o)\left(\frac{1}{\rho_o} - \frac{1}{\rho_s}\right). \tag{2.8}$$

At shocks these equations must be satisfied simultaneously with the integration of the equations of motion (2.1) through (2.3) in neighboring regions of continuous flow.

2.1.2 Characteristic Equations

Partial differential equations can be classified according to their mathematical properties. The equations of unsteady compressible fluid flow are of "hyperbolic" type. A distinguishing property of hyperbolic equations is the existence of certain characteristic lines in the plane of independent variables (in this case r and t), usually called simply characteristics.

Along a characteristic, the dependent variables satisfy a certain differential relation known as a compatibility relation. Such relations provide the key to the computational technique known as the method of characteristics.

By using the sound speed c, we can put Equations (2.1) and (2.2) in ordinary differential form on certain lines (the characteristics) in the r, t plane. These characteristic equations (or compatibility relations) take the form

$$\frac{dp}{\rho c} + du + \nu \frac{uc}{r}\, dt = 0 \tag{2.9}$$

on the first family of characteristics

$$dr = (u + c)\, dt \tag{2.10}$$

and

$$\frac{dp}{\rho c} - du + \nu \frac{uc}{r}\, dt = 0 \tag{2.11}$$

on the second family of characteristics

$$dr = (u - c)\, dt. \tag{2.12}$$

We observe that Equation (2.3) is already in the differential form

$$de + pd\left(\frac{1}{\rho}\right) = 0 \tag{2.13}$$

on the particle paths

$$dr = u\, dt. \tag{2.14}$$

Therefore there are three families of lines in the r,t plane along which the equations of continuous (but possibly nonisentropic) flow can be written in ordinary differential form.

Computationally, we can take advantage of these properties, because the compatibility relations contain ordinary first-order derivatives rather than partial derivatives. Therefore these relations lend themselves to numerical integration in cases not solvable analytically. However, it may be seen that the characteristic lines, along which the solution can be obtained by integrating the compatibility relations, are themselves defined by nonlinear differential equations. Therefore the characteristics depend on the solution and must be determined simultaneously with it.

Physically, the characteristics can be interpreted as lines along which infinitesimal disturbances (wavelets) of pressure and other flow variables can propagate. In the r, t plane we can represent graphically the propagation of

pressure waves and the motion of gas particles. Characteristics are thus signals which carry information about local flow disturbances to other parts of the fluid at later times.

A further physical interpretation of the characteristic lines defined by (2.10) and (2.12) is as follows: An infinitesimal wave or acoustic signal will travel with the local sound velocity $\pm$ c relative to the fluid, which moves with the local particle velocity u. Hence, relative to a stationary observer, sound signals will travel with the velocity $u \pm c$, the double sign respectively referring to signals moving in the direction of increasing or decreasing r relative to fluid particles.

2.1.3 Equations of State

The equations of state used in the present study to represent explosive detonation products and air are of the form of Equation (2.4). Energy is imparted to the surrounding gas as the products of detonation of a solid explosive expand adiabatically from the Chapman-Jouguet (CJ) detonation state. In order to determine the way in which the energy is released from the detonation products, the explosive equation of state must represent correctly the expansion isentrope of the products. This so-called CJ isentrope must correspond to correct values of pressure, density, internal energy, sound speed, and detonation velocity in the CJ state.

A well known solid explosive for which an equation of state of the form of (2.4) is available is pentolite (50/50 TNT/PETN) of initial density 1.65 g/cm^3. Thermochemical calculations[7] give the following values for the CJ detonation state of this explosive:

$$p_{CJ} = 0.2452 \text{ mb}$$

$$\rho_{CJ} = 2.210 \text{ g/cm}^3$$

$$c_{CJ} = 0.5714 \text{ cm/}\mu\text{sec}$$

$$D = 0.7655 \text{ cm/}\mu\text{sec}$$

$$e_{CJ} = 0.0775 \text{ mb-cm}^3\text{/g}$$

where D is the detonation velocity, and 1 megabar (mb) = 10^{12} dynes/cm^2. The chemical energy e_o released in the detonation must satisfy the jump condition (^{o}2.8) with the subscript s denoting the CJ state. It has the value $e_o = 0.05866$ mb-cm^3/g

(1402 cal/g). An equation of state of the form of (2.4) which represents all of these properties adequately is

$$p = (A+B\rho)\ \rho e + C\rho^3 \qquad (2.15)$$

where the constants A, B, and C are given by

$$A = 0.35$$

$$B = 0.1243\ cm^3/g$$

$$C = 0.1279\ mb\text{-}cm^9/g^3$$

These constants match the CJ conditions as well as the ideal gas behavior of the products in the limit of very low pressure and density.

The equation of state of air used in the present work is taken to be that of an ideal gas with a ratio of specific heats $\gamma = 7/5$. The ideal-gas equation of state in the form of (2.4) is

$$p = (\gamma - 1)\ \rho e \qquad (2.16)$$

Variations of γ corresponding to real-gas behavior can also be incorporated into the present formulation provided γ can be expressed in terms of the other state variables in Equation (2.16). However, estimates indicate that real-gas effects will persist momentarily only within a few charge radii of the explosive, a region in which geometric and other details of explosive placement are negligible for reasons discussed earlier.

2.1.4 Dimensionless Variables

The equations of motion (2.1) through (2.3) and their counterparts in ordinary differential (characteristic) form contain quantities with dimensions involving the usual length, time, and force or mass units. These equations apply for any physically consistent system of units.

It is convenient to work with variables in dimensionless form in order to bring out the natural scaling relationships (and limitations on scaling) among the variables. It is

easily shown that the governing equations can be made dimensionless by the choice of any three dimensionally independent parameters of the system, such as the ambient pressure p_o, the explosive energy yield W, and the ambient sound speed c_o or density ρ_o. Furthermore, with such a choice the equations of motion in terms of the dimensionless variables have exactly the same form as the dimensional equations.

For our purposes an appropriate set of dimensionally independent parameters will consist of a characteristic pressure p^* and density ρ^*, which may be taken as the ambient values of these quantities, and an explosion energy yield W^*, which may be taken as the yield of, say, one explosive charge in the problem. The dimensionless independent variables are then

$$\bar{r} = r \left(\frac{p^*}{W^*} \right)^{1/3} \tag{2.17}$$

$$\bar{t} = t \left(\frac{p^*}{W^*} \right)^{1/3} \left(\frac{p^*}{\rho^*} \right)^{1/2} \tag{2.18}$$

The pressures and densities are scaled respectively by p^* and ρ^*, internal energy by p^*/ρ^*, and velocities by the square root of this ratio. The usual cube-root yield scaling of distance and time is immediately evident in Equations (2.17) and (2.18). For these variables to be dimensionless W^* must be measured in energy units consistent with the units of force and length in which the other dimensional parameters are measured. Conversion of W^* in terms of the weight of a given solid explosive is readily accomplished through the detonation energy per unit weight of the material.

While the ideal-gas equation of state (2.16) is invariant under a transformation to dimensionless variables, this is not true of the detonation-product equation of state (2.15), since the latter involves the dimensional constants B and C. The numerical values of the dimensionless equivalents of these empirical constants will depend on the choice of characteristic pressure and density. Therefore the scaled (dimensionless) results in any problem will depend on the choice of reference values of pressure and density. However, this dependence is confined to details of the behavior in the region of the explosion products, and its effect on scaling of the far-field results to different atmospheric conditions will be weak.

2.2 Numerical Methods

Application of the method of characteristics to specific problems consists of numerical integration using the finite-difference equivalents of Equations (2.9) through (2.14) together with shock relations and the applicable interface or boundary conditions. At each step of such calculations, values of the dependent variables are known at previously calculated discrete points in the r, t plane. The solution is advanced in time from prescribed initial data by solving simultaneously the finite-difference equivalents of (2.9), (2.11), and (2.13) written between known points and the point to be determined.

It should be recalled that the characteristic lines and particle paths in the r,t plane represented by Equations (2.10), (2.12), and (2.14), on which the respective compatibility relations apply, are not known beforehand, and are determined as the solution progresses. At each step of the computations, suitable average values of nonderivative coefficients in the difference equations must be used. In general this requires an iterative procedure to determine the location of each new point simultaneously with solving for values of the dependent variables at the new point.

There are two basically different ways in which the properties of characteristics can be used to construct numerical solutions. One of these, referred to as the natural-grid method, is to obtain the solution along particular members of each of the families of characteristic lines determined continuously as the solution is advanced. The other, called the fixed-time method, uses the properties of characteristics to relate the flow at the beginning and end of a prescribed time interval at each step of the calculations. The former method is useful in certain special cases, particularly for isentropic flows. The latter method, due to Hartree[4], provides results in the form of profiles of pressure and velocity at fixed times, and has several advantages over the natural-grid method for problems of the type we consider in the present work. In the following paragraphs we outline calculations using the two methods, discussing the fixed-time method in substantially more detail, since it was utilized for most of the calculations reported here.

2.2.1 Natural Grid Method

At a typical interior (continuous) point of the solution, calculations using the natural-grid method proceed as follows:

Assume the solution to be known at points 1 and 3 in Figure 1, and suppose that no shock waves are present locally. The solution is to be found at point 2', the intersection of two characteristic lines of opposite families with the particle path through point 2 on the line joining 1 and 3. Between 1 and 2' Equations (2.9) and (2.10) apply, while between 3 and 2' Equations (2.11) and (2.12) apply. Equations (2.13) and (2.14) hold along the particle path joining 2' with 2, where values of required variables at the latter point are obtained by interpolation between known values at 1 and 3. Finally, values of p and e at 2' must satisfy the equation of state. Thus in computations the new point 2' is tentatively located using (2.10) and (2.12) with the values of u and c at 1 and 3. The first approximations to p and u at 2', obtained from (2.9) and (2.11), are successively improved using (2.13) and (2.14) together with the equation of state, until all conditions relating the points in the diagram are satisfied simultaneously within a prescribed convergence criterion.

In the present work we used the natural-grid method to determine certain features of the early expansion of the explosion gases. The procedure in this application is described in more detail in Section 3.2.1.

2.2.2 Fixed Time Method

One disadvantage of the solution on a natural characteristic grid as outlined in Section 2.2.1 is that the solver has no control over the points at which the solution gets determined. Investigation of coalescing blast waves from explosive charges requires results in the form of spatial distributions (e.g., the pressure profiles) at prescribed times, and a considerable problem would arise of two-dimensional interpolation in the characteristic mesh. For most of the present work we use a method which overcomes this difficulty by defining the mesh points in advance in both space and time and performing the interpolation as the calculation proceeds. This fixed-time method has the advantage that the interpolations required are always one-dimensional, and the results at any stage of the solution are always available in the form of profiles with respect to distance at fixed times. In either method, it can be shown that the truncation error incurred by replacing the differential equations by their difference equivalents is of the order of h^2, where h is a measure of arc length along the characteristic lines between points at which the solution is determined in the r, t plane[5].

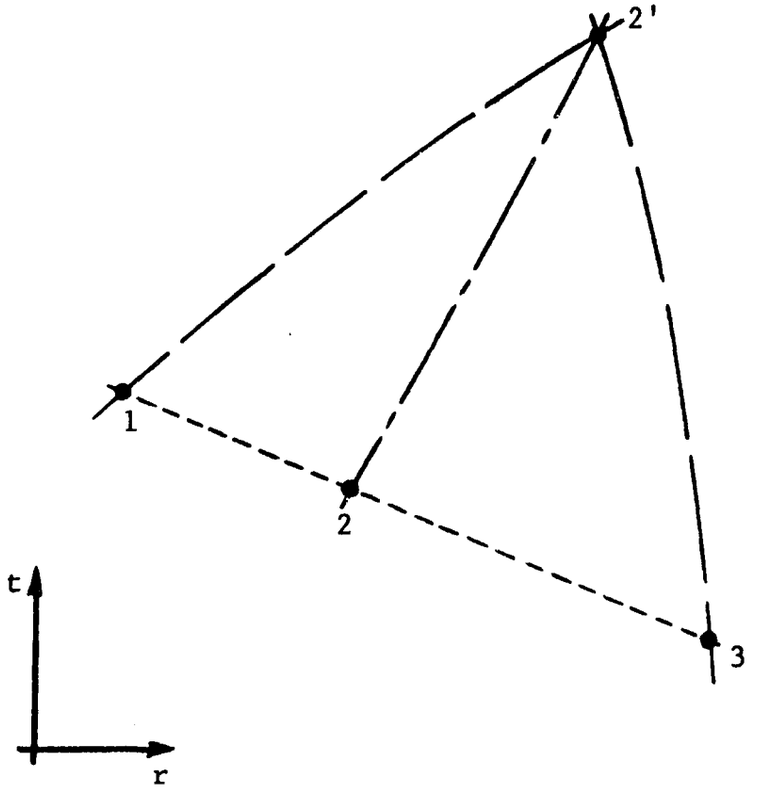

Figure 1 Characteristic Relations at a Typical Point

In the present work we devised a version of the fixed-time method in which computations are performed following particle trajectories in the r, t plane, and which accommodates any equation of state of the form of (2.4). Thus, we can follow the expansion of detonation products described by Equation (2.15) as well as the resulting pressure field in the surrounding air.

In the following paragraphs we outline the order of calculation at a typical interior point and at a blast wave moving into undisturbed air. These typify the most frequently utilized calculation routines in the type of problem studied in this work. Other considerations encountered in developing numerical solutions are also summarized.

2.2.2.1 Typical Interior Point

Assume the solution is known at fluid elements occupying positions 1, 2, and 3 in a continuous region at time t (Figure 2). The solution is required at point 2', which represents the new position at t + Δt of the particle that was located at point 2 at time t.

The characteristic lines of the first and second families passing through 2' meet the base line at a and b. Let double subscripts denote quantities averaged arithmetically between the points so indicated. Equations (2.9) through (2.14) are written in finite-difference form as follows:

$$\left(\frac{1}{\rho c}\right)_{a2'} (p_{2'}-p_a) + (u_{2'}-u_a) + \nu \left(\frac{uc}{r}\right)_{a2'} \Delta t = 0 \qquad (2.19)$$

$$r_a = r_{2'} - (u+c)_{a2'} \Delta t \qquad (2.20)$$

$$\left(\frac{1}{\rho c}\right)_{b2'} (p_{2'}-p_b) - (u_{2'}-u_b) + \nu \left(\frac{uc}{r}\right)_{b2'} \Delta t = 0 \qquad (2.21)$$

$$r_b = r_{2'} - (u-c)_{b2'} \Delta t \qquad (2.22)$$

$$e_{2'} = e_2 - p_{22'} \left(\frac{1}{\rho_{2'}} - \frac{1}{\rho_2}\right) \qquad (2.23)$$

$$r_{2'} = r_2 + u_{22'} \Delta t \qquad (2.24)$$

To determine the location of 2' and the values of the dependent variables there, first estimate $r_{2'}$ from (2.24) by assuming $u_{2'} = u_2$.

Also assume initially that p, ρ, and c at 2' have the same values as at 2. Calculate r_a and r_b in first approximation from (2.20) and (2.22), taking as initial guesses for u and c at a and b their values at 1 and 3, in order to compute the required averages. Using these values of r_a and r_b, compute u, p, ρ, and c at a and b from their values at 1, 2, and 3, by means of second-order interpolation formulas.

Compute the averages of the quantities $1/\rho c$ and uc/r required in (2.19) and (2.21). Solve (2.19) and (2.21) for $p_{2'}$ and $u_{2'}$.

Compute $\rho_{2'}$ and $e_{2'}$ by solving (2.23) simultaneously with the applicable equation of state (2.15) or (2.16). Compute $c_{2'}$ from the right member of (2.5).

Test whether the successive values of $p_{2'}$ and $u_{2'}$ so calculated satisfy prescribed numerical convergence criteria. If they do not, repeat the process using the current values of the dependent variables at 2' as new initial guesses.

2.2.2.2 Shock Wave Point

In the present numerical method, shocks are accounted for independently as they propagate through the mesh of particle trajectories. At a shock, the jump conditions (2.6) through (2.8) must be solved simultaneously with the equations of one of the characteristic families in the region behind the shock.

Consider a shock moving rightward into a region of known conditions (Figure 3). Denote the state ahead of the shock by the subscript zero. Assume the solution is known at points 1, 2, and Z, the last being a previously calculated point on the shock. The shock state at S is to be determined.

The characteristic line of the first family passing through S meets the base line at point a. The shock equations (2.6) through (2.8) are applicable as they stand. In addition, the shock position is given in finite-difference form by

$$r_s = r_z + U_{zs}\Delta t \qquad (2.25)$$

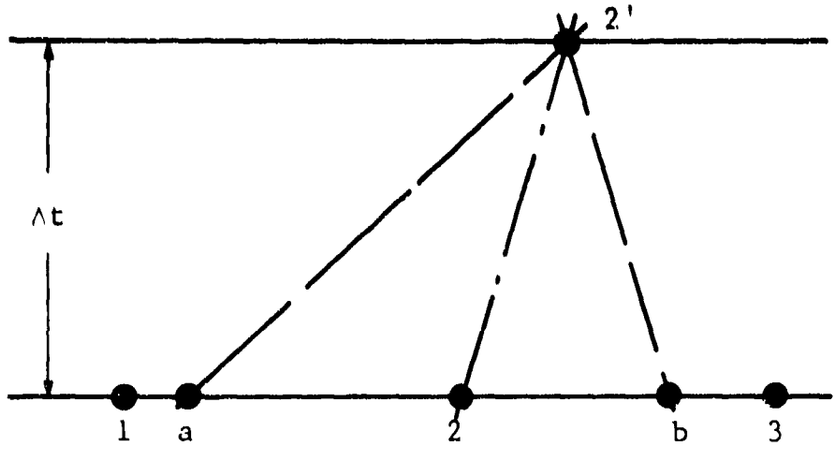

Figure 2 Fixed-Time Calculation at an Interior Point

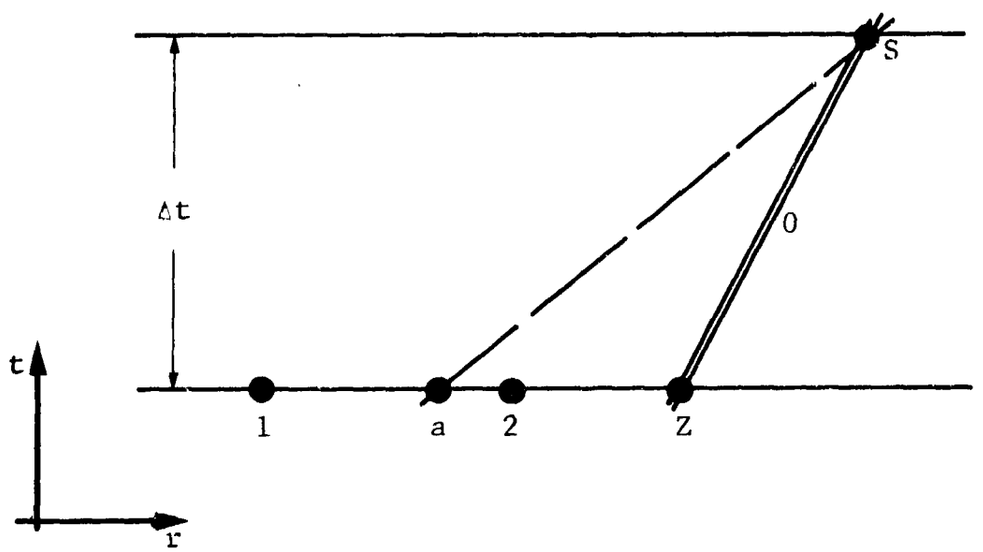

Figure 3 Fixed-Time Calculation at a Shock

where the double subscript denotes the average of values at the indicated points. Equations (2.19) and (2.20) apply between S and a, with subscript s replacing 2'. The procedure for determining the solution at S is as follows:

First, estimate r_s from (2.25) assuming initially $U_s = U_z$. Also assume initially that $u_s = u_z$. Solve (2.6) and (2.8) simultaneously with the equation of state for p, ρ, and e at S. Compute c_s from the right member of (2.5). Initially this process gives the same values of state variables as at Z, but the values will change in subsequent iterations.

Compute r_a from (2.20), taking as initial guesses for u and c at a their values at 2, in order to compute the required average. Using this estimate of r_a, compute u, p, and ρ at a from their values at 1, 2, and Z by means of second-order interpolation formulas. Compute c_s from (2.5).

Form the averages of the quantities $1/\rho c$ and uc/r required in (2.19). Solve (2.6) and (2.19) simultaneously for p_s in terms of the current value of ρ_s. Compute e_s and an improved value of ρ_s by solving (2.8) simultaneously with the equation of state. Compute u_s from (2.6), and U_s from (2.7).

Test whether the successive values of p_s and u_s satisfy prescribed convergence criteria. If they do not, repeat the process using the current values of U and u at S as new initial guesses. It has been found that this process always converges successfully. Other iteration schemes for determining shock wave points were also attempted, but were found to diverge when the shock moves into a field having a strong pressure gradient.

2.2.2.3 Special Points

Special situations encountered in the computations include boundary and interface points, and points adjacent to shocks. At boundaries either u or p is prescribed, and calculations must be made using the given boundary value in the characteristic relations of one family only. At a material interface the calculations are essentially the same as at an interior point, except that different equations of state apply to either side of the interface.

At an interior point adjacent to a shock, one of the characteristics extended backward from the new position of the point may intersect the shock rather than the previous fixed-time line. If this happens, it is necessary to

apply the characteristic relations between the new position of the point and the intersection of the characteristic with the shock. Values of variables at the intersection are obtained by linear interpolation along the shock trajectory.

Other situations which require special treatment, but which are encountered relatively less frequently as a solution is developed numerically, include the interaction of a shock with a material interface or with another shock. The former interaction occurs when a detonation wave emerges at the boundary of an explosive charge, while the latter takes place when two blast waves moving in the same direction eventually coalesce.

2.2.2.4 Addition of New Points

To advance the solution of the blast field in air exterior to the explosion gas sphere to the times and positions of interest requires the addition of new particle trajectories at the leading shock, thereby expanding the computed field. As the computed field expands, it is necessary also to reduce the density of computed particle trajectories so as to maintain approximately uniform resolution of the blast pressure field gradients.

We devised a point addition routine which insures a controllable level of computational accuracy. New particle trajectories are introduced at the leading shock as the shock traverses equal radial intervals in the undisturbed air ahead of the shock. The required radial interval Δr is determined from

$$\Delta r = \frac{\rho_s^o}{\rho_o} \Delta r^o \qquad (2.26)$$

where ρ_o is the undisturbed air density, ρ_s^o is a reference (or initial) value of shock density, and Δr^o is an input constant characterizing the desired spatial resolution of the results. This criterion results in zones of approximately equal mass between computed trajectories. This point addition method was found to provide relatively uniform resolution of blast pressure gradients.

2.2.2.5 Stability and Radial Zoning

It is known from the structure of the governing equations that the solution at a typical interior point in

the r, t plane depends only on previous data within a region bounded by characteristics of the first two families intersecting at the new point. This defines a so-called domain of dependence of the point. Thus in Figure 2, for example, the solution at 2' depends only on previous data along the base line between a and b.

In the fixed-time method, values of variables at a and b are determined from their values at 1, 2, and 3, using second-order interpolation formulas. Consequently, any change of properties at 1 or 3 will influence the results at 2', in effect broadening the numerical domain of dependence of 2'. Any error introduced because of this effect is small and has been found to decrease gradually with time[6].

In order to insure stability of the calculations, the magnitude of the time increment Δt is limited by the condition

$$\Delta t \leq \Delta r/c \qquad (2.27)$$

where Δr is the spatial interval between two neighboring previously calculated data points, and c is the local value of the sound speed. With this criterion, points a and b in Figure 2 always lie between 1 and 3. In practice, to determine the next time step the current spatial distribution of points is scanned and Δt is obtained as the least value of $\Delta r/c$ for the current profile. Thus a refinement or coarsening of the spatial distribution of data points is always accompanied by a corresponding refinement or coarsening of the time step. The total computational effort in a given problem therefore varies roughly as the square of the spatial resolution required.

We have found that, with the method of adding new points at the leading shock described in Section 2.2.2.4, radial intervals Δr between points in the profile at any time are such that $\Delta r/c$ tends to be nearly uniform throughout the profile. Since for stability the time step Δt in the fixed-time computation method is obtained as the least value of $\Delta r/c$ for the profile, the inequality $\Delta t \leq \Delta r/c$ tends to be marginally satisfied at all intervals Δr. Under this condition the fixed-time method approximates one form of the natural-grid method of characteristics, which is subject only to truncation (grid size) error and not to errors in the numerical domain of dependence of calculated points.

A simple automatic rezoning scheme was adopted for use in computing the far-field blast pressures. Periodically, alternate particle trajectories are deleted as the computed field expands and the available data storage is filled. With rezoning, the new point addition criterion is relaxed so that the stability criterion $\Delta t \leq \Delta r/c$ continues to be satisfied nearly uniformly for all radial intervals Δr, but with more economical resolution of the profile.

3. INITIAL EXPLOSION BEHAVIOR

In order to determine an appropriate model for the initial formation of the air shock from an explosive charge, we examined some aspects of spherical charge detonation and the early expansion of the explosion gas. In this section we describe calculations of the pressure and velocity fields in a centrally initiated pentolite sphere, and some features of the initial unsteady expansion of the detonation product gas.

3.1 Spherical Charge Detonation

Radial distributions of pressure, density, internal energy, and particle velocity in the detonation products of a spherical charge represent initial conditions on the subsequent blast field in the surrounding gas. These profiles are obtained at the instant the detonation wave resulting from the central initiation emerges at the surface of the spherical charge.

Walker and Sternberg[7] analyzed the underwater detonation of pentolite spheres using the equation of state (2.15), and gave the pressure profile in the detonation products. However, the distributions of other state variables were not reported. In the present work we independently obtained the necessary spatial variation of all state variables in the products.

Although the details of the pressure profile in the detonation products at early times are unimportant at distances larger than a few charge radii, it is essential to start a blast problem with internally consistent initial data. This is because the initial data must reflect accurately the total explosive energy release. When the charge detonation process terminates, the chemical energy released by detonation is in the form of internal and kinetic energies of the products. The pressure and velocity profiles must be consistent in the sense that the total energy so represented must equal the chemical energy released by detonation.

3.1.1 Equations of Motion

Central point initiation of a spherical charge is assumed to result in a stable Chapman-Jouguet detonation of constant velocity D, a property of the particular explosive and loading density. The flow profile consists of a detonation front followed by a centered rarefaction called a Taylor wave. The central region of the detonation products will be at a uniform state during the process. The flow behind the front is isentropic.

The equations of motion are (2.1) and (2.2) with $\nu = 2$ for spherical flow. The energy equation (2.3) for isentropic flow simplifies to

$$\frac{dp}{d\rho} = c^2 \tag{3.1}$$

where the sound speed c in the products is determined from the right member of (2.5) for the equation of state (2.15).

At the detonation front the usual shock equations (2.6) through (2.8) apply, except that e_o, the internal energy ahead of the shock, is replaced by the detonation energy per unit mass of the explosive. In addition, at the head of the wave the Chapman-Jouguet hypothesis states that

$$u + c = D \tag{3.2}$$

Finally, the energy yield W is proportional to the mass of the charge:

$$W = 4\pi\rho_o e_o r_o^3/3 \tag{3.3}$$

where ρ_o and r_o are the initial charge density and radius.

A similarity solution exists for this problem, so that the results can be expressed in terms of the single independent variable $z = r/t$. At the detonation front $z = D$. In particular, when the front emerges at the surface of the charge, the energy released is given by Equation (3.3).

The equations of motion are invariant under a transformation to dimensionless variables formed by using any three dimensionally independent parameters to define the scales of force, length, and time. We select as dimensional parameters the explosive energy yield W together with the pressure and density of the ambient atmosphere. The specific values of these parameters are immaterial except insofar as the values of the dimensionless equivalents of explosive properties and of the constants B and C in the equation of state (2.15) are affected by the choice of normalizing pressure and density. The dimensional CJ properties and constants in the equation of state listed in Section 2.1.3 were normalized using the standard atmospheric pressure $p^* = 1.013 \times 10^{-6}$ mb and density $\rho^* = 0.001226$ g/cm^3.

3.1.2 Detonation Wave Profiles

When the transformation is made to the similarity variable z, it is found that the derivatives du/dz and dp/dz are infinite at the detonation front. Therefore a cusp exists in the pressure profile at the front. It is necessary to regard u instead of z as the independent variable in order to integrate the governing equations numerically.

Equations (2.1), (2.2), and (3.1) can then be written

$$\frac{dz}{du} = \frac{z[(z-u)^2-c^2]}{2c^2u} \tag{3.4}$$

$$\frac{d\rho}{du} = \frac{\rho(z-u)}{c^2} \tag{3.5}$$

$$\frac{dp}{du} = \rho(z-u) \tag{3.6}$$

Equations (3.4) through (3.6) were integrated numerically for the pentolite equation of state (2.15) using a fourth-order Runge-Kutta scheme.

Integration was performed inward from the detonation front, at which z = D and all dependent variables have their CJ values, to the tail of the Taylor rarefaction, at which the particle velocity is zero. This occurs at approximately $r = 0.45\ r_o$; that is, the radius of the central sphere of uniform state is about 45 percent of the charge radius. The resulting profiles of pressure in atmospheres, and of dimensionless particle velocity, are shown in Figure 4 as functions of r/r_o at the instant the detonation front emerges at the surface of the charge.

3.1.3 Detonation Energy Check

At the detonation front z = D, the detonation velocity, while at the tail of the Taylor wave u = 0 and $z = c_i$, the sound speed in the central sphere of uniform state. These are singular points, since at z = D the derivatives du/dz and dp/dz are infinite, while at $z = c_i$ the same derivatives are indeterminate. It can be proved, however, that at $z = c_i$, du/dz = 0 for any physically realistic equation of state of the explosion gas.

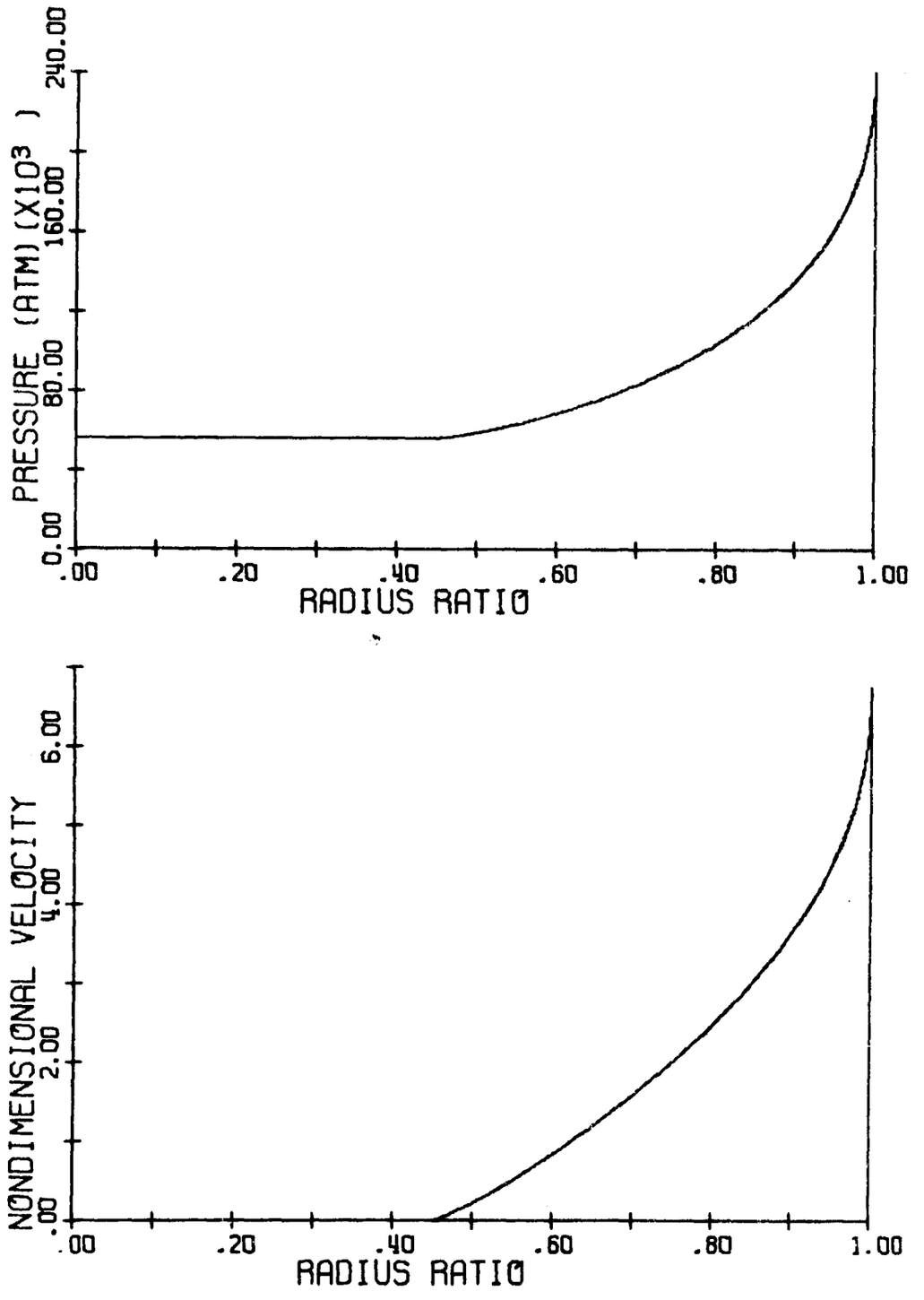

Figure 4 Spherical Charge Detonation Wave Profiles

The singular nature of the pressure and velocity profiles at the head and tail of the Taylor wave complicates somewhat the numerical integration required to obtain the profiles in the neighborhood of these points. To test the validity of the detonation wave profiles of Section 3.1.2, we evaluated numerically the energy balance equation which states that the total potential and kinetic energy at the instant that detonation is complete must be equal to the chemical energy stored initially in the charge. In terms of the similarity variable z, the energy balance reads

$$\rho_o e_o D^3 = \rho_i e_i c_i^3 + 3 \int_{c_i}^{D} \rho(e+u^2/2)\, z^2 dz \qquad (3.7)$$

where ρ and e are the density and internal energy, and subscripts o and i denote properties in the unreacted state and in the central sphere of uniform state after reaction. Thus e_o is the detonation energy per unit mass of explosive material.

Numerical evaluation of the integral on the right in Equation (3.7) was performed using an approximation of the integrand consistent with the fourth-order Runge-Kutta numerical integration of the wave profiles previously reported. It was found that the energy balance equation (3.1) is satisfied within 0.14 percent when the Taylor profile is resolved with 200 points.

3.2 Explosion Gas Expansion

When the detonation front emerges at the surface of a centrally initiated spherical charge, the high-pressure detonation product gas contacts the surrounding air. This drives a strong shock into the air, while the product gas sphere expands through a strong, inward-traveling rarefaction wave. The wave is a centered rarefaction, since it propagates on a fan of characteristics all of which originate from the charge boundary at the time the detonation wave emerges.

3.2.1 Centered Expansion Wave

The principal features of the early expansion of the explosion gas are shown schematically in Figure 5. The detonation front OA emerges at the charge boundary r_o at point A. The Taylor wave following the front occupies OAB, and OCB is the central region of uniform state. The detonation wave profiles previously reported apply at $t=t_A$. The region ABT is the inward-traveling expansion wave in the explosion gas, centered at A. The line AI is the interface between the explosion gas sphere and the air, while AS is the air shock.

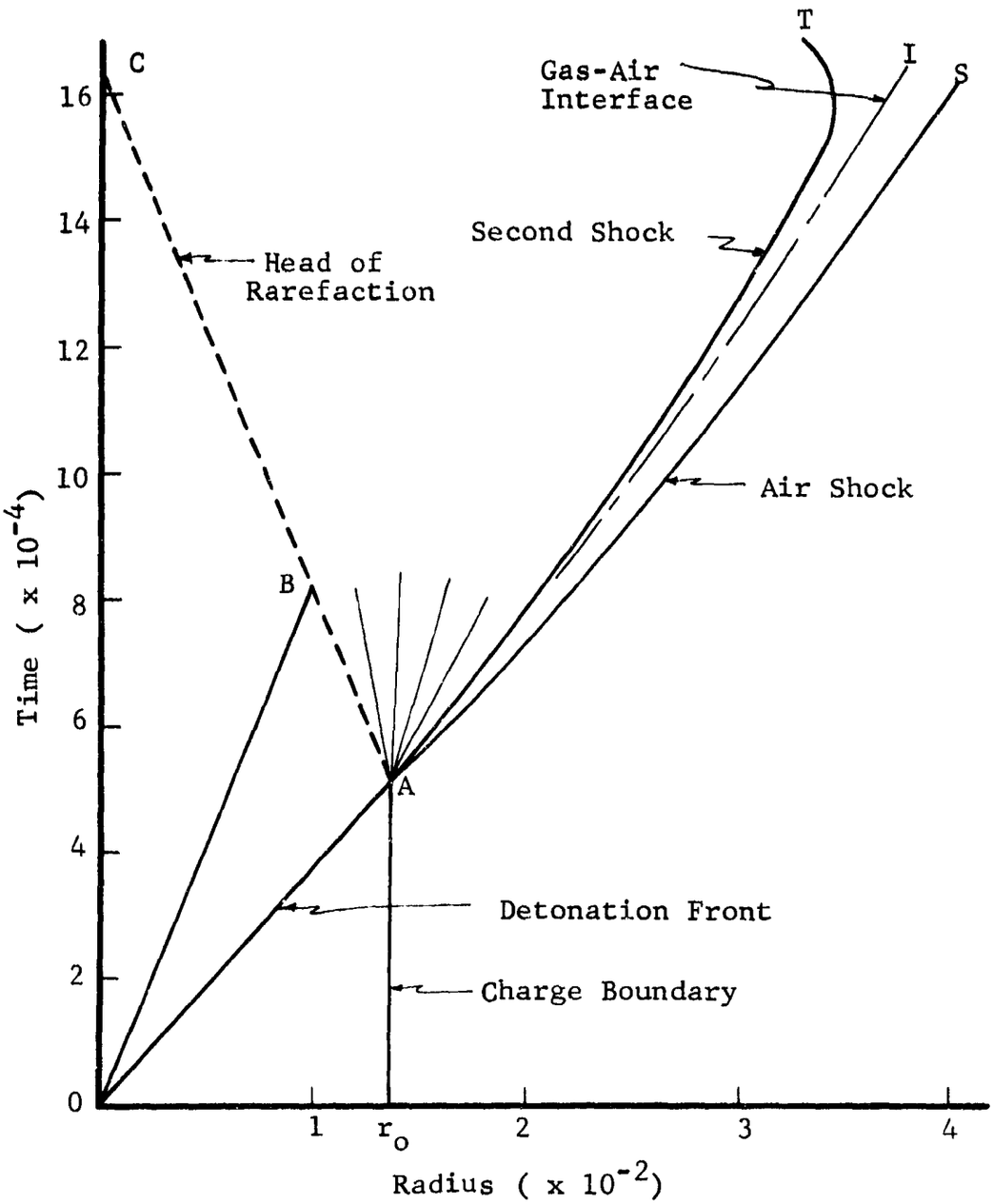

Figure 5 Early Expansion of Explosion Gas

At A, the pressure drops instantaneously from the detonation-front value to the initial pressure of the air shock which is established at that point. The initial air shock strength at A is determined by requiring that the instantaneous values of shock pressure p_s and particle velocity u_s also satisfy the compatibility relation for isentropic expansion of the explosion gas. The instantaneous compatibility relation

$$\frac{du}{d\rho} = -\frac{c}{\rho} \tag{3.8}$$

and the energy equation (3.1) for isentropic expansion were integrated numerically using a fourth-order Runge-Kutta scheme, for the equation of state (2.15) of pentolite detonation products. The integration proceeded from the Chapman-Jouguet values of all the variables until a pair of pressure-velocity values was found which also satisfies the air shock relations. Using the ideal-gas equation of state for air, we found the initial value of the air shock pressure at A to be 847 atm, a value consistent with an empirical fit of experimental data on air shock pressures close to spherical pentolite charges.[5]

To compute the pressure field in the centered fan ABT, it is first necessary to determine properties along the head characteristic ABC. On this curve $dr=(u-c)dt$, while values of u and c are functions of r/t from the Taylor wave solution in OAB. In terms of the similarity variable $z=r/t$, the parametric equations of the slightly curved segment AB of the head characteristic are

$$\frac{Dt}{r_o} = \exp\left[-\int_D^z \frac{dz}{z-u+c}\right] \tag{3.9}$$

and

$$r = zt. \tag{3.10}$$

Equation (3.9) is readily evaluated numerically. The straight segment BC is given by $dr = -c_i dt$, since $u=0$ and $c=c_i$, a constant, in the central region of uniform state. The solution in the entire fan ABT can then be determined from known boundary values of all the variables along the head characteristic.

Because the expansion of the detonation products in the centered fan ABT is isentropic, it is convenient to compute the field in the fan using a natural characteristic grid as outlined

in Section 2.2.1, rather than the fixed-time method of computation. With isentropic flow it is not necessary to follow the motion of fluid particles, and the natural-grid method in this case requires no interpolations in the lattice.

To determine the field in the fan, it is necessary to resolve the instantaneous pressure drop at A into a finite number of steps. The difference between the instantaneous values of (u-c) at the head and tail of the fan was divided into 40 equal intervals. This defines a family of 39 characteristics interior to the fan, all originating from A.

Let C^+ and C^- denote characteristics of the first and second families, respectively. The curved segment AB of the head C^- characteristic was resolved with 50 data points. The calculation proceeds from the head outward to the tail of the fan. A typical lattice element is shown in Figure 6. Points 1 and 2 are previously calculated data points. Point 3 is determined by the following procedure:

Initially, assume u_3, c_3, and all other dependent variables at point 3 to be the averages of their values at 1 and 2. Estimate r_3 and t_3 from the C^+ and C^- characteristic equations

$$r_3 - r_1 = (u+c)_{13}(t_3-t_1) \qquad (3.11)$$

$$r_3 - r_2 = (u-c)_{23}(t_3-t_2) \qquad (3.12)$$

where double subscripts denote average values between the indicated points.

Compute p_3 and u_3 by solving simultaneously the compatibility relations corresponding to (3.11) and (3.12).

Using a Newton-Raphson iteration method, compute e_3 and ρ_3 by solving simultaneously the equation of state and the energy equation written in difference form between points 1 and 3. Compute c_3 from the definition of the sound speed for the explosion gas equation of state.

Test whether the successive values of p_3 and u_3 satisfy prescribed numerical convergence criteria. If they do not, repeat the process using the current values of the dependent variables at 3 as new initial guesses.

On the first calculation step from the origin of the fan, the C^- characteristics through points 1 and 3 of Figure 6

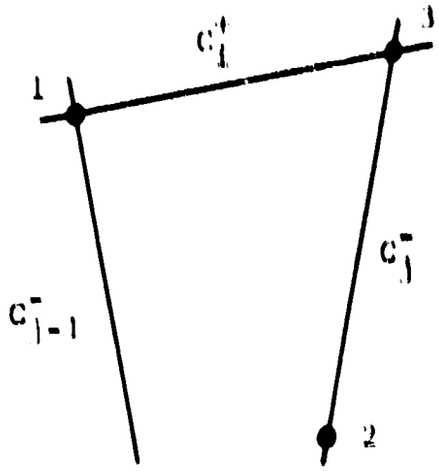

Figure 6 Natural-Grid Lattice Element

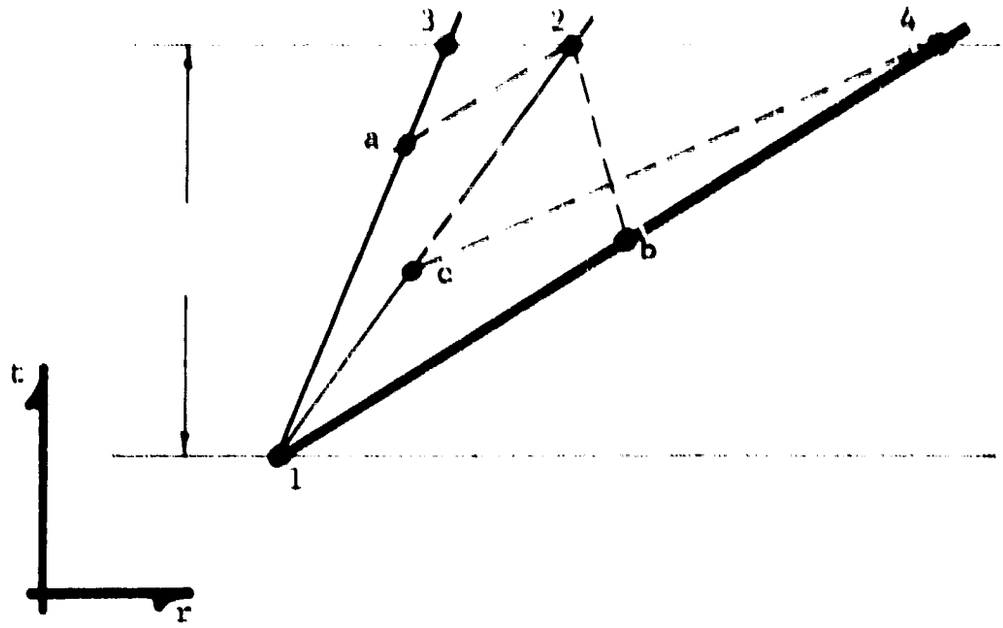

Figure 7 Initial Fixed - Time Calculation

intersect at point 2, which in that case corresponds to the fan origin. However, the calculation on the first step does not differ from that at a typical later step. One simply assigns to point 2 the appropriate pressure-velocity state from those into which the fan is initially subdivided.

The field in the entire fan is determined by the foregoing procedure. However, the expansion near the tail of the fan is so severe owing to spherical divergence that the pressure drops below that of the air shock. The overexpansion must be compensated for through an inward-traveling shock which forms along the tail characteristic of the fan (AT in Figure 5). This shock is initially of zero strength, but gradually increases in amplitude, propagating into the known field of the fan.[8] The shock, though traveling inward relative to the fluid, is swept outward at early times owing to the particle velocity induced in the expansion. The inward-traveling shock is determined jointly with the solution of the air shock and the pressure field in the adjacent air.

3.2.2 Air Shock at Early Times

The field between AS and AT in Figure 5 is determined by the normal fixed-time computation scheme. This field is bounded by two shocks, each propagating into a known region, and contains a material interface line AI.

An exceptional aspect of the procedure is the initial time step. In Figure 7, point 1 is the origin of the air shock. The initial shock pressure at point 1 is known from the instantaneous pressure drop at the charge boundary described in a preceding paragraph. Initially the inward-traveling shock between points 1 and 3 is of zero strength, and coincides with the tail of the centered fan in the explosion gas. The initial time step is arbitrary, but is chosen consistent with the resolution of the field in the fan.

Point 2 on the interface and point 4 on the shock are determined simultaneously by applying compatibility relations on characteristics extended backward from these points, and jump conditions across the shock at point 4. First-order interpolation formulas are used for the values of dependent variables at points a, b, and c. Otherwise, the procedure is the same as that for shock wave and interface points in the fixed-time method.

After the initial time step, the fixed-time scheme is applied in the usual way to the field between the two shocks. At early times after the process starts, the inward-facing shock remains weak and can be treated as coincident with the tail of the centered rarefaction in the explosion gas. We performed calculations of the gas expansion and air shock during the time when the strength of the inward shock is negligible.

The pressure profile shortly after the detonation wave emerges at the charge boundary is shown in Figure 8.

At later times, jump conditions would have to be applied to determine the location and strength of the inward-traveling shock as the solution progresses. This process was found to be quite difficult to treat numerically. The inward-traveling shock gives rise to a series of weak outward-propagating after-shocks at late times,[9] but these will appear behind the negative-pressure phase in the tail of the resulting far-field blast pulse and will not affect the coalescence of main shocks from sequential explosions. Calculation of the far-field blast pressures is simplified by omitting these details of the initial unsteady expansion of explosion gas.

Because the explosion gas expansion is adiabatic, the energy W_t transferred to the air at any time is obtained as the work of the pressure forces at the gas-air interface:

$$W_t = 4\pi \int_{r_o/D}^{t} pur^2 dt \qquad (3.13)$$

The result obtained by evaluating the integral in Equation (3.13) along the trajectory of the gas-air interface gives the energy W_n remaining in the explosion gas sphere at any time, since

$$W_n = W - W_t \qquad (3.14)$$

where W is the explosive energy of the charge. This property must hold for any model of the behavior of the explosion gas sphere used to calculate far-field blast pressures.

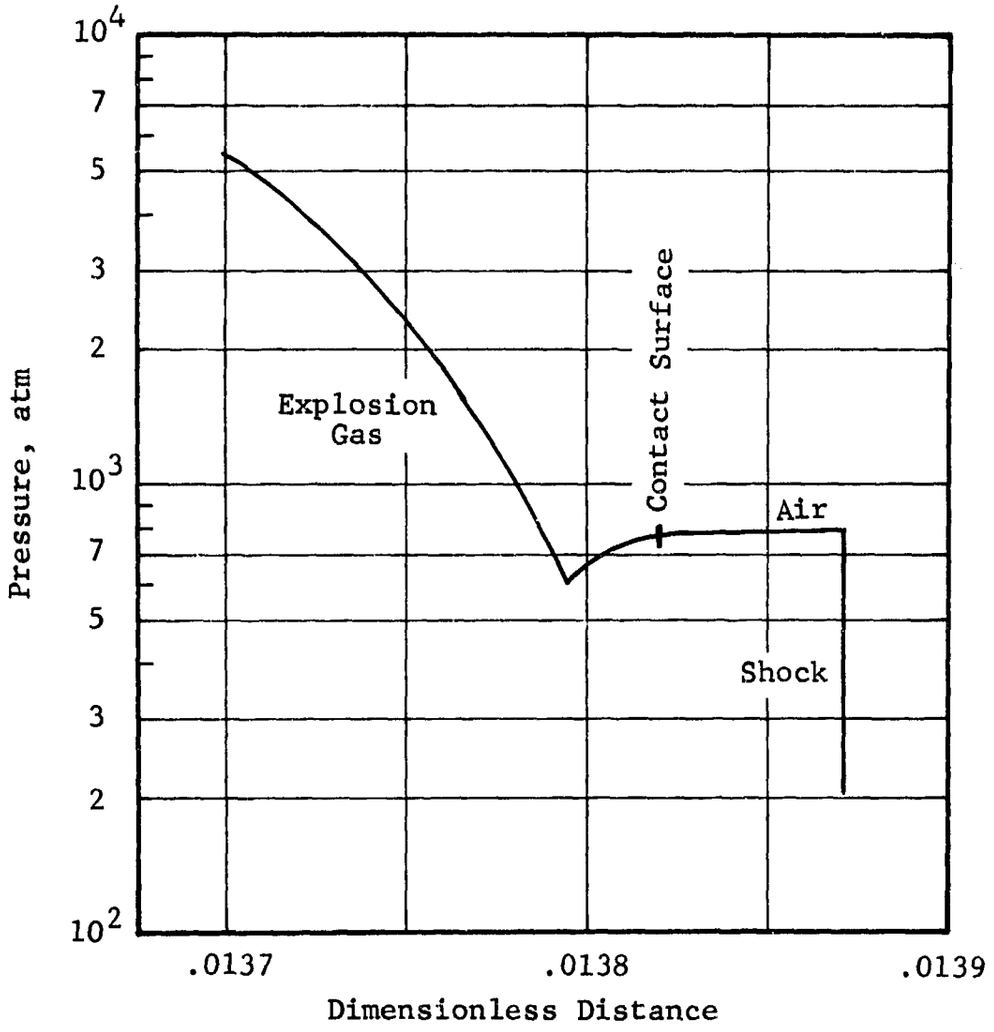

Figure 8 Pressure Profile at Early Time
Charge Radius = 0.01357

4. FAR FIELD AIR BLAST ANALYSIS

Computer programs were written in FORTRAN IV programming language, using the fixed-time characteristic scheme detailed in Section 2.2.2, to calculate the far-field propagation of air blast from spherical explosions. In this section we describe an application of the code to the single point explosion problem, for which an exact solution is available. This provides a test of the accuracy of the numerical method. We discuss the simplified model of the explosion gas sphere used to calculate far-field propagation, and the method used to insert subsequent explosions. Results are presented for the peak overpressures and pulse separations from sequential explosions.

4.1 Point Source Explosion

Among the few known exact solutions to problems of unsteady nonisentropic flow is the case of a strong spherical blast wave produced by instantaneous energy release at a point. The available exact solution for this problem provides a useful test of the accuracy of the numerical method described in Section 2.2.2, and of the performance of the compute. code developed in the present work.

We obtained the numerical solution of the single explosion problem using as initial data the pressure, velocity, and energy density profiles which characterize the strong point explosion. The numerical solution developed from these initial data must reproduce the blast field given by the exact solution at all later times.

4.1.1 Similarity Solution

The exact solution of the point explosion problem was obtained by Sedov[10] under the assumptions that the energy is released instantaneously at a point in a perfect gas, and that the ambient atmospheric pressure p_o is negligibly small compared to the shock front pressure p_s. With these assumptions the resulting profiles of the dependent variables p, ρ, and u remain self-similar at all times after the explosion. That is, the ratios of these variables to their shock front values (subscript s) are functions only of r/r_s, where r_s is the shock radius at any time. The functions are expressed parametrically in terms of an intermediate variable V for $\gamma = 7/5$ as follows, where $6/7 \leq V \leq 1$:

$$\frac{r}{r_s} = V^{-2/5} \, (7V-6)^{2/19} \, [(15-8V)/7]^{-173/380} \qquad (4.1)$$

$$\frac{p}{p_s} = V^{6/5} (6-5V)^{-7/3} [(15-8V)/7]^{173/60} \quad (4.2)$$

$$\frac{\rho}{\rho_s} = (7V-6)^{15/19} (6-5V)^{-10/3} [(15-8V)/7]^{865/228} \quad (4.3)$$

$$\frac{u}{u_s} = V \frac{r}{r_s} \quad (4.4)$$

The shock front values of these quantities vary with time as follows:

$$r_s = \left(\frac{KW}{\rho_o}\right)^{1/5} t^{2/5} \quad (4.5)$$

$$p_s = \frac{2}{15} (KW)^{2/5} \rho_o^{3/5} t^{-6/5} \quad (4.6)$$

$$\rho_s = 6\rho_o \quad (4.7)$$

$$u_s = \frac{1}{3} \left(\frac{KW}{\rho_o}\right)^{1/5} t^{-3/5} \quad (4.8)$$

where W is the energy release, ρ_o is the ambient atmospheric density, and the constant K = 1.175. By Equations (4.1) and (4.5), the ratio of any dependent variable to its shock front value is constant on any line $r/t^{2/5}$ = constant, for given values of W and ρ_o. Such a line is called a similarity line.

Choosing W and ρ_o as reference quantities to normalize the results simplifies the expressions (4.5) through (4.8). Because the ambient atmospheric pressure is absent from the problem, the pressure scale may be selected arbitrarily. This reflects the similarity property of the results. The shock pressure p_s at a particular time may be selected as the scale of pressure. This will define the time scale via the dimensionless equivalent of Equation (4.6).

4.1.2 Numerical Solution

The center of the blast sphere ($r = 0$) in the point explosion problem is a singularity at which the sound speed is infinite. Consequently, the behavior near the center cannot be treated numerically. We developed the numerical solution in a region of the r,t plane bounded by a constant time line and by the similarity line $r = 0.8\ r_s$. On the constant time line, the initial data are given by Equations (4.1) to (4.4), and the initial dimensionless shock pressure was taken as unity. On the similarity line the particle velocity was prescribed using Equations (4.4) and (4.8). The initial data were resolved with 20 equally spaced points on the initial time line. Calculations were continued until the shock pressure decreased to 1 percent of its initial value.

The computed field and the pressure profile are shown in Figures 9 and 10 at the time when the shock pressure has decreased by about one order of magnitude from its initial value. At this time the largest relative error in the dependent variables is less than 0.4 percent. The profile is resolved with 23 points. The new particle trajectories introduced at the shock more than compensate for the number which have left the field through the back boundary, a similarity line in this problem.

The computed field and the pressure profile are shown in Figures 11 and 12 at the time when the shock pressure has decreased to about 1 percent of its initial value. The relative error in the results along the last line of computation is less than 0.05 percent. The maximum error in the pressure at the shock front, incurred at a relatively early time, is about 0.3 percent. The pressure profile is resolved with 50 points at this time.

Two factors contribute to the level of accuracy attained in this test problem. First, as the solution is advanced, the same relative pressure drop (about 60 percent of the peak value in the profile) is resolved with a progressively larger number of computed points, and the field was not rezoned at intermediate time steps.

The second and possibly more important factor is that the method of adding new points at the leading shock tends to maintain a nearly uniform value of $\Delta r/c$ throughout the profile in this problem. On the other hand, we resolved the initial data profile with equally spaced points. Therefore at early times $\Delta r/c$ is not approximately uniform throughout the profile, and we immediately begin to incur errors in the computed results as indicated in Figure 9. However, by the time the shock pressure has decreased by about an order of magnitude at the final time line of Figure 9, the majority of the 23 points which resolve the pressure profile are points added during

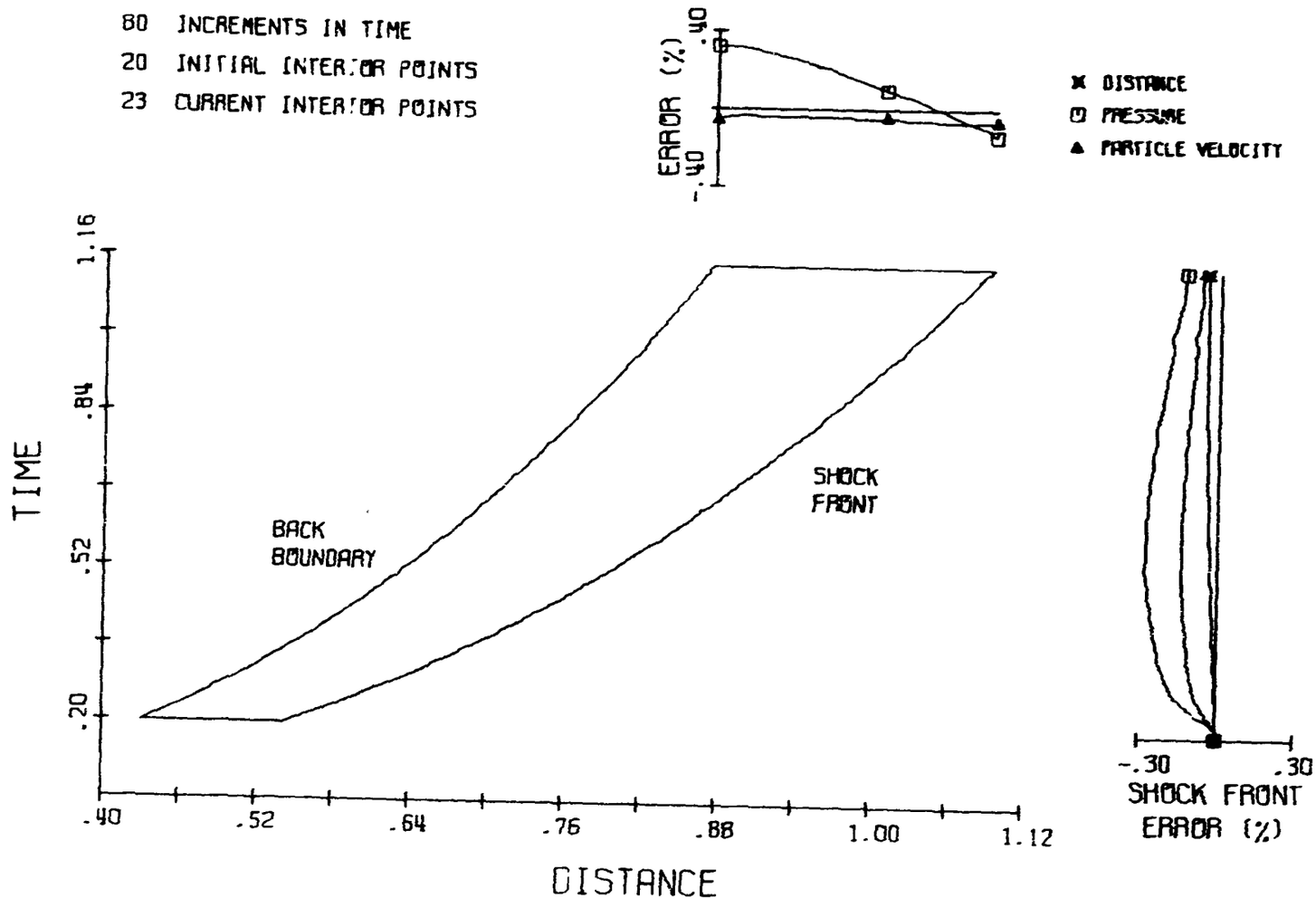

Figure 9 Point Explosion Field at $p_s = 0.12$

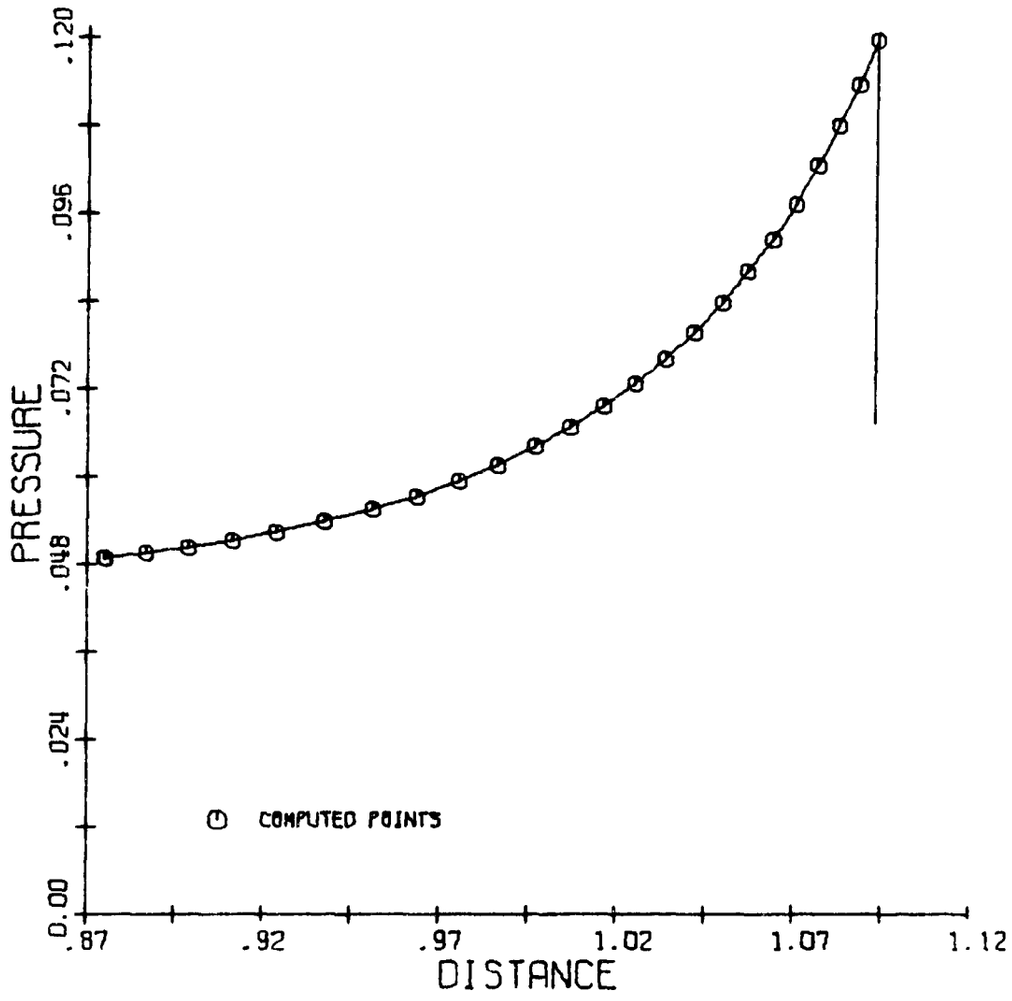

Figure 10 Point Explosion Pressure Profile at $p_s = 0.12$

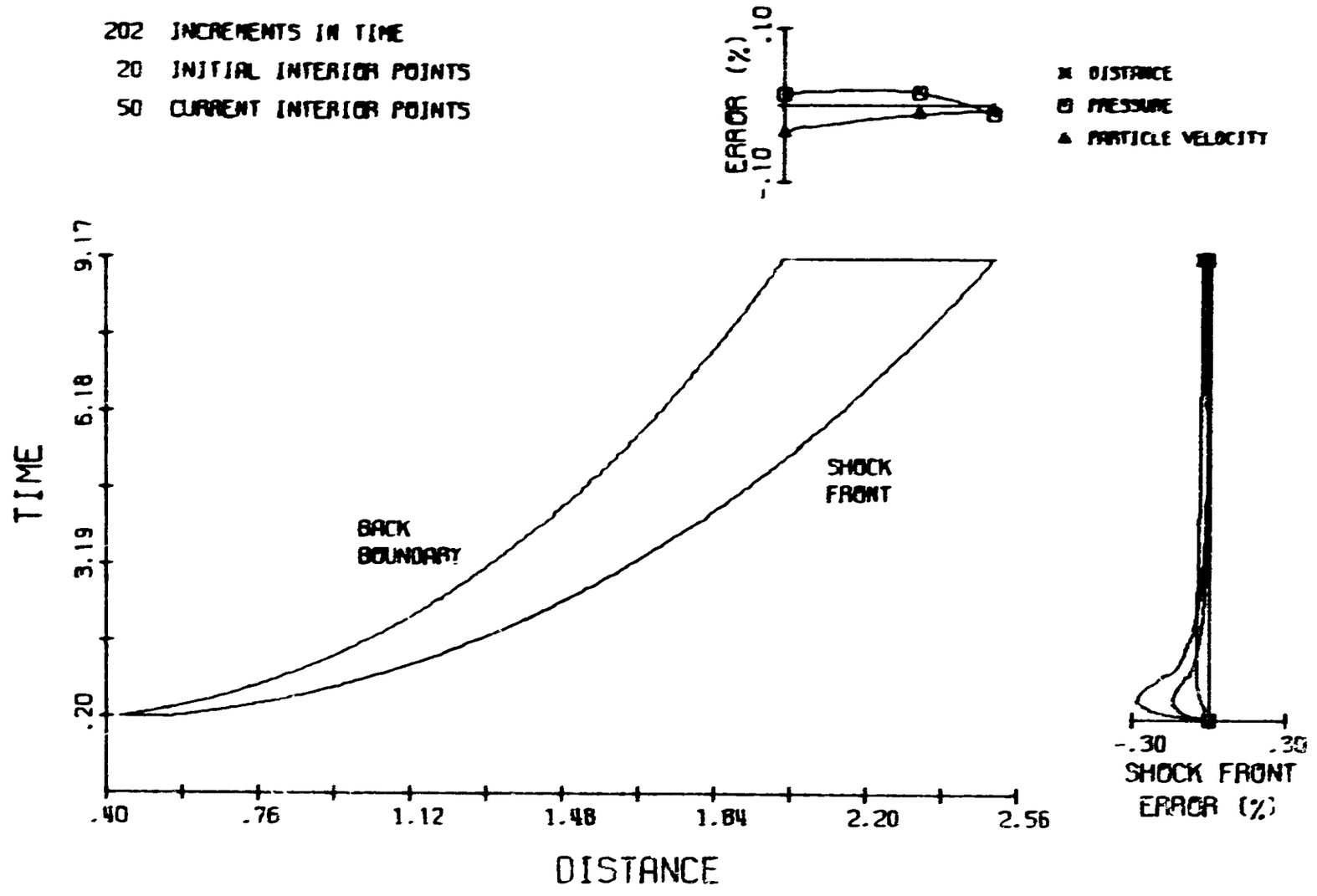

Figure 11 Point Explosion Field at $p_s = 0.01$

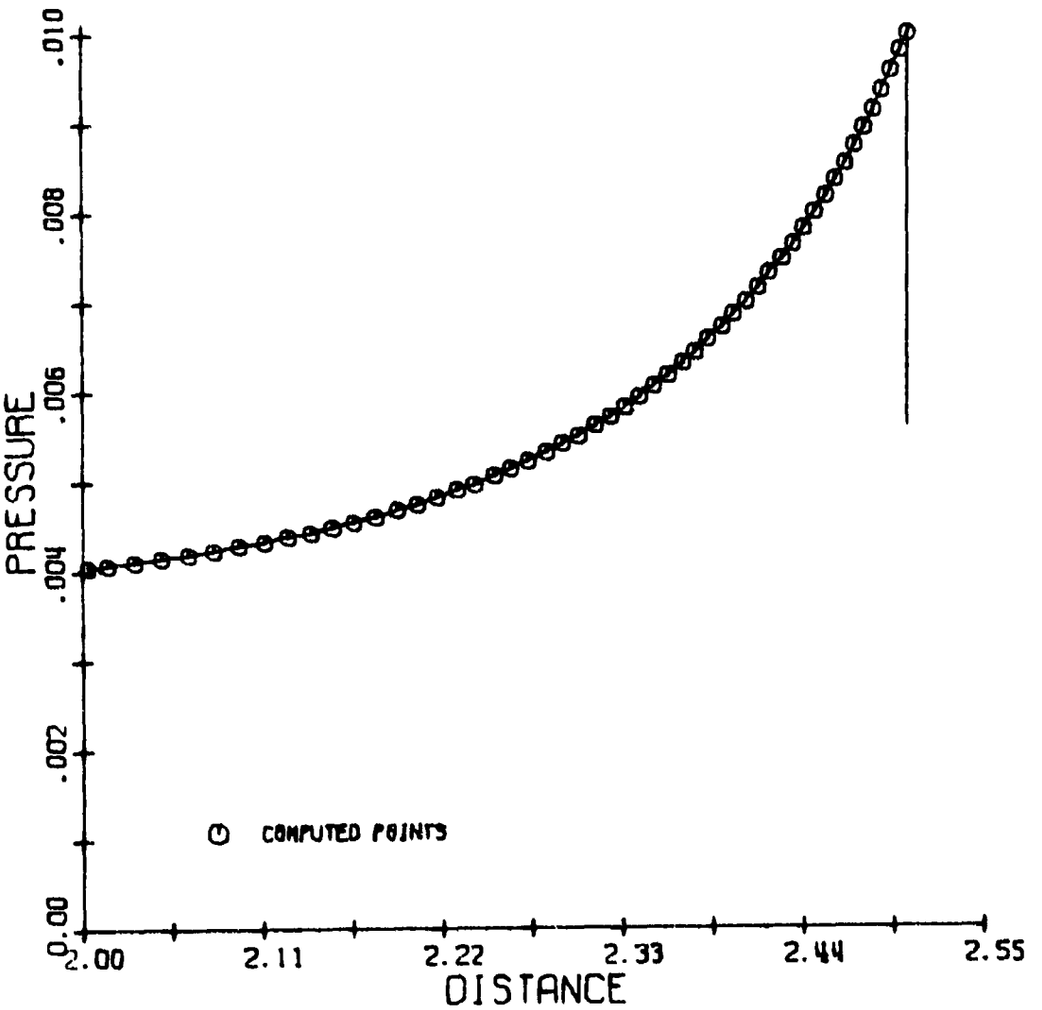

Figure 12 Point Explosion Pressure Profile at $p_s = 0.01$

computation. Most of the 20 initial particle trajectories have left the computed field through the back boundary. The accuracy of the results at the shock front and in the profile at this time has begun to improve significantly. By the time the shock pressure has decreased to 1 percent of its initial value (Figure 11), the effects of initial data resolution have vanished, and the agreement of the computed results with the exact solution is excellent.

4.2 Initial Conditions

In order to compute far-field blast pressures from explosions, it is essential to reduce the level of detail retained in calculations of the explosion gas sphere itself. The blast field in air at late times can be followed satisfactorily by treating the explosion gas at these times as an adiabatic sphere of uniform state. The equivalent uniform gas sphere is established on the basis of the total energy content of the explosion gas.

4.2.1 Uniform Explosion Gas Sphere

In a pentolite charge the head characteristic of the centered rarefaction originating from the charge boundary reaches the center at a dimensionless time of 0.001647 (point C in Figure 5). This corresponds to a scaled time $t/W^{1/3} = 0.01705$ msec/lb$^{1/3}$, a value nearly two orders of magnitude smaller than the shortest scaled delay time interval of interest between successive explosions in situations of practical interest. Therefore the charge detonation and the early unsteady expansion of the explosion gas sphere take place in a time interval that is insignificant compared with the times associated with far-field propagation.

As initial and boundary conditions for computing the far-field propagation, we replace the explosive charge by a sphere of detonation product gas having the same total energy and mass as the original explosive, at uniform but time-varying pressure.

The particle velocity in the gas sphere is zero except at the boundary, where it is equal to the gas-air interface velocity. Consequently the energy is entirely in the form of internal energy. The initial pressure in the sphere is determined from the requirements that the total energy and mass are the same as those of the original explosive, and that the gas satisfies the detonation product equation of state (2.15). Subsequently the energy of the sphere decreases according to Equations (3.13) and (3.14).

During the motion the pressure in the gas sphere is a function of boundary radius through isentropic expansion corresponding to the equation of state (2.15), while at the sphere boundary the pressure depends on the interface velocity as well through the compatibility relation for unsteady flow in the adjacent atmosphere.

It has been shown for a single TNT explosion that the effect of explosion-product mass on the blast wave is negligible beyond a shock radius at which a mass of air ten times the charge mass is engulfed.[9] For pentolite of initial density 1.65 g/cm^3 and air at standard atmospheric conditions, this would correspond to a scaled shock radius $R/W^{1/3} = 3.15$ ft/lb$^{1/3}$, considerably less than the smallest scaled radius of interest to the present work (~7 ft/lb$^{1/3}$). Therefore the explosion gas sphere can safely be represented as an equivalent uniform region at late times in the present work. It has also been shown[11] that late-stage equivalence holds between single explosions of equal energy but different mass, in that the shock pressures are the same at equal distances. If in addition the explosions are of equal mass, late-stage equivalence also holds for details of the interior structure of the blast fields.

4.2.2 Insertion of Successive Charges

A subsequent explosion is inserted computationally by increasing the current values of total energy and mass in the explosion gas sphere by the energy and mass of the second charge. The energy and density of the gas sphere are increased uniformly over the sphere volume at the time of the subsequent explosion. This neglects the time of propagation of the shock from the subsequent charge through the gases of the first explosion. The instantaneous pressure increase is uniquely determined from the increase of internal energy and density, and from the requirement that the explosion products continue to satisfy the equation of state (2.15). This process immediately initiates a second air shock at the boundary of the gas sphere, and tends to underestimate the separation between the two main shocks in the surrounding air.

At all times the unsteady blast field in the surrounding air is computed in the normal manner by the fixed-time method of characteristics. Within the framework of this model, the effects of any number of successive explosions originating from the same center can in principle be studied numerically. In the present work, however, we have restricted attention to problems involving two or three successive explosions.

4.3 Computed Results

The program for computation of air blast from explosions was coded in FORTRAN IV programming language for execution on a CDC 6600 machine. The general equations of plane, cylindrical, and spherical flow were coded so as to retain generality for all one-dimensional flows. The factor ν in Equation (2.1), which defines the dimensionality of the problem, is an input constant.

We applied the code to sequential spherical explosion problems to predict blast wave coalescence phenomena. Problem conditions were selected so as to duplicate those of several of the scale-model tests described in Section 5. Detonation properties of pentolite, for which the computations were performed, are quite similar to those of plastic explosive C-4, which was used in the experiments. Computations are performed internally with dimensionless variables, but the resulting times and distances are scaled by the TNT equivalent of the total weight of explosive detonated on a rigid ground surface. Therefore the results are applicable to any explosive weight for the conditions of charge weight ratio and scaled time delay considered here.

For conditions equivalent to those of the experiments described in Section 5 (2 lb of C-4 detonated on a rigid surface), the time delays and charge weight ratios for which computations were performed are listed in Table 1. For the three-charge problems the indicated delay is that between the first two detonations; the third explosion was introduced at the instant of coalescence of the first two shocks.

Table 1

Time Delays by Computer Run Number

Time Delay (msec)	Charge Weight Ratio			
	1:1	2:1	1:2	1:1:1
0.8	1	6		9
1.5	2	7	8	10
2.2	5			
2.9	3			
5.7	4			

In each case we continued the calculations beyond coalescence, if it occurred, or until the results were sufficient to provide a basis for understanding the behavior of successive pulses in the experiments. Time separations of the pulses at

various distances were obtained by cross-plotting the normally output results, which are in terms of pressures and positions at fixed times.

The results for scaled time separation between leading and trailing shocks are shown as functions of scaled distance in Figures 13, 14, and 15. For a given time delay between detonations, the time separation between two successive shocks vanishes when coalescence occurs.

Peak pressures of the successive shocks are shown as functions of distance for each computed case in Figures 16 through 25. In these figures, the pressure-distance curve for a leading shock terminates when it is overtaken by a trailing shock. The pressure-distance curve of the trailing shock is joined continuously with that of the coalesced wave, except for a possible discontinuity of slope at coalescence (e.g., see Figure 16). The following general features of the computed results are noted:

- The computational model simulates a situation in which each observation point is equidistant from two sequentially detonated, spatially separated charges (as on the lateral blast gage line of the experiments described in Section 5), and has an unobstructed view of both.

- The distance at which coalescence occurs tends to be underestimated for very short time delays (5.5 $ft/lb^{1/3}$ compared with an experimental value of 7.3 $ft/lb^{1/3}$ for a scaled time delay of 0.6 $msec/lb^{1/3}$ reported in Section 5). This is because the second explosion is modeled by adding its energy and mass uniformly over the gas bubble of the first explosion at the instant of the second detonation. This effectively assumes an infinite propagation speed of the second shock in the products of the first explosion. The agreement improves rapidly with increasing time delay, however, as this effect becomes relatively less important.

- The peak pressure of a coalesced wave is substantially the same as that from the simultaneous explosion of the total weight of explosive in the event, as confirmed extensively in the experiments reported in Section 5.

- For long time delays there is no tendency for the successive blast pulses to coalesce. In fact, for a scaled time delay of 4.2 $msec/lb^{1/3}$ (the largest considered) with equal charge weights, the second shock travels in the negative pressure phase of the blast pulse from the first explosion.

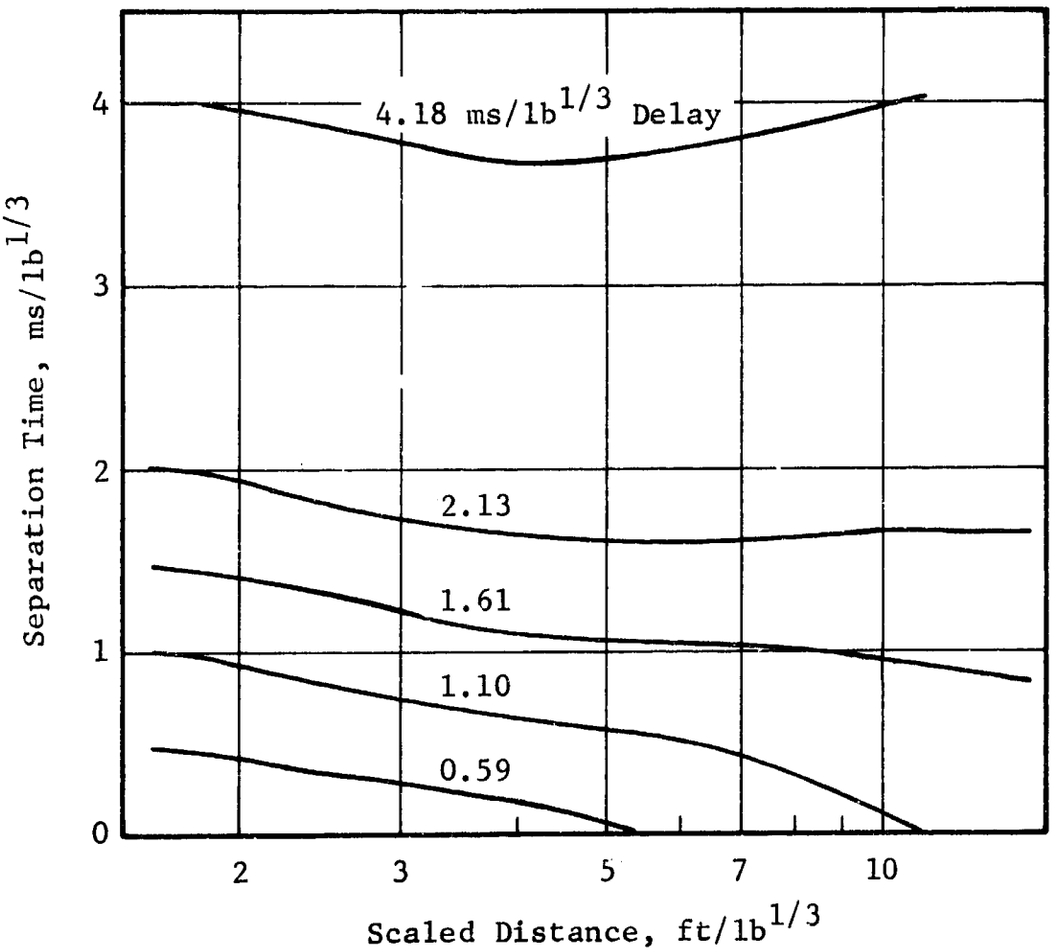

Figure 13 Computed Pulse Separation Times, Charge Weight Ratio 1:1

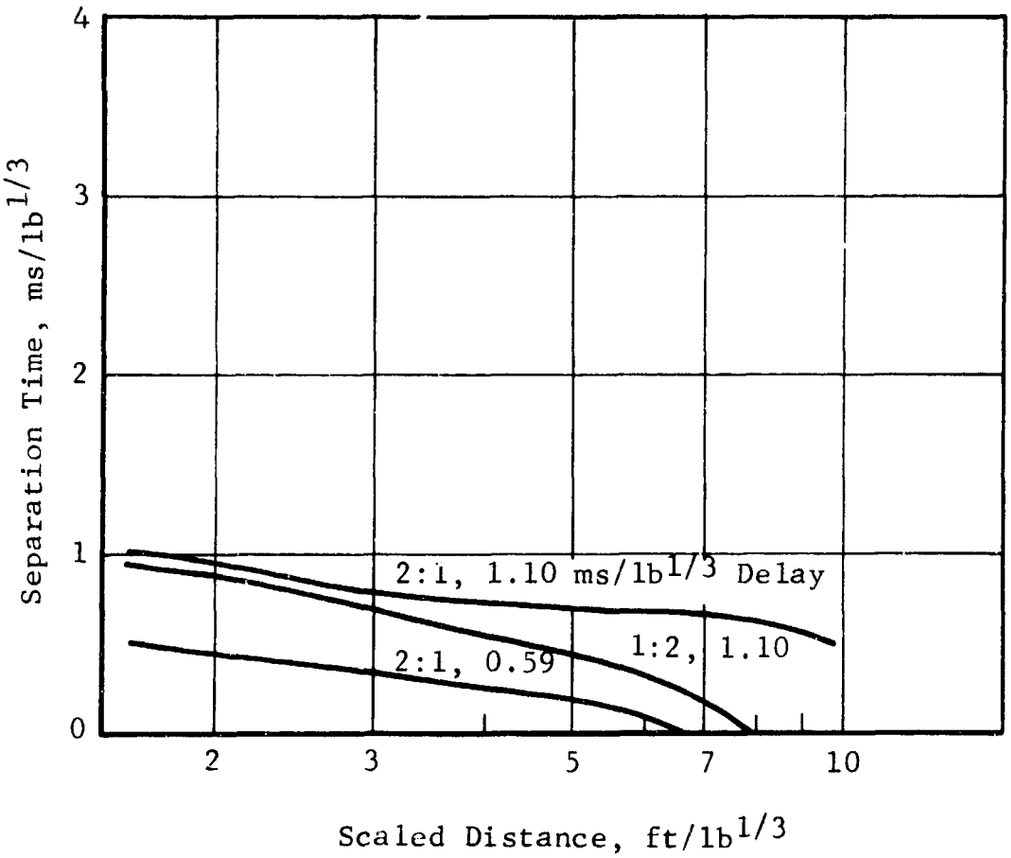

Figure 14 Computed Pulse Separation Times, Charge Weight Ratio 2:1 and 1:2

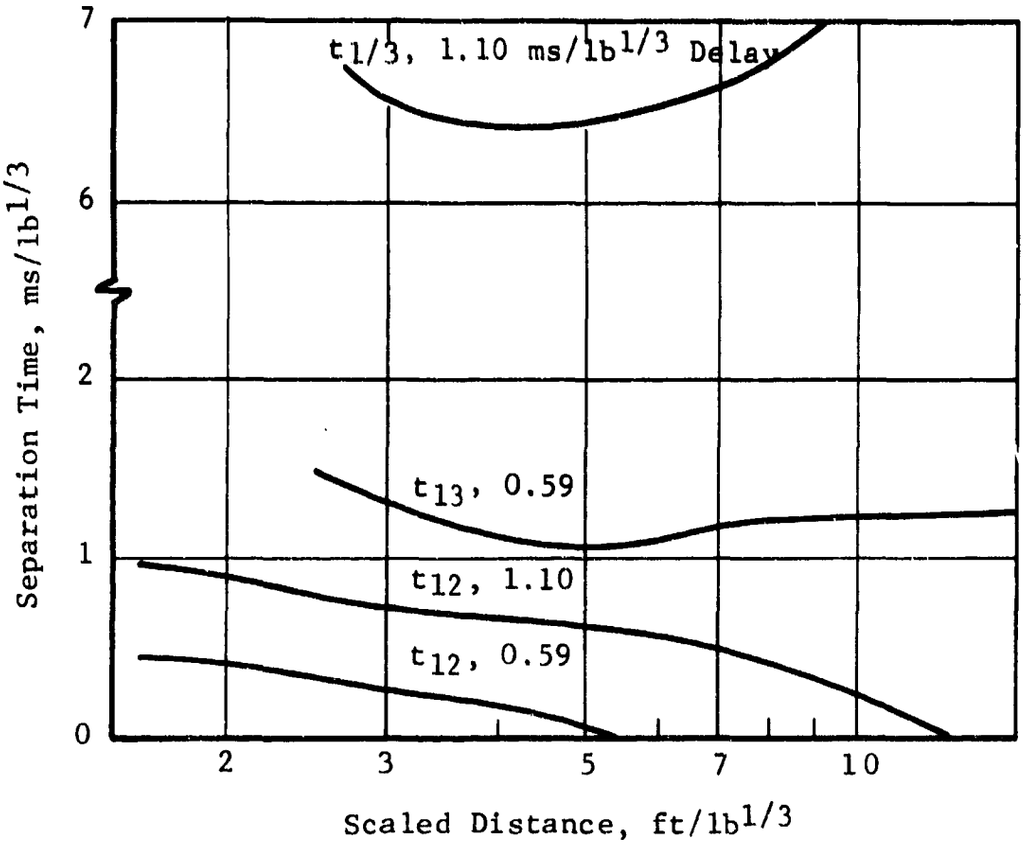

Figure 15 Computed Pulse Separation Times, Charge Weight Ratio 1:1:1

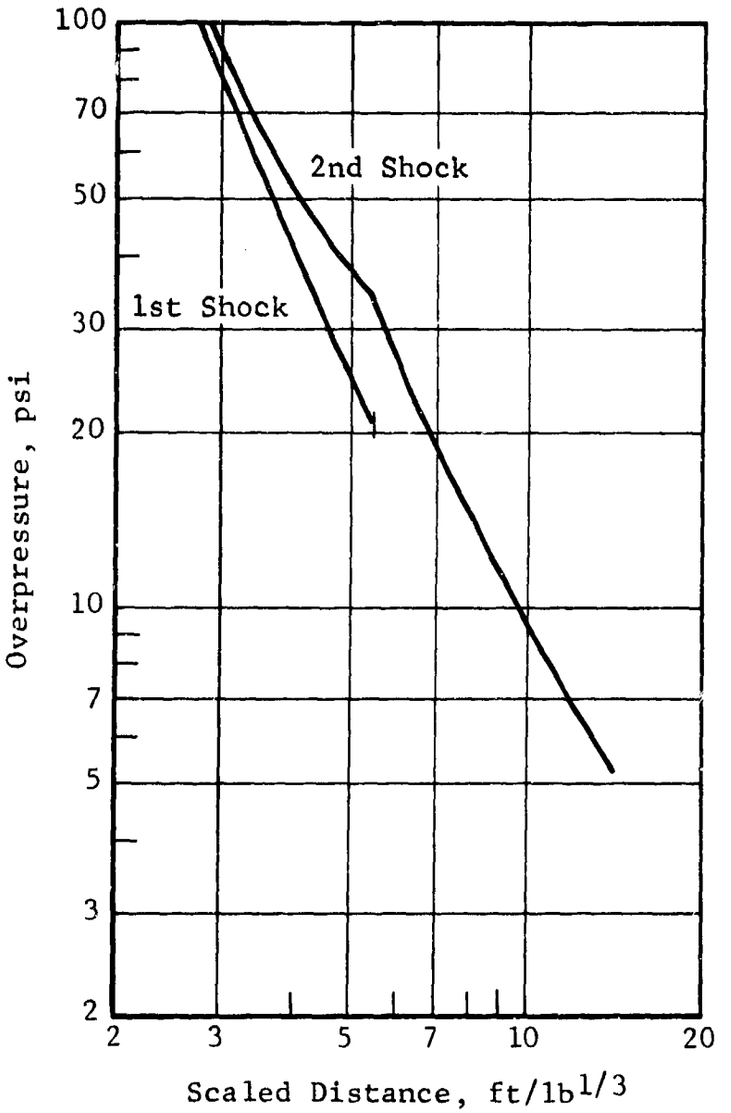

Figure 16 Pressures, Run No. 1, Charge Weight Ratio 1:1, Time Delay 0.59 ms/lb$^{1/3}$

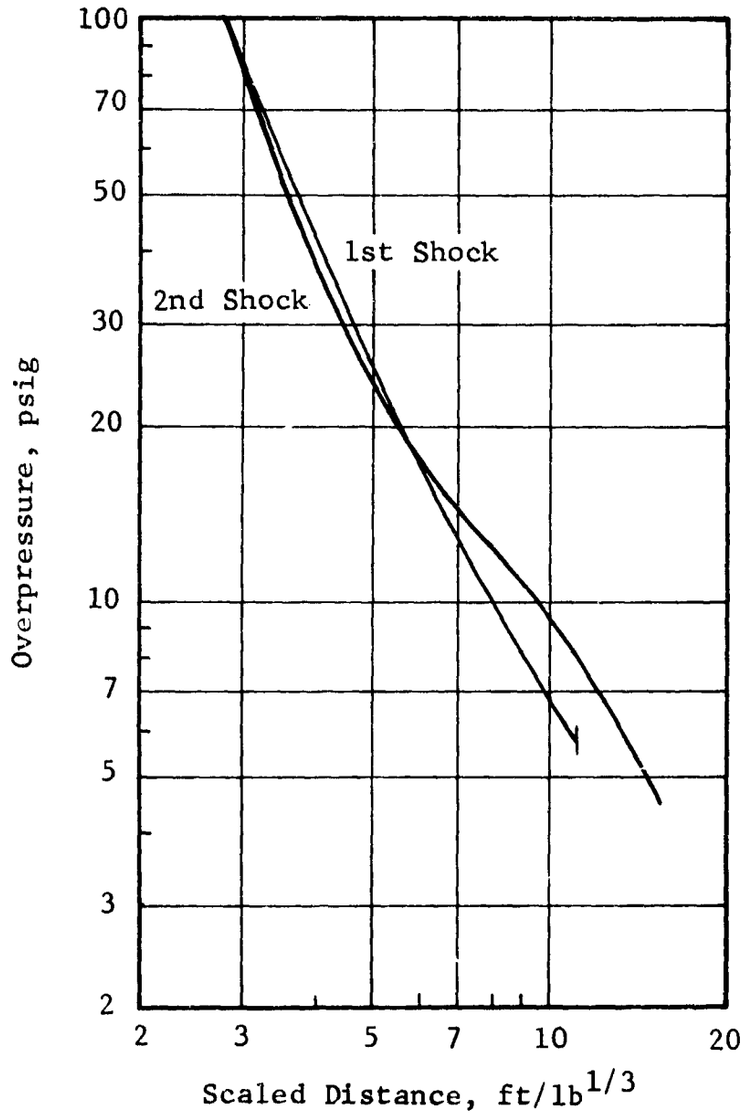

Figure 17 Computed Pressures, Run No. 2, Charge Weight Ratio 1:1, Time Delay 1.10 ms/$lb^{1/3}$

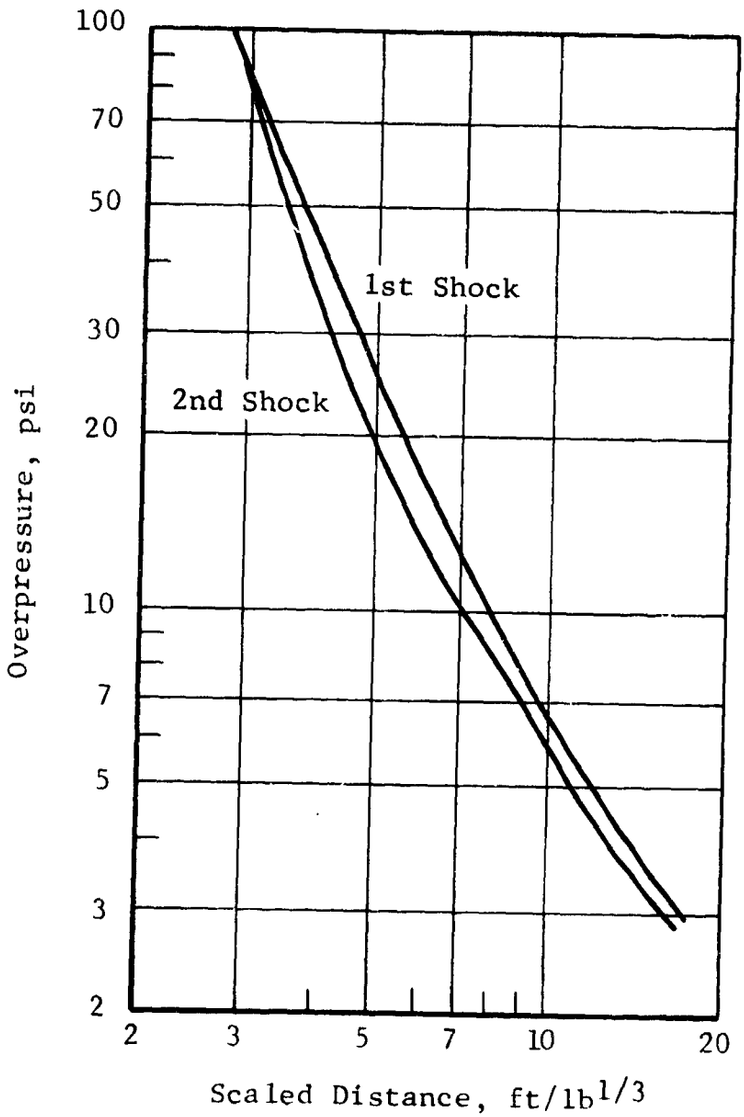

Figure 18 Pressures, Run No. 5,
Charge Weight Ratio 1:1,
Time Delay 1.61 ms/lb$^{1/3}$

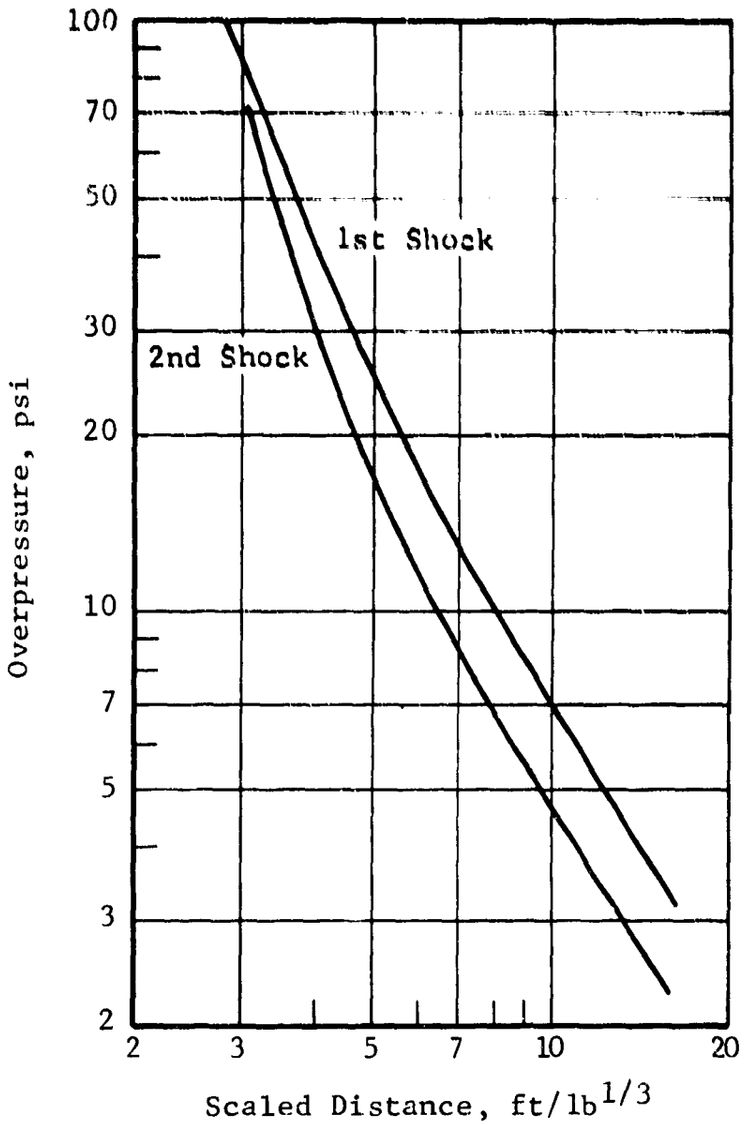

Figure 19 Pressures, Run No. 3, Charge Weight Ratio 1:1, Time Delay 2.13 ms/$lb^{1/3}$

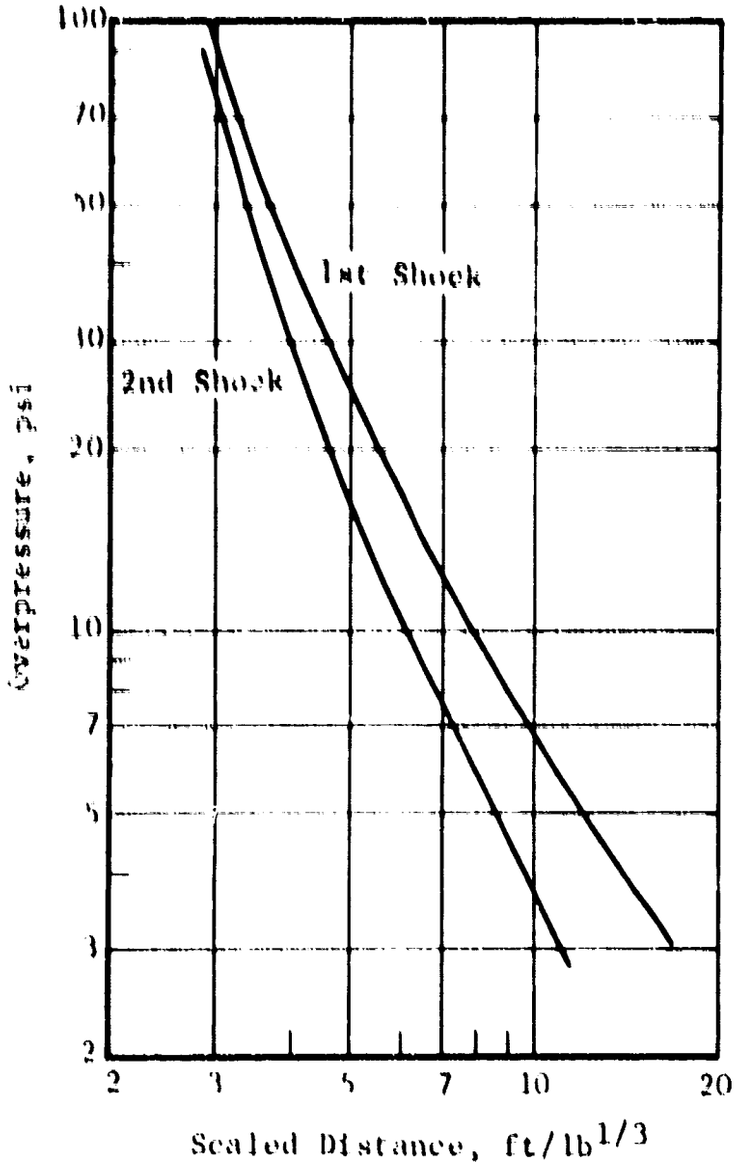

Figure 20 Pressures, Run No. 4, Charge Weight Ratio 1:1, Time Delay 4.18 ms/lb$^{1/3}$

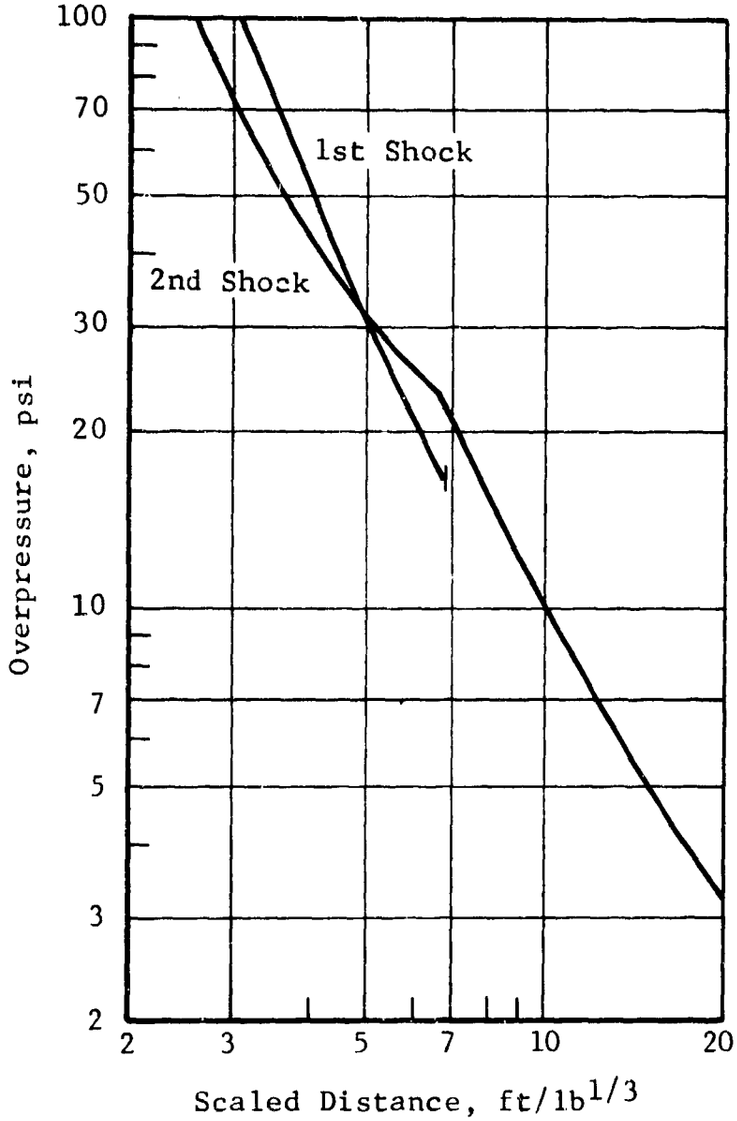

Figure 21 Pressures, Run No. 6, Charge Weight Ratio 2:1, Time Delay 0.59 ms/$lb^{1/3}$

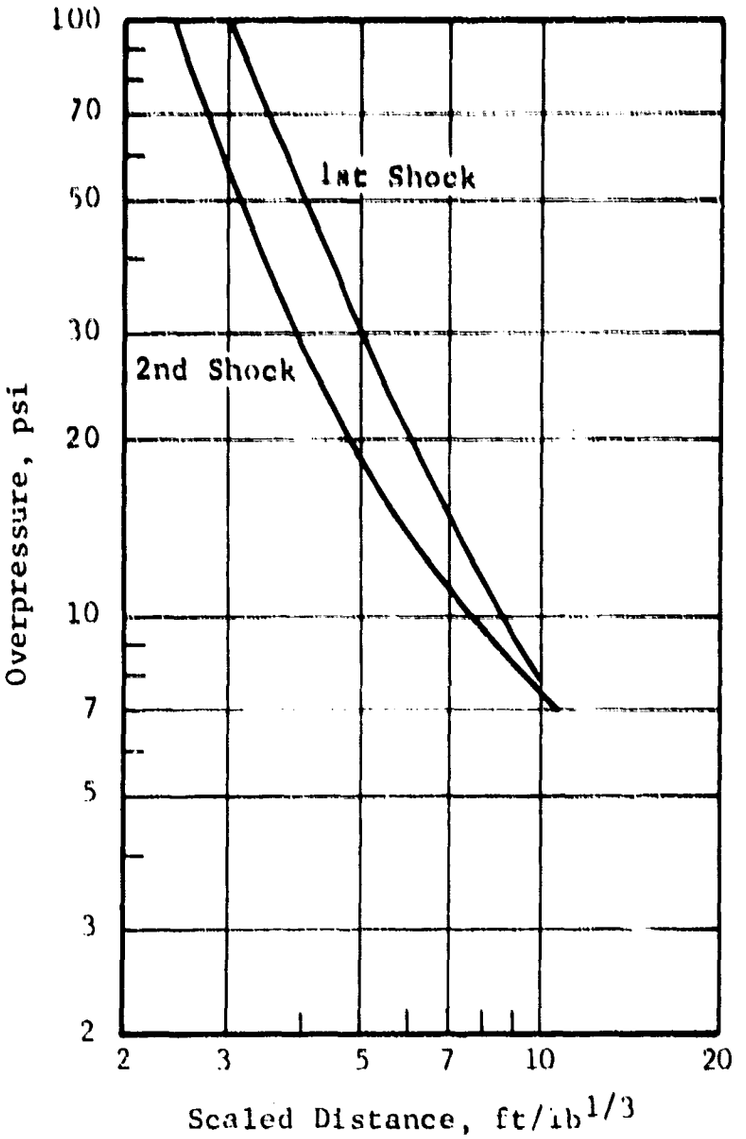

Figure 22 Pressures, Run No. 7, Charge Weight Ratio 2:1, Time Delay 1.10 ms/lb$^{1/3}$

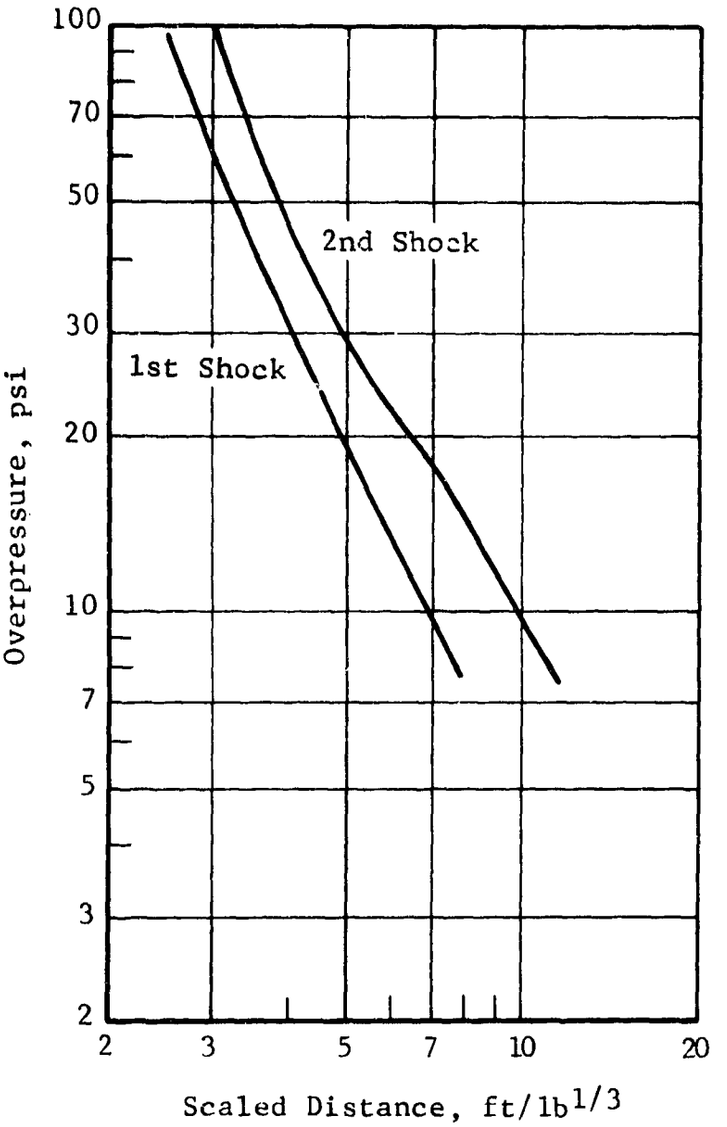

Figure 23 Pressures, Run No. 8, Charge Weight Ratio 1:2, Time Delay 1.10 ms/lb$^{1/3}$

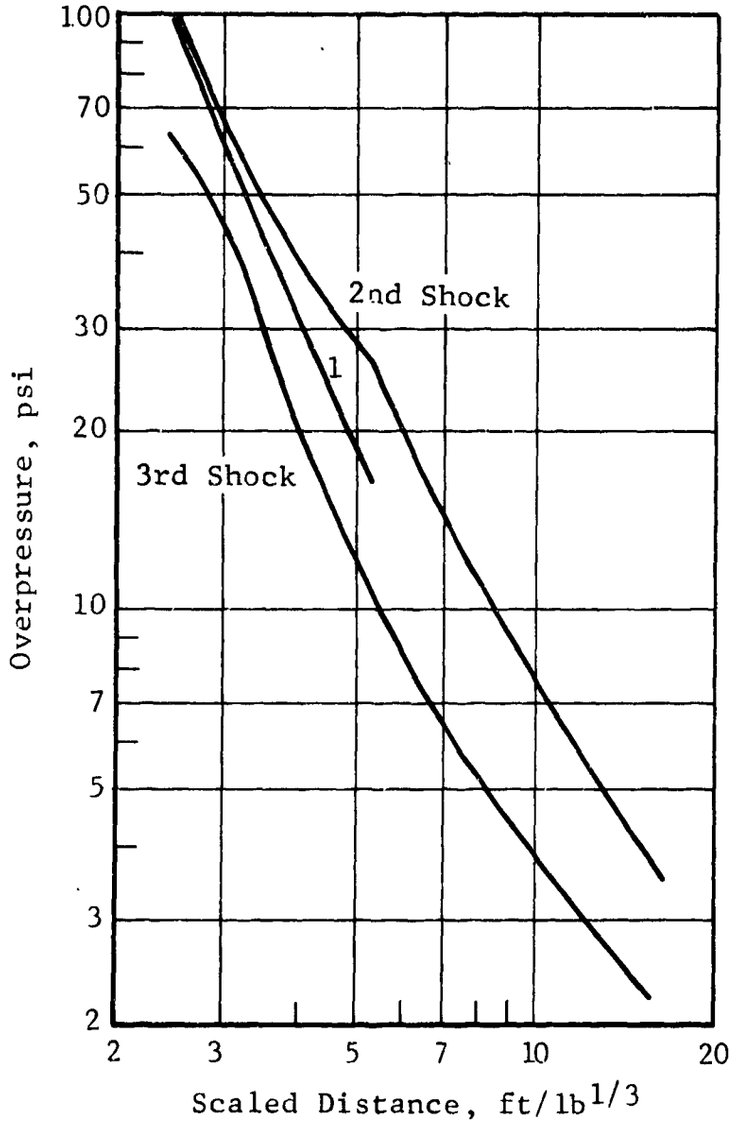

Figure 24 Pressures, Run No. 9, Charge Weight Ratio 1:1:1, Time Delay 0.59 ms/lb$^{1/3}$

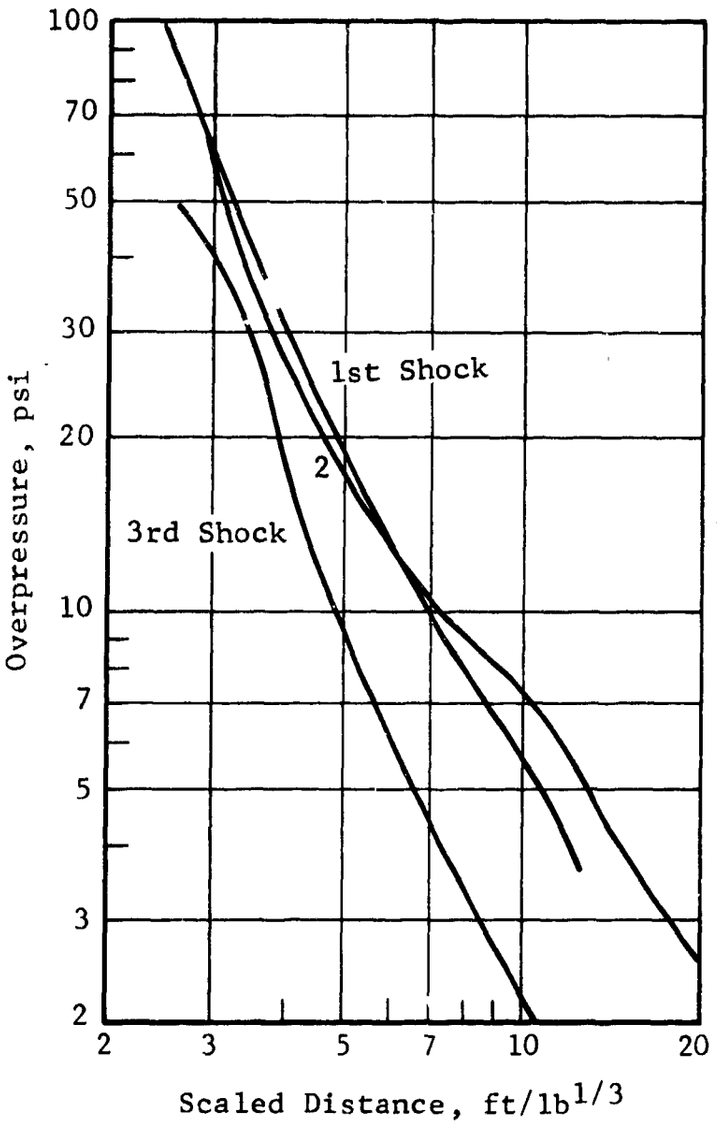

Figure 25 Pressures, Run No. 10, Charge Weight Ratio 1:1:1, Time Delay 1.10 ms/lb$^{1/3}$

5. SEQUENTIAL EXPLOSION EXPERIMENTS

A series of 20 small-charge experiments was designed in conjunction with the theoretical investigation to explore the effects of delay time between sequential explosions on the coalescence of successive blast pulses produced by the explosions. The experiments were designed to validate and extend the numerical predictions of the main effects of delay time and charge weight ratio at several distances from the explosion site. Other factors such as charge separation distance and firing sequence with respect to charge position were held fixed.

The relationships between explosion delay time and distance from the explosion site can be visualized in terms of a data map in the plane of these two independent variables. For short delay times the blast pulses from two successive explosions will coalesce to form a single pulse at sufficiently large distances from the explosion site. A curve of critical delay times (or equivalently, marginal coalescence) defines the boundary between conditions which produce coalescence and those which do not. Moreover, it is one curve of a family of contours of constant pulse separation. All contours of nonzero pulse separation will lie to one side of the curve of marginal coalescence. The goal of the analysis and experiments has been to establish this type of map. It is essential to obtain wide coverage in terms of such a data map, because useful values of pulse separation (that is, those sufficiently long so that the explosions can safely be considered nonsimultaneous) must eventually be selected on the basis of criteria involving the effects of blast on the structures of interest.

5.1 Test Arrangement

Experiments were conducted with two sequential explosions in which the ratio of the weights of successively fired charges was 1/2, 1, and 2. A few experiments were also conducted with three sequential explosions. The total charge weight in each experiment was 2 lb. Blast pressure measurements were made at six locations on each of two gage lines axial and transverse to the line of centers of the charges. All pressure gage signals were recorded on magnetic tape.

5.1.1 Explosive Charges

Hemispherical charges of plastic explosive C-4 (91% RDX + 9% plasticizer), were used for all experiments. The charges were formed by pressing a pre-weighed quantity of

explosive into specially fabricated molds. The pressing was done by remote control. The diameters of the 2/3-, 1-, and 4/3-lb charges were nominally 3-1/2, 4, and 4-1/2 in., respectively. The charges were initiated in programmed sequence by fast-functioning M-36 type electric detonators (National Northern Div., Atlantic Research Corp.) with 1/2-in. by 1/2-in. cylindrical tetryl pellets as boosters. The time delay between the first and second explosions was obtained by using electronic waveform and pulse generators (Tektronix Type 161 and 160, respectively) to trigger a thyratron-controlled 4-mfd, 330-v firing circuit to energize the second detonator at the preselected delay time. In the experiments with three explosions, the time delay between the second and third charges was obtained by using a length of 18 gr/ft detonating cord (DuPont Detacord) having a detonation speed of 23 ft/msec.

5.1.2 Test Fixture

In the test configuration the charges rested on a 1-in. thick steel base plate, and were separated by a steel dividing wall to prevent sympathetic detonation. The dividing wall was 6 in. high by 1 in. thick. The distance between centers of two charges was 10 in. A sketch of the test fixture is shown in Figure 26. The test fixture was built to accommodate three-charge experiments by adding a second dividing wall and replaceable insert plate.

5.2 Instrumentation

Pressure measurements were made at six stations on each of two blast gage lines. The gage lines were axial and transverse to the line of centers of the charges. The pressure transducers were installed flush with the ground surface in mechanically isolated steel mounting plates on the centerlines of two 75-ft long by 10-ft wide concrete slabs. A general view of the test area is shown in Figure 27. Figure 28 shows a typical gage installation in the 6-in. by 1/2-in. cover plate of the centerline conduit through which the transducer cables of each blast line were carried.

The actual time delays between sequential explosions were monitored by use of ionization probes placed at the charge centers. The time of initiation of each charge was recorded on magnetic tape.

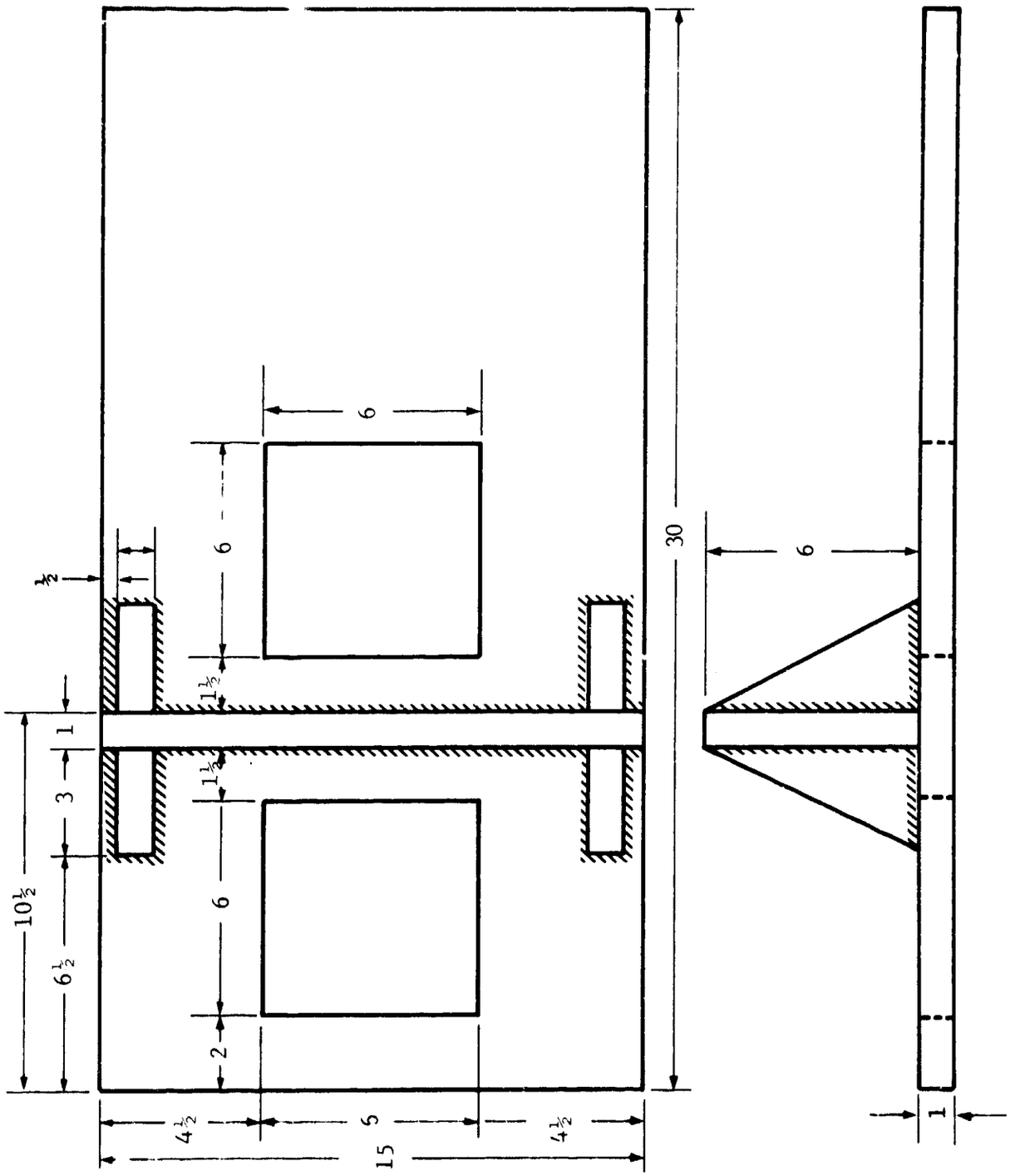

Figure 26 Test Fixture

Figure 27 Air Blast Gage Lines

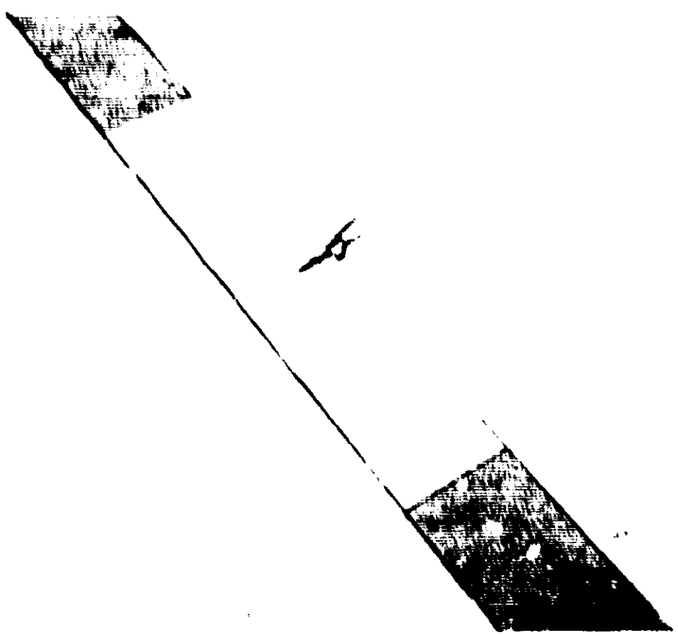

Figure 28 Photocon Gage Installation

5.2.1 Pressure Measuring Systems

Three types of pressure transducers were employed in the test program: the Model 603A and Model 601H manufactured by the Kistler Instrument Co. (KIC) and the Photocon Research Products Corp. (PRP) Type 752-40 psig.

The KIC transducers are of the piezoelectric type, employing crystalline quartz as a sensing element. Pressure applied to the diaphragm of the transducer is converted to a force acting on the quartz crystal sensing element, which in turn generates an electrical charge output proportional to the applied pressure. The transducer is a charge generator and the basic sensitivity of the unit is expressed in picocoulombs per psi. A charge amplifier is used in conjunction with the transducer to convert the generated charge to an equivalent voltage signal.

A pre-test evaluation of the charge amplifier (KIC Model 566) showed the band pass and noise of the unit to be functions of the ratio of the feedback capacitance to the input capacitance. A transfer function setting of 10 mv/pcb was selected in order to maintain a reasonable signal-to-noise ratio. This setting provides a frequency response to 15 kHz.

The Photocon Type 752-40 psig transducer has a dynamic range of 0 to 40 psig and frequency response of 0 to 10 kHz. The diaphragm of the transducer, in conjunction with an insulated stationary electrode, forms an electrical capacitor. The pressure to be measured is applied to the diaphragm causing a change in capacitance proportional to the applied pressure. The transducer capacitance and a built-in inductance form a tuned radio-frequency circuit. The tuned circuit is line-coupled by means of a low impedance cable to a Dynagage system consisting of an oscillator-detector circuit and a cathode-follower amplifier. The changes in capacitance produce changes in the diode detector impedance, and thereby produce a signal voltage proportional to the applied pressure.

5.2.2 Recording Instrument

Hewlett Packard (HP) Model 8875A differential amplifiers were used to condition the data signals for magnetic tape recording. These units were used to provide a voltage gain and impedance match between the pressure measuring system and magnetic tape recorder.

The data signals were recorded on an Ampex series CP-100 magnetic tape recorder. This unit is equipped with 13 fm recording tracks for data recording, and a single channel of direct recording for time base signals. The tape recorder conforms to specifications for the IRIG intermediate band.

5.2.3 Data Reproduction

Oscillograph reproductions were made from the magnetic tape recordings by employing the HP Model 8875A amplifiers to drive a Consolidated Electrodynamics Corp. (CEC) Recording Oscillograph Type 5-124. The oscillograph is equipped with CEC Type 7-363 galvanometers for recording the data signals on oscillograph paper.

Most of the data was recorded at a tape speed of 60 ips and reproduced at a tape speed of 3.75 ips, resulting in a frequency division of 16. The oscillograph paper speed was 128 ips. For these conditions, the oscillogram has a horizontal resolution of 488 μsec/in. and an effective frequency response from dc to 20 kHz, referred to real time.

5.2.4 Block Diagram

A block diagram of the record-reproduce instrumentation system is shown in Figure 29. In addition to the equipment described above, the monitoring and signal control equipment is shown.

The data channels were monitored and an electrical calibration signal was recorded on each data track immediately preceding each test run. The electrical calibration signal is a voltage simulation of a predetermined pressure level. This signal is used in data reduction and to verify the integrity of the record/reproduce system.

5.2.5 Calibration Procedures

The following paragraphs describe in general terms the techniques used to calibrate the pressure transducers used in the test program. The primary purpose of the calibration series is to establish the sensitivity factor K of the transducer. The KIC pressure transducers were calibrated statically and dynamically in the pre-test calibration series and statically in the post-test calibration series. The Photocon pressure measuring systems were calibrated statically in both the pre-test and post-test calibration series.

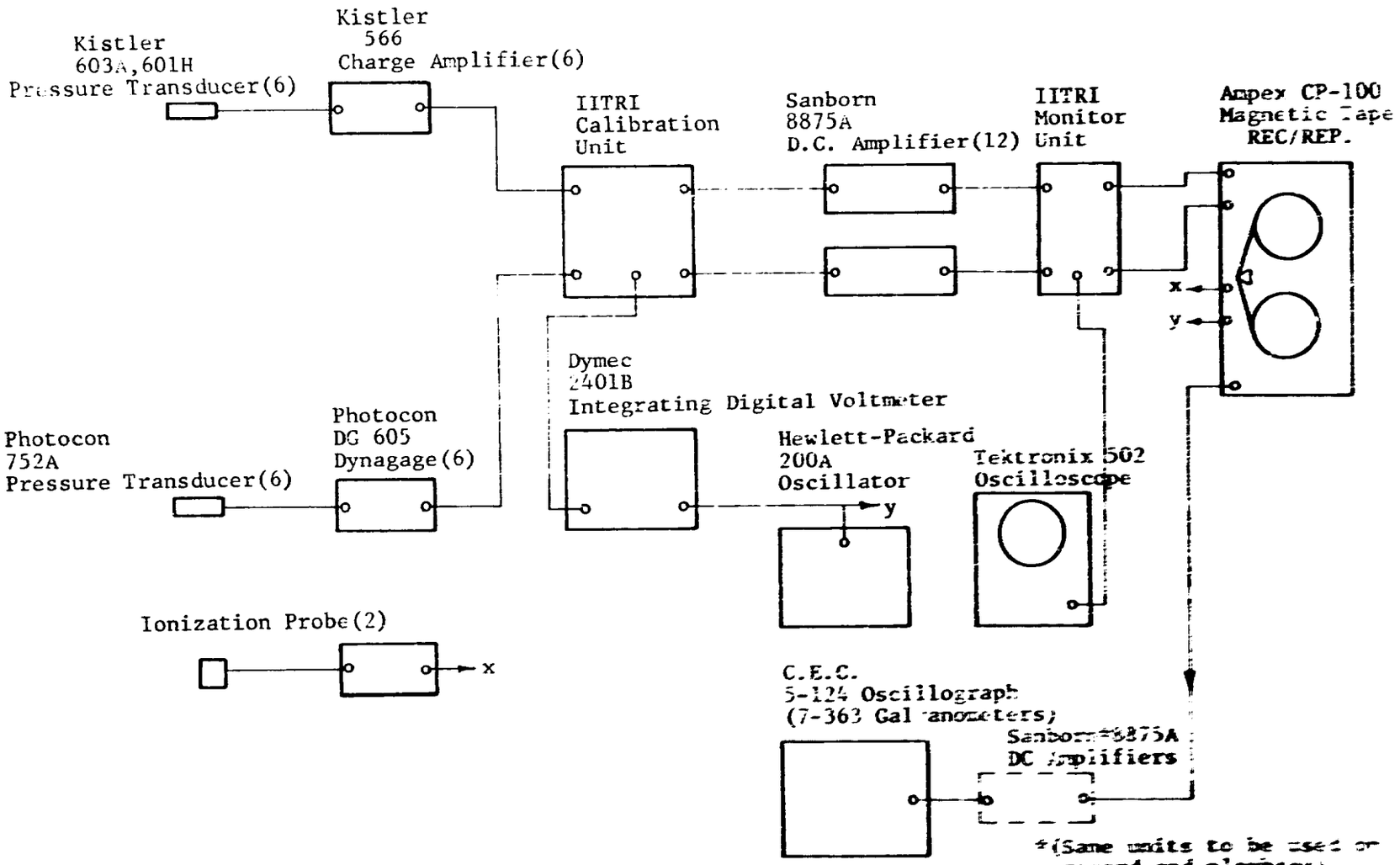

Figure 29 Block Diagram of Record-Reproduce Instrumentation

5.2.5.1 Static Calibration

Each KIC pressure transducer was placed in a Plexiglas mount. The transducer was held in place by applying a torque of about 8 in.-lb to the retaining piece. The Photocon transducers (752-40 psig) were removed from their water-cooled flame shields and placed in a mounting adapter, designed to provide flush mounting of the diaphragm. The mounted transducers in turn were placed in the expansion chamber of the calibration fixture.

The calibration fixture consists of an expansion chamber with a volume less than 2 in^3 and a compressed-air chamber with a volume of 380 in^3. The chambers are separated by an electrically operated solenoid valve. The pressure in the compression chamber was monitored by using a pressure transfer standard (Seegers 55 2455-A) for the KIC units and by a mercury manometer for the Photocon systems. When the solenoid valve is operated, the transducer is subjected to a pressure rise (the rise time is about 2 msec). The applied pressure causes a voltage to be generated at the output of the signal conditioning amplifier.

The KIC transducer sensitivity factor K is the output voltage of the charge amplifier V divided by the charge amplifier setting C and the applied pressure p.

$$K = \frac{V}{Cp} \text{ (pcb/psi)} \qquad (5.1)$$

Similarly, the sensitivity factor K for the Photocon Research systems is the output voltage from the dynagage V divided by the applied pressure p.

$$K = \frac{V}{p} \text{ (volts/psi)} \qquad (5.2)$$

The KIC transducers were calibrated at eight points in the range 0-150 psi and the Photocon systems were calibrated at 5 points in the range 0-10 psi. The quantity $\bar{K}$ for the range is the arithmetic mean of the values of K determined at all the points. The values of $\bar{K}$ for the pre-test and post-test calibration series are shown in Table 2.

Table 2

Pressure Transducer Calibrations

Kistler Model Number	Transducer S/N	Pre-Test Static Calibration $\overline{K}$ (pcb/psi)	Post-Test Static Calibration $\overline{K}$ (pcb/psi)	Dynamic Calibration $\overline{K}$ (pcb/psi)	Percent Deviation τ_{100}
601H	18697	1.144	1.124	1.147	4.0
601H	14300	1.025	1.035	1.038	12.6
601H	17764	1.082	1.076	1.042	5.5
603A	2569	0.346	0.351	0.352	4.0
603A	2666	0.319	0.321	0.312	7.0
603A	2668	0.332	0.331	0.336	4.8
603A	2573	0.349	0.341	0.347	1.7
603A	2670	0.335	0.343	0.345	5.2
603A	2655	0.335	0.329	0.319	4.4

Photocon Model Number	System Number	Transducer S/N	Pre-Test Static Calibration $\overline{K}$ (volts/psi)	Post-Test Static Calibration $\overline{K}$ (volts/psi)
752-3196-40	A1-1	4044	0.332	0.332
752-3196-40	A2-2	4046	0.332	0.335
752-3196-40	A3-3	4142	0.379	0.357
752-3196-40	A4-4	4099	0.358	0.333
752-3196-40	A5-5	4104	0.355	0.367
752-3196-40	A6-6	4110	0.303	0.314
752-3196-40	A4-7	4150	0.277	0.283
752-3196-40	A4-8	4083	0.269	0.276

5.2.5.2 Dynamic Calibration

The KIC pressure transducers were dynamically calibrated in a 2-in. shock tube. The transducers, installed in the mountings previously described, were flush-mounted in the walls of the shock tube in three radial configurations. The transducers were subjected to flat-topped shock pulses of six different amplitudes in the range 14.6 psi to 162.5 psi.

The distance between each transducer was accurately measured; therefore the average shock velocity could be determined. Five velocity readings were averaged. The shock pressure was computed from the measured shock velocity using the Rankine-Hugoniot relations.

The sensitivity factor K for each pressure level and the average sensitivity factor $\bar{K}$ for the range were determined in the manner previously described.

The rms deviation for $\bar{K}$ was determined by the relationship:

$$r = \left[\frac{1}{N} \sum_{i=1}^{N} (\bar{K} - K_i)^2 \right]^{1/2} \qquad (5.3)$$

The percent deviation was determined by the relationship:

$$r_{100} = \frac{2r}{\bar{K}} \times 100 \ (\%) \qquad (5.4)$$

Using a factor of 2 in the numerator of (5.4) gives a confidence level of 95.5 percent. The results of dynamic calibration are also presented in Table 2.

5.3 Experimental Results

The experiments were planned so as to give adequate coverage or density of data in the most interesting ranges of explosion delay time and scaled distance. For two-explosion experiments, we used equal 1-lb charges, and 2/3- and 4/3-lb charges (to give charge weight ratios of 1/2 and 2). For three-explosion experiments, we used

equal 2/3-lb charges. A total of 20 tests of this kind were carried out. In addition, a reference shot utilizing a single 2-lb sphere of C-4 was fired.

The positioning of gages by type was the same on both blast lines. Table 3 summarizes the nominal pressure levels and distances at which gages were located in each blast line. These distances were selected on the basis of the nominal peak pressures shown in the table for a ground surface explosion of 2 lb of TNT[12]. The explosive C-4 is about 25 percent more energetic per unit weight than TNT, since its heat of detonation is 1.37 kcal/g compared with 1.10 kcal/g for TNT[13]. The scaled distances shown in the table referenced to TNT, are based on 2 lb total charge of C-4 in each experiment, which is equivalent to 2.50 lb of TNT. The actual peak pressures observed at the gage stations in the reference test with a 2-lb sphere of C-4 were correspondingly somewhat higher than the nominal peak pressures on the basis of which the gage positions were originally selected (Figure 30).

Table 3

Pressure Gage Positions

Nominal Pressure* (psi)	Distance (ft)	Gage Type	Scaled Distance** ($ft/lb_{TNT}^{1/3}$)
20	8.8	KIC 603A	6.5
10	12.2	KIC 603A	9.0
5	18.4	KIC 601H	13.6
2.5	28.4	PRP 752A	20.9
1.2	50.4	PRP 752A	37.1
1	57.0	PRP 752A	42.0

*From 2 lb of TNT at distances shown.

**Based on TNT equivalent of 2 lb total charge of C-4 in each experiment.

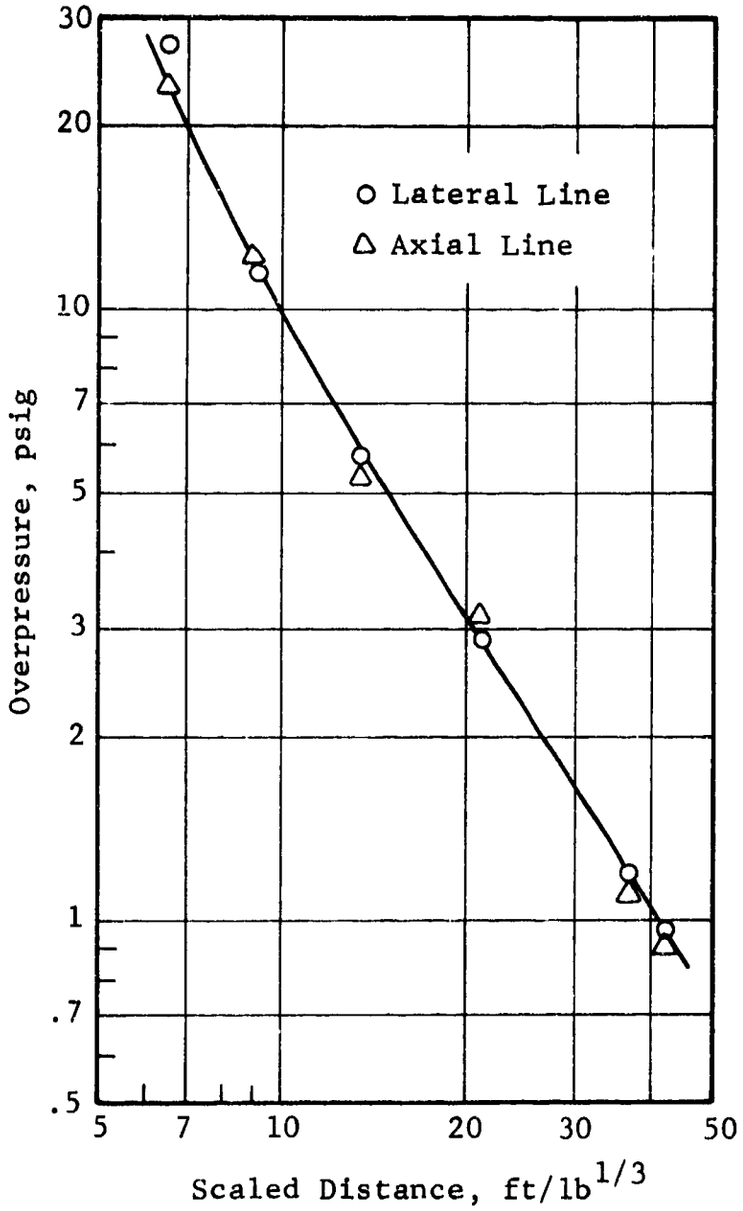

Figure 30 Pressure - Distance Curve for C-4

Sequential explosion experiments were conducted at time delays ranging from 0.8 to 5.7 msec at intervals of 0.7 msec. The actual delay, observed in each experiment on the ionization probes, was always within 0.1 msec of the programmed delay. The nominal delays at which the shots were fired are given in Table 4.

A typical set of pressure-time records from successive gages in the line transverse to the line of centers of the charges is shown in Figure 31. These records are taken from Test 16. Coalescence of the waves from the two explosions is clearly evident.

Time separations and peak pressures from all the experiments are plotted in the figures on succeeding pages. Time and distances are scaled by the TNT equivalent of the total amount of explosive present. Therefore the results are applicable to any explosive weight in the types of situations tested. In the following paragraphs we give general conclusions and inferences drawn from the experimental results.

5.3.1 Equal-Charge Experiments

Eight experiments were conducted with two 1-lb charges of C-4 in each test. A photograph of the experimental setup with two charges is shown in Figure 32. On each figure showing peak pressure data points plotted against scaled distance, the reference curve of Figure 30 for the total quantity of explosive involved is superimposed for comparison. The reference curve corresponding to half the total quantity is also shown, terminated at the experimentally determined point of coalescence.

The following principal features were observed from the records:

- The firing sequence of the charges, together with the presence of the dividing wall, has a relatively strong effect on coalescence on the line of gages axial to the line of centers of the charges. In all tests we fired the charge farther away from the axial line first. This enhances coalescence on the axial line relative to that on the transverse line. Overlaying the two sets of time separation curves shows that the effect of firing sequence is roughly equivalent to reducing the time delay by about 1.8 msec, or about 1.3 msec/$lb^{1/3}$ based on the TNT equivalent of the total charge present.

Table 4

Programmed Delays by Shot Number

Nominal Delay (msec)	Charge Weight Ratio			
	1:1	2:1	1:2	1:1:1
0.8	12	17		
1.5	11	16	24	28
2.2	10	18	22	29
2.9	13		23	
3.6	9	19		30
4.3	14		25	31
5.0	15			
5.7	20			

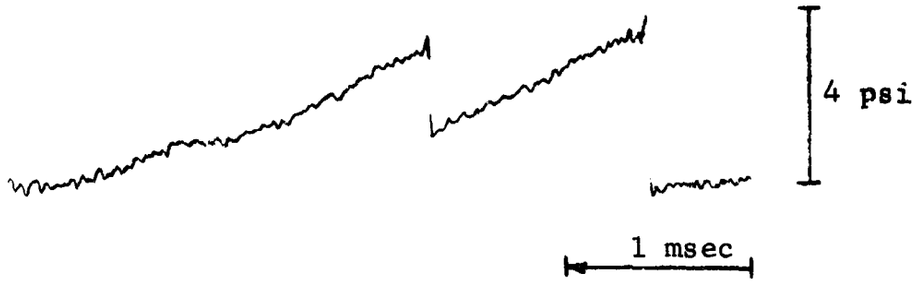

Scaled Distance 13.5 ft/lb$^{1/3}$

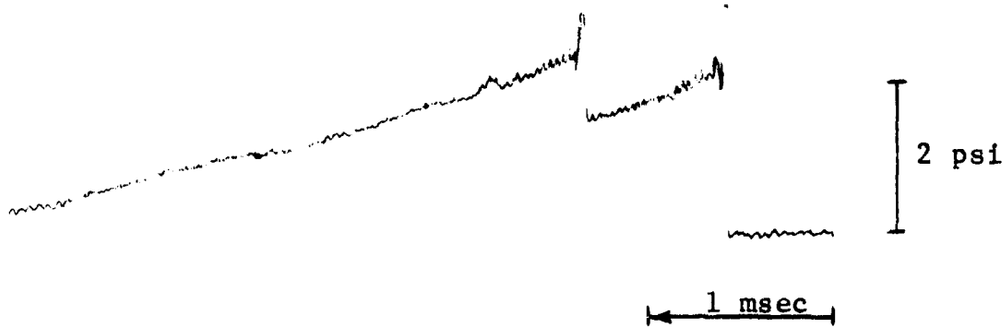

Scaled Distance 20.9 ft/lb$^{1/3}$

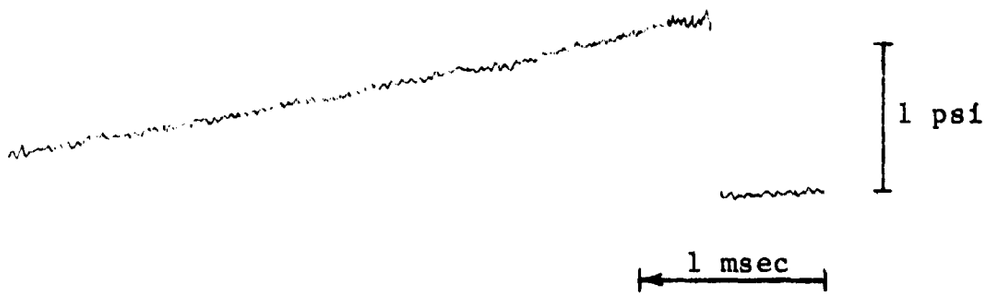

Scaled Distance 37.1 ft/lb$^{1/3}$

Figure 31 Pressure Records, Lateral Line, Shot No. 16, Charge Weight Ratio 2:1, Time Delay 1.16 ms/lb$^{1/3}$

Figure 10 Two Charge Experimental Setup

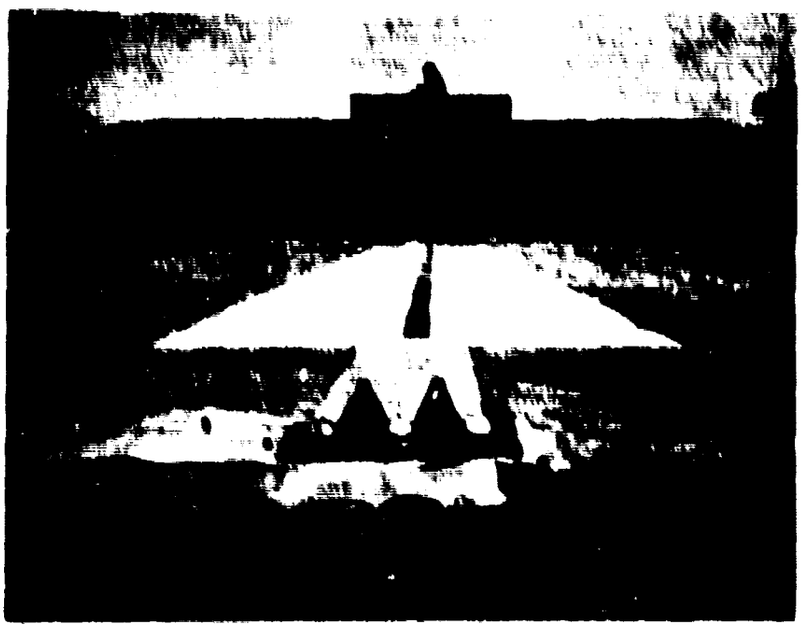

Figure 11 Three-Charge Experimental Setup

- A further effect of the firing sequence and the dividing wall is that the pressure of the leading shock in the uncoalesced wave on the axial line lies considerably below the reference curve for half the quantity of explosive involved. Similarly, the coalesced wave at the close-in stations lies somewhat below the reference curve for the total quantity; the peak pressure in the coalesced wave on the axial line tends to recover, however, and indeed decays somewhat more slowly than the reference curve for the total quantity at more distant stations.

- The trailing blast pulse in the uncoalesced wave is quite peaked at close-in stations, the pressure being comparable to the reference curve for the total explosive quantity well before coalescence occurs. This effect is illustrated in the data shown for the lateral gage line in Figure 41.

- For long delay times when coalescence does not occur, the pressure of the trailing shock may fall below even the reference curve for half the total quantity. The reason for this is that for a sufficiently long time delay the trailing pulse travels in the negative pressure region of the tail of the leading wave, and in fact the pulse separation tends to increase as the double wave propagates.

- In all cases when coalescence occurs the resultant shock pressure is essentially that from a single explosion of the total quantity of explosive involved.

- In the lateral direction, there is substantially no tendency for the shocks to coalesce for time delays larger than 4.3 msec, or 3.2 msec/$lb^{1/3}$ based on the TNT equivalent of the total charge in the event. The tendency to coalesce was observed on the axial line in all experiments. However, since the effect of firing sequence on the axial line is equivalent to reducing the scaled time delay by 1.3 msec/$lb^{1/3}$, it can be inferred that there will be no tendency for the shocks to coalesce in the axial direction if the scaled time delay exceeds 4.5 ft/$lb^{1/3}$.

5.3.2 Unequal-Charge Experiments

Eight experiments were conducted with two unequal charges totaling 2 lb of C-4 charge weight. In four of these, the 4/3-lb charge was fired first, and in the other four the 2/3-lb charge was fired first. In each case the charge fired first was in the location farther from the axial line of blast gages. The reference curve for the total explosive quantity is given in all figures showing pressure data, and the reference curve corresponding to the weight of the first charge is shown up to the point of coalescence.

The general conclusions reached regarding the results of the equal-charge experiments also apply to the unequal-charge experiments. In addition, we find that

- Coalescence occurs more readily when the successive charges are in the ratio of 1:2, and less readily for the ratio 2:1, than with equal charges.

- There is no tendency for the shocks to coalesce on the lateral blast line when the scaled time delay is greater than about 2.6 msec/lb$^{1/3}$ for charge weights in the ratio 2:1, and greater than about 3.7 msec/lb$^{1/3}$ for charge weights in the ratio 1:2. As in the case of equal charges, the enhancement of coalescence in the axial direction relative to the lateral direction is equivalent to a reduction of the time delay by about 1.3 msec/lb$^{1/3}$.

5.3.3 Three-Charge Experiments

Four experiments were conducted with three equal 2/3-lb C-4 charges, the time delays between successive charges being equal. A photograph of the experimental setup with three charges is shown in Figure 33. The charge farthest from the axial blast gage line was fired first, the middle charge second, and the nearest charge last.

The reference curve for the total explosive quantity is given in all figures showing pressure data, together with the reference curves for 1/3 and 2/3 of the total quantity where applicable up to coalescence. In general, we found from this brief series that

- The third pulse tends to overtake the second before the second overtakes the first.

- After coalescence of all three pulses occurs, the pressures are essentially the same as those from a single charge of the total quantity of explosive in the event.

5.4 Comparisons

A large-scale test was conducted in April 1968 at the Naval Weapons Center[3] with two 5000-lb charges detonated with a nominal delay of 20 msec between explosions. An analysis of the published data shows that the two shocks coalesced at approximately 230 ft from the site of the explosions. The scaled time delay in this test is $20/(10{,}000)^{1/3} = 0.93$ msec/lb$^{1/3}$ based on the total TNT charge weight in the event, and the scaled coalescence distance is $230/(10{,}000)^{1/3} = 11$ ft/lb$^{1/3}$. We found in our experiments with two equal charges that for time delays of 0.6 and 1.1 msec/lb$^{1/3}$ the respective coalescence distances are 7.3 and 13.0 ft/lb$^{1/3}$ along the (lateral) gage line analogous to that in the NWC test (Line A) on which the coalescence data were reported[3]. Thus for a scaled time delay of 0.93 msec/lb$^{1/3}$ our test results predict a coalescence point at about 11 ft/lb$^{1/3}$, in full agreement with the NWC test result. Moreover, our pressure data are in good overall agreement with the findings of the NWC test.

In a series of small-scale tests with two 1/4-lb charges, Kaplan[2] reported the result of an experiment in which the time delay was 2.73 msec, or 3.2 msec/lb$^{1/3}$ if we assume that the total charge weight in his experiment was 1/2 lb of C-4 or a similar energetic explosive. A pressure record from this test shows two pulses separated by a time interval apparently about equal to the explosion time delay. One of our equal-charge experiments was fired at approximately the same scaled time delay. At this time delay we found no appreciable tendency for the shocks to coalesce; this agrees qualitatively with the reported result. Other tests[2] with two 1/4-lb charges involved time delays well below 1 msec/lb$^{1/3}$; single pulses were observed at gage stations from 16 to 37 ft/lb$^{1/3}$. In our tests with short time delays we found coalesced waves at all but the closest gage stations, in agreement with the reported observations.

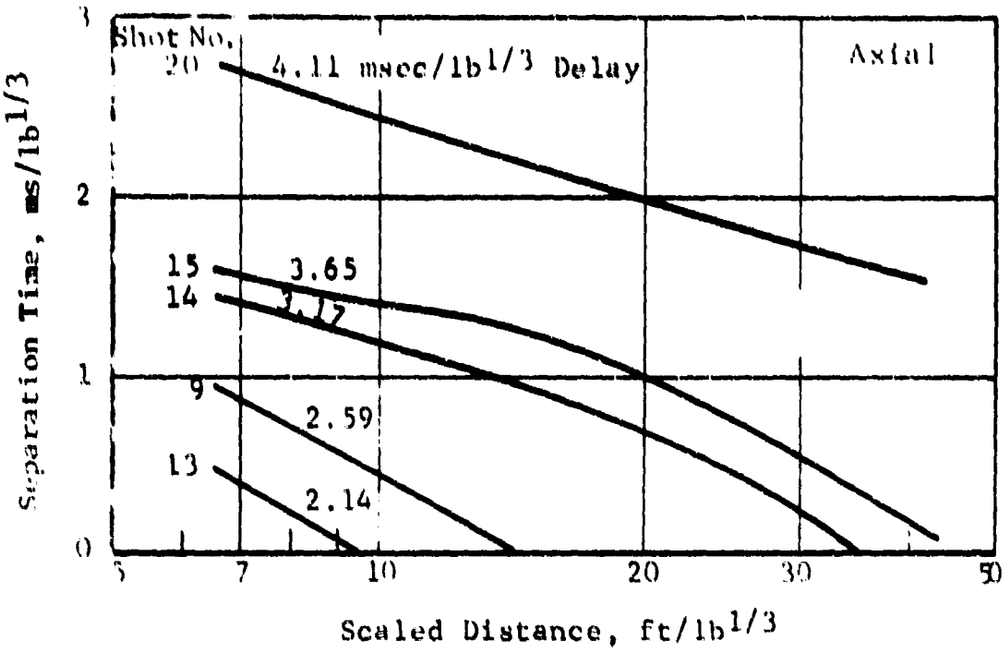

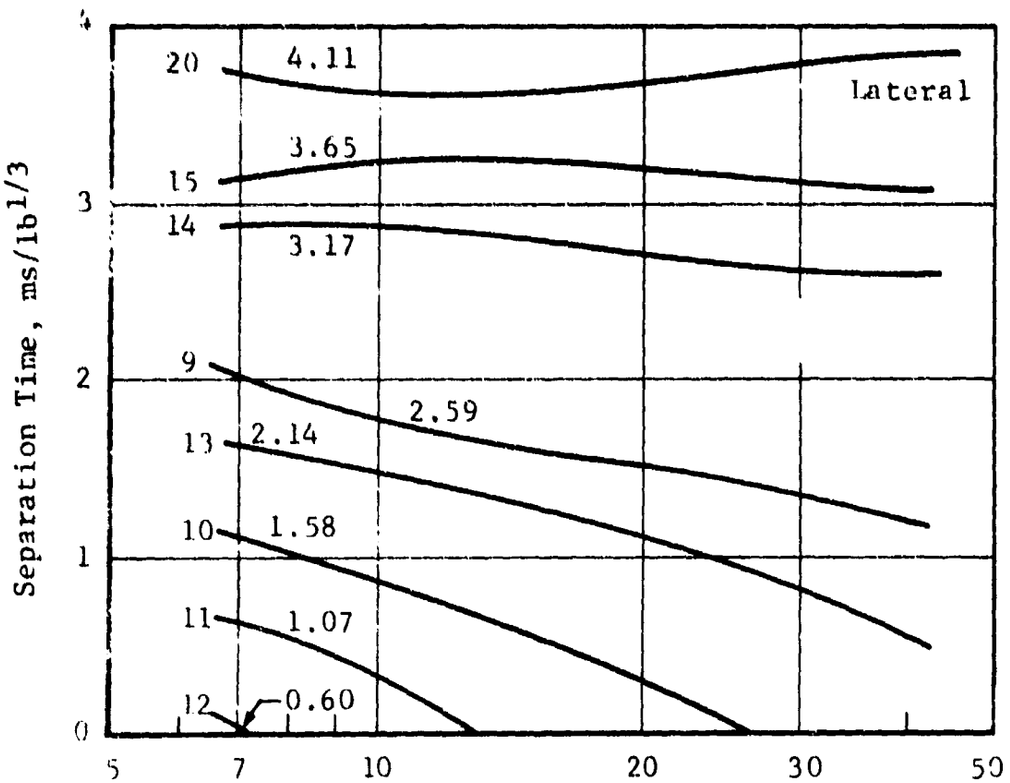

Figure 34 Pulse Separation Times, Charge Weight Ratio 1:1

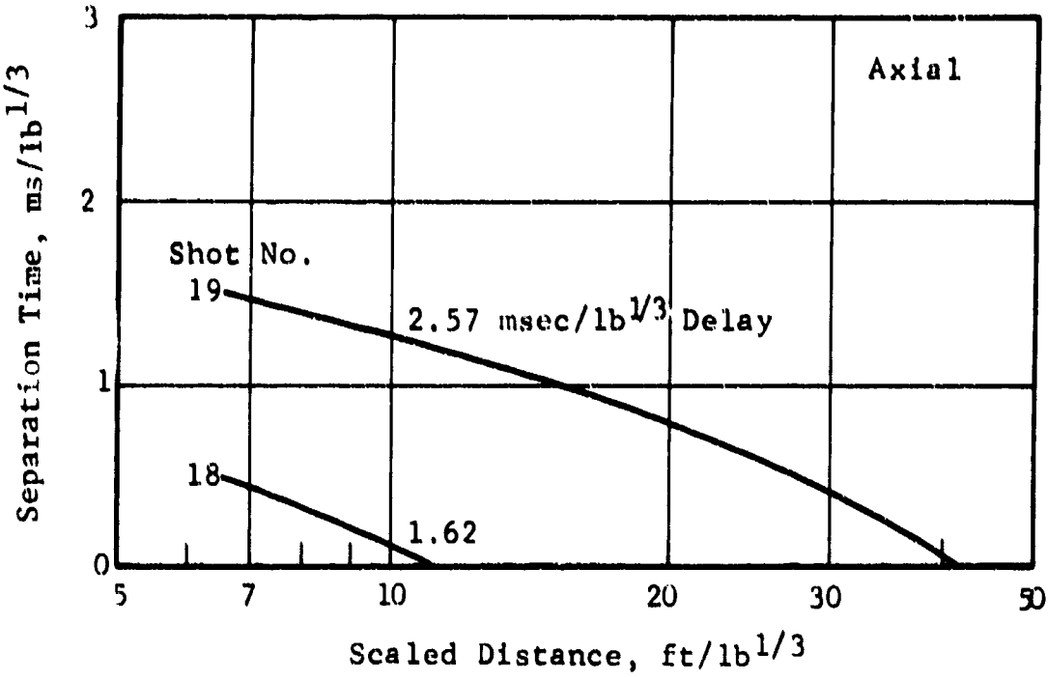

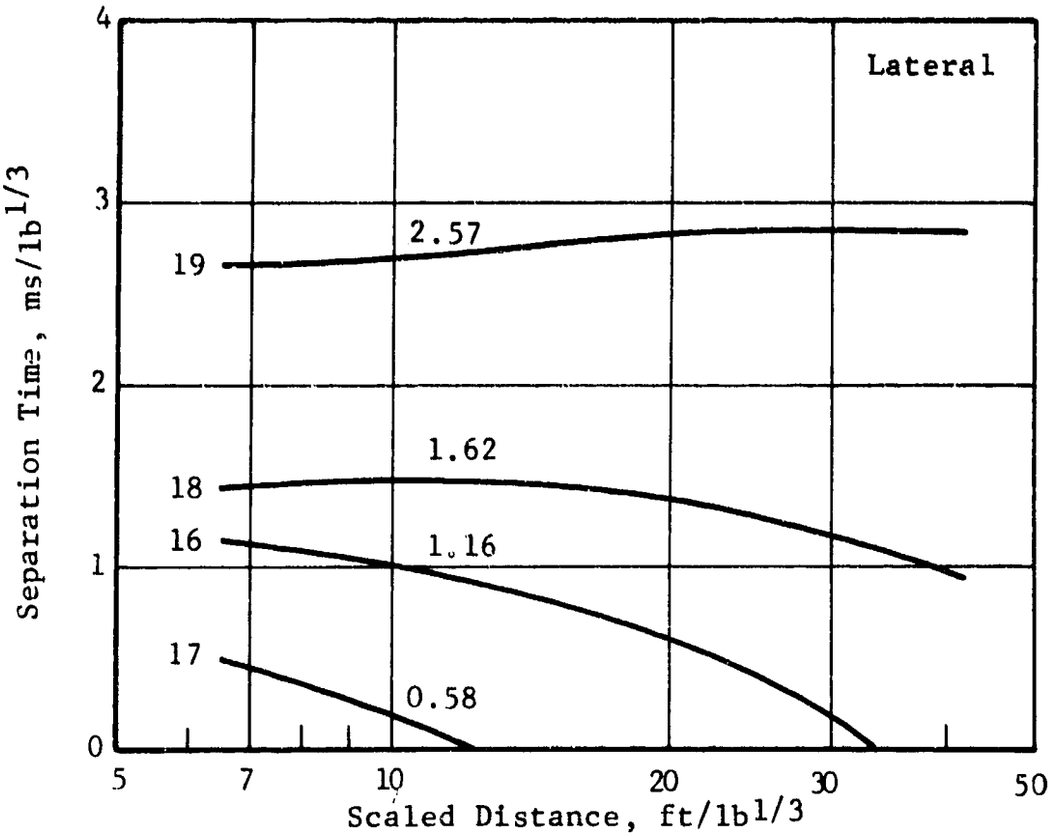

Figure 35 Pulse Separation Times, Charge Weight Ratio 2:1

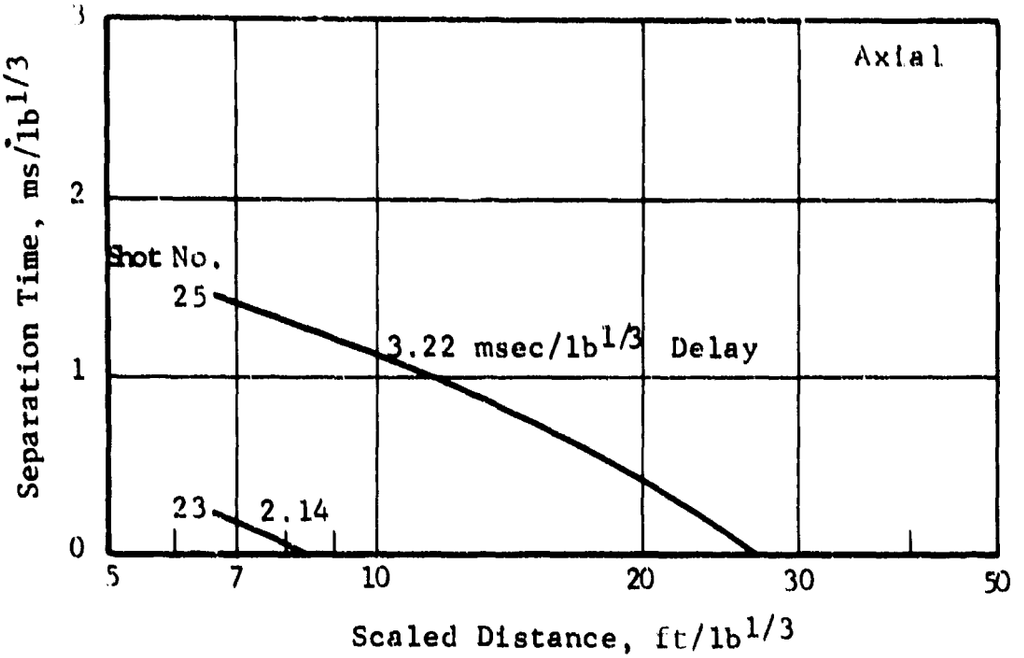

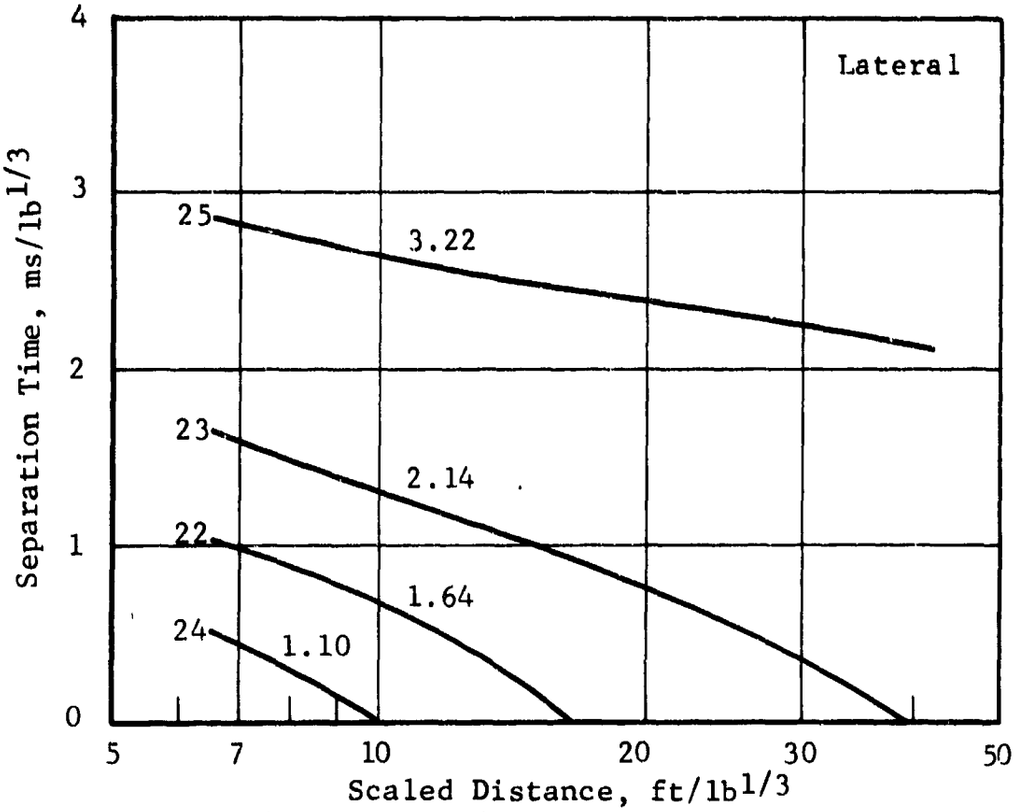

Figure 36 Pulse Separation Times, Charge Weight Ratio 1:2

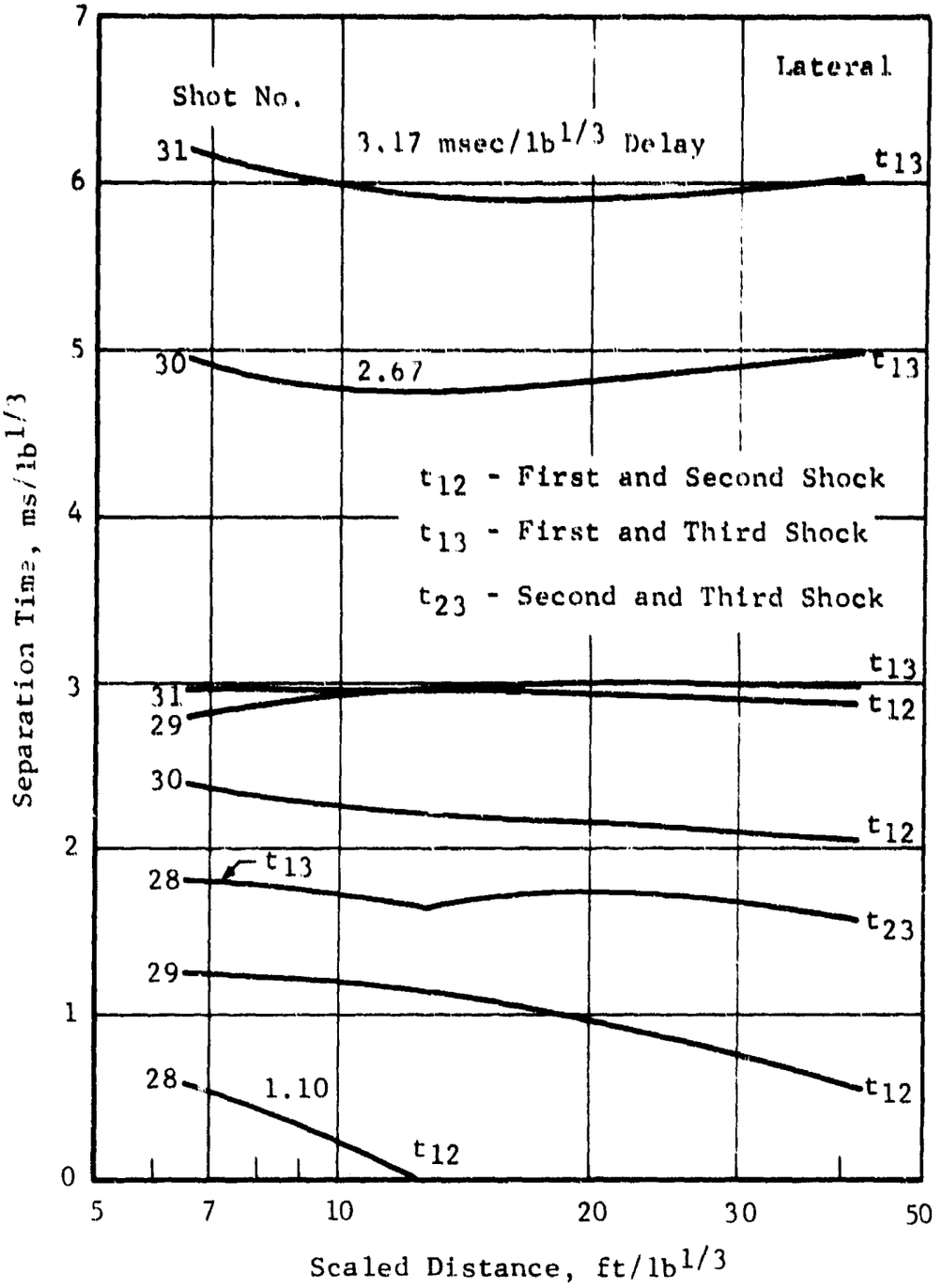

Figure 37 Pulse Separation Times,
Charge Weight Ratio 1:1:1

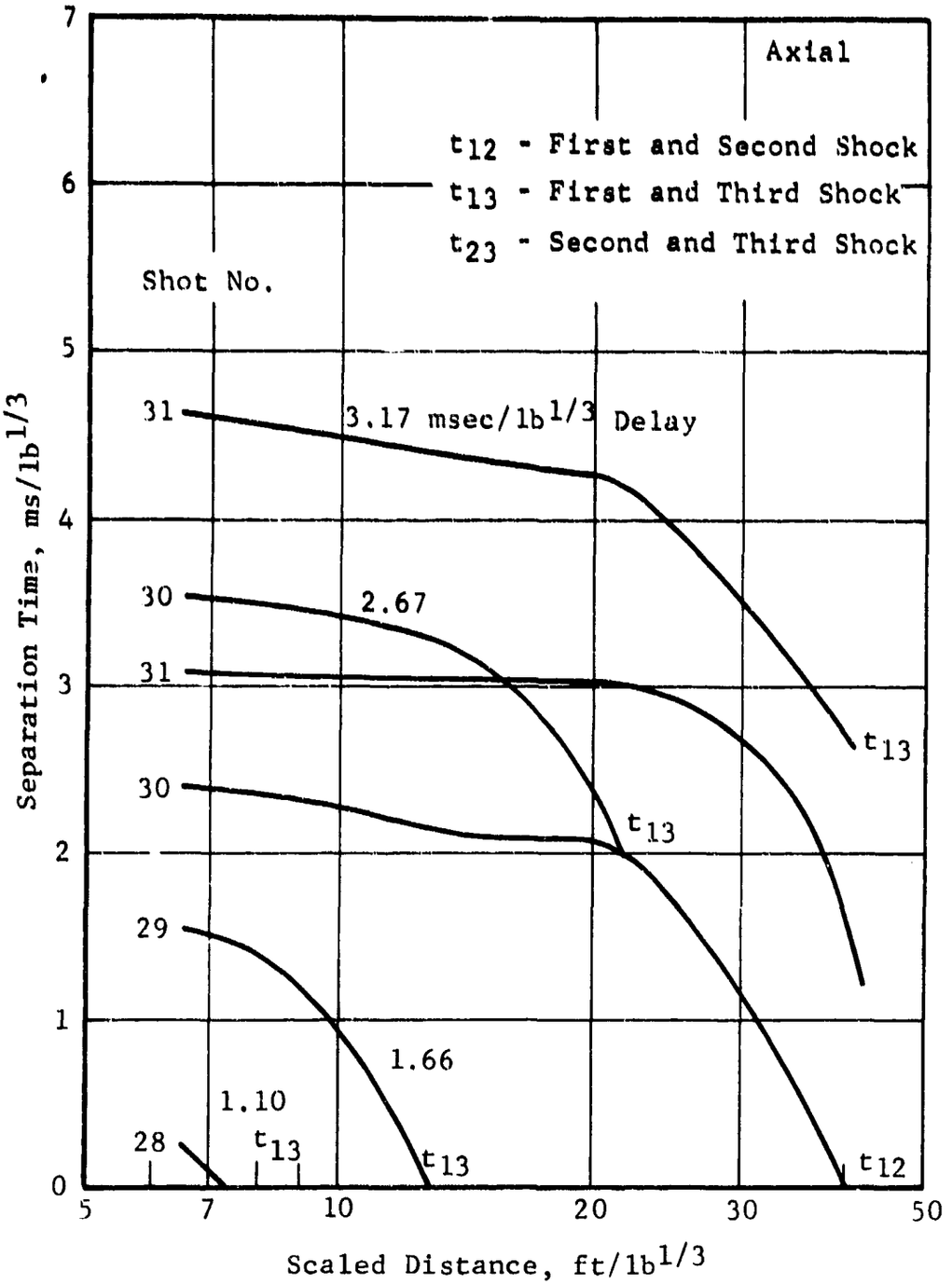

Figure 38 Pulse Separation Times, Charge Weight Ratio 1:1:1

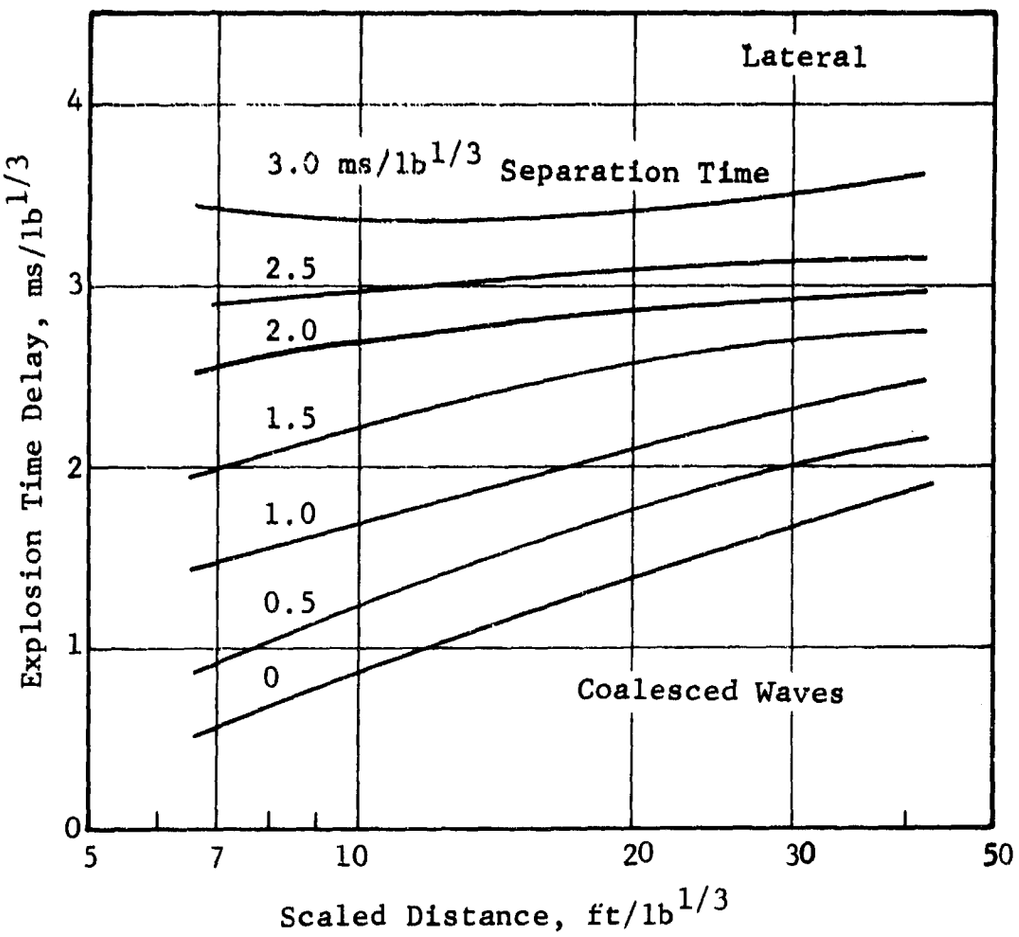

Figure 39 Coalescence Map, Charge Weight Ratio 1:1

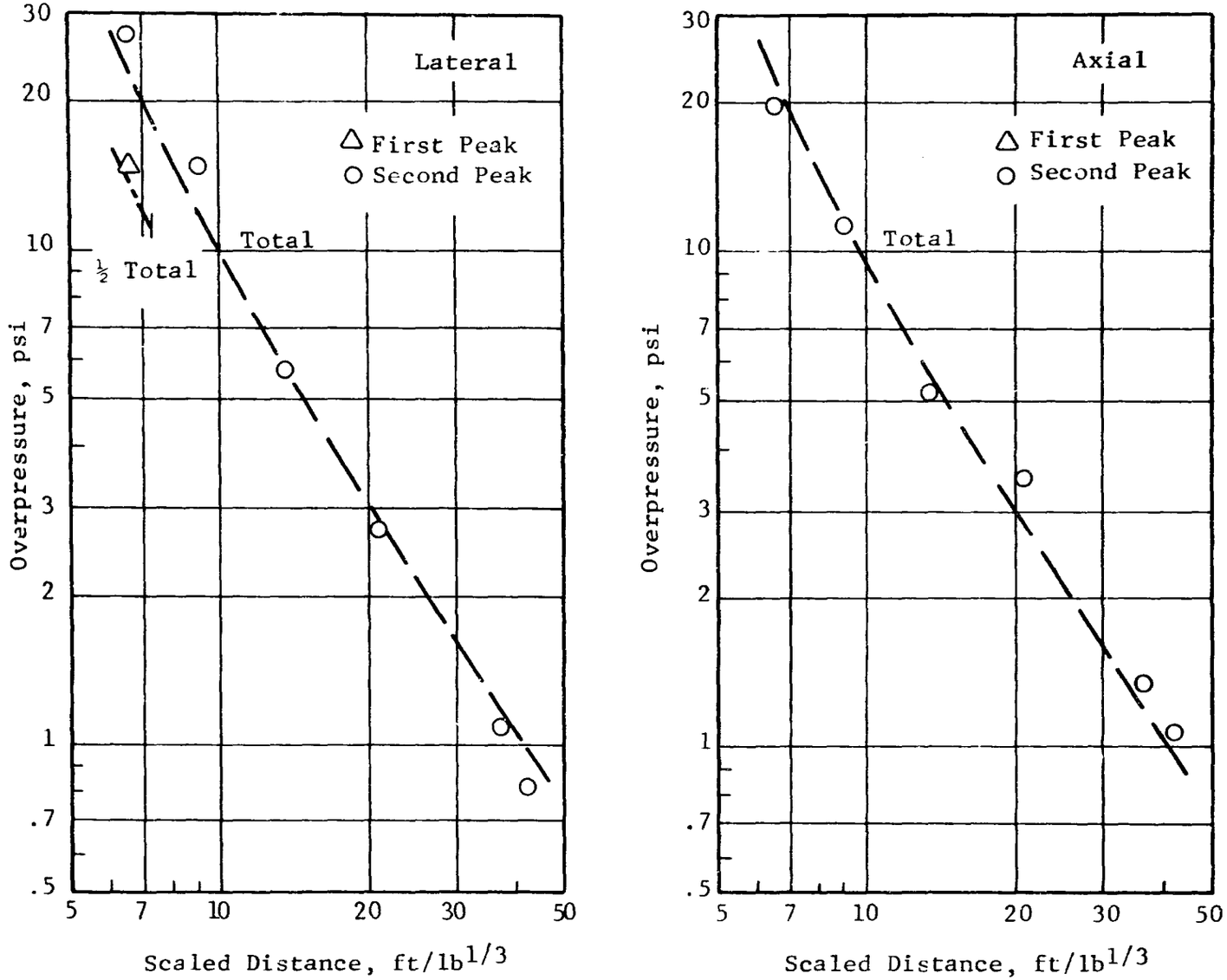

Figure 40 Pressures, Shot No. 12, Charge Weight Ratio 1:1, Time Delay 0.60 ms/lb$^{1/3}$

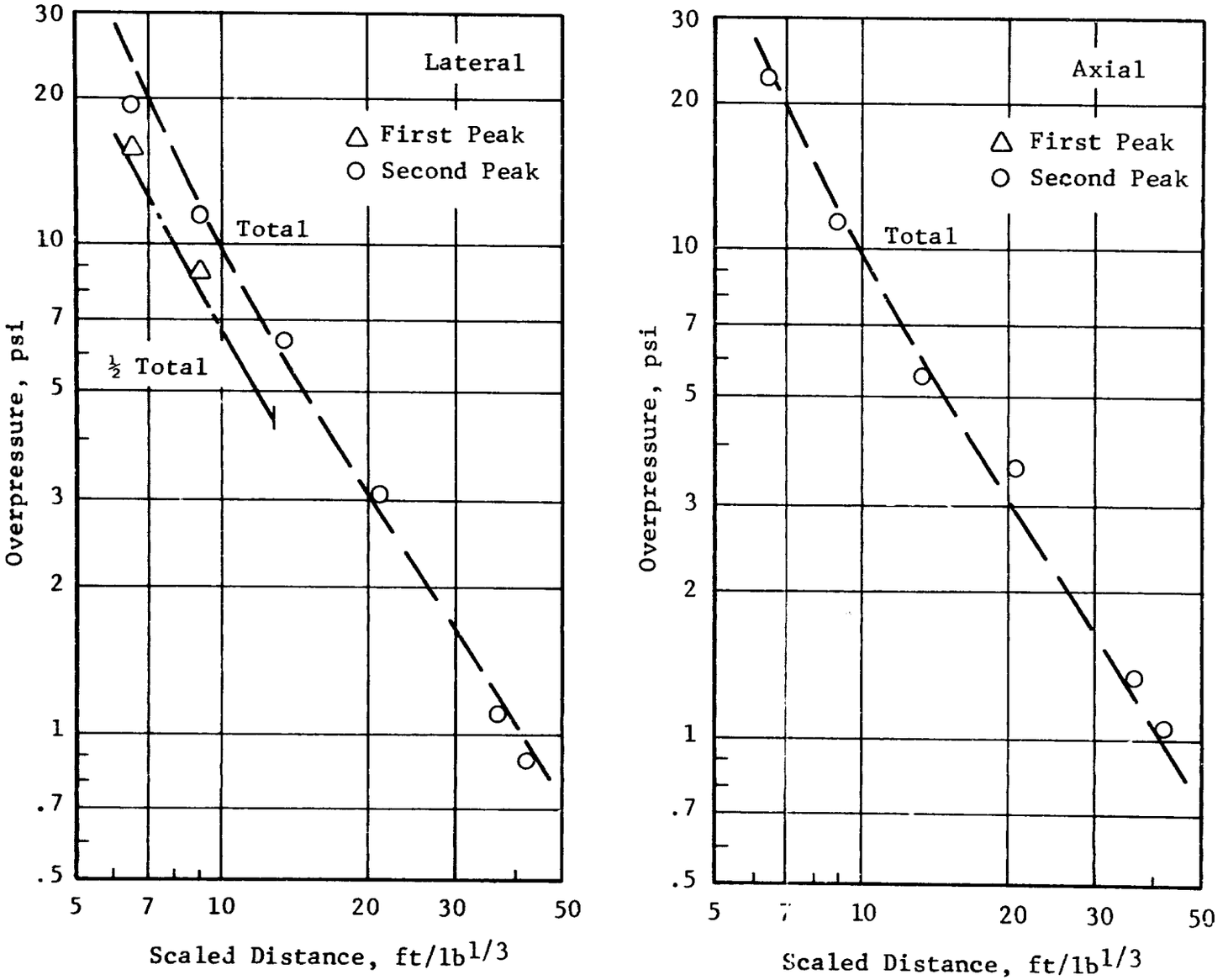

Figure 41 Pressures, Shot No. 11, Charge Weight Ratio 1:1, Time Delay 1.07 ms/$lb^{1/3}$

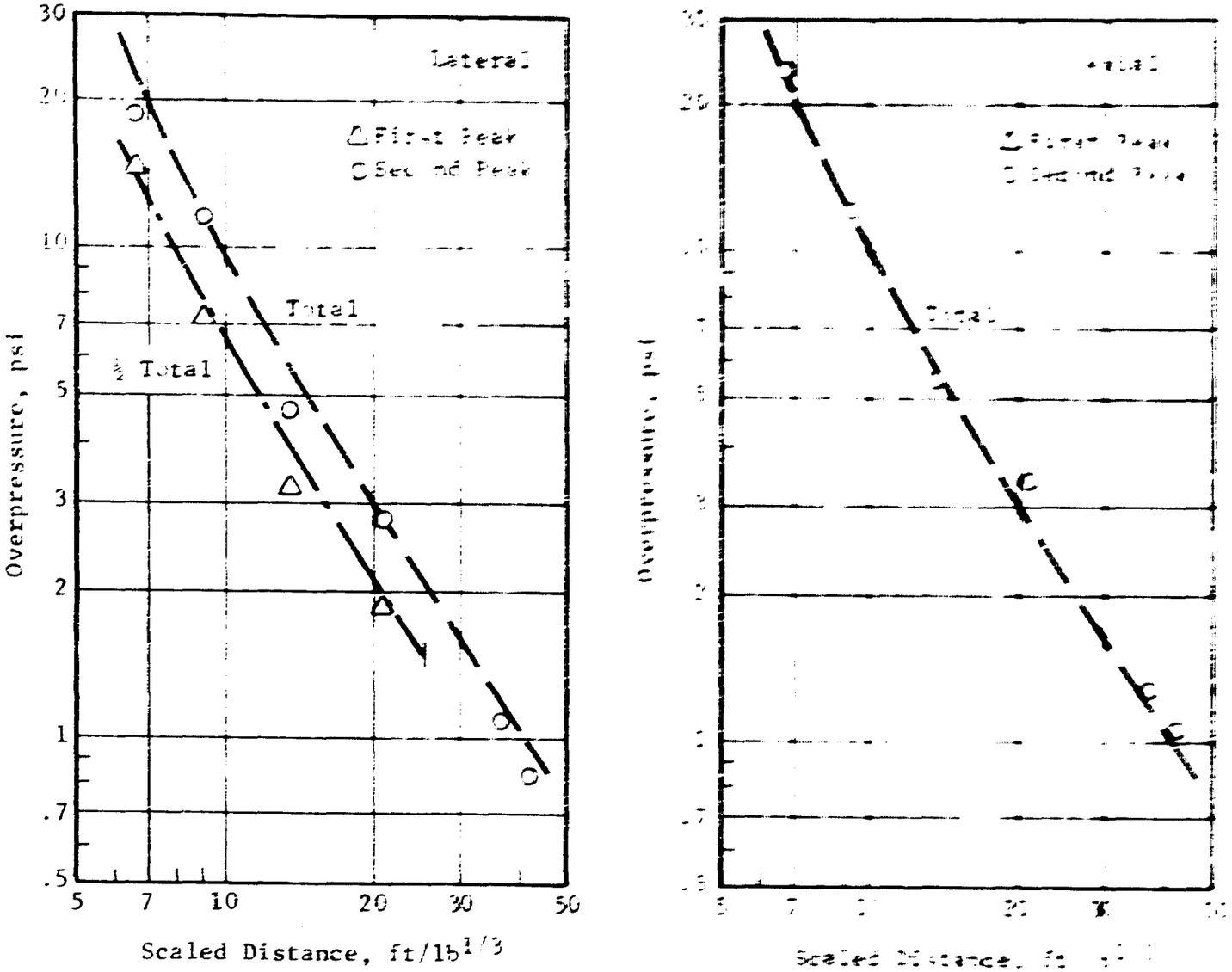

Figure 42 Pressures, Shot No. 10, Charge Weight Ratio [illegible], Time Delay [illegible] ms [illegible]

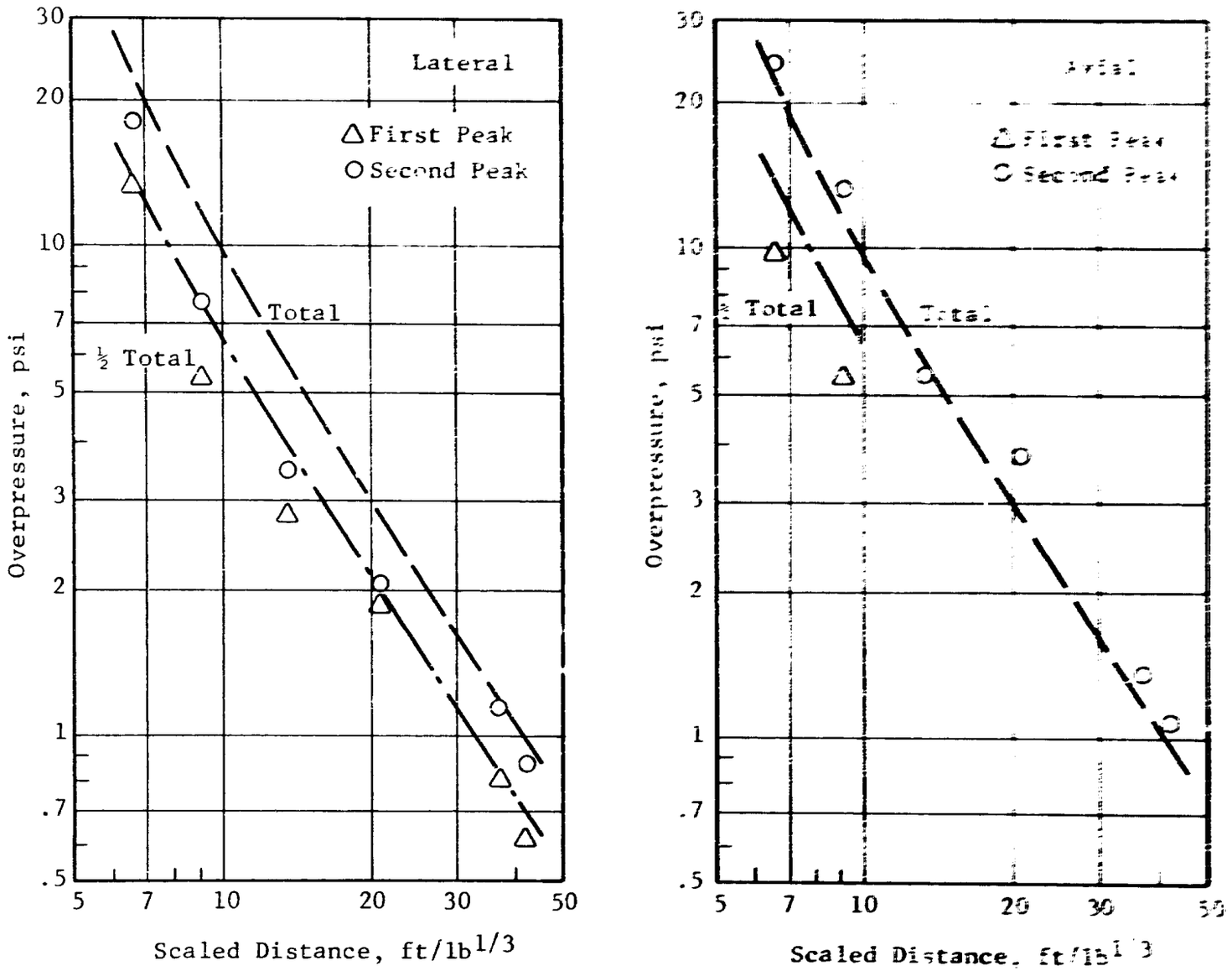

Figure 43 Pressures, Shot No. 13, Charge Weight Ratio 1:1, Time Delay 2.14 ms/lb$^{1/3}$

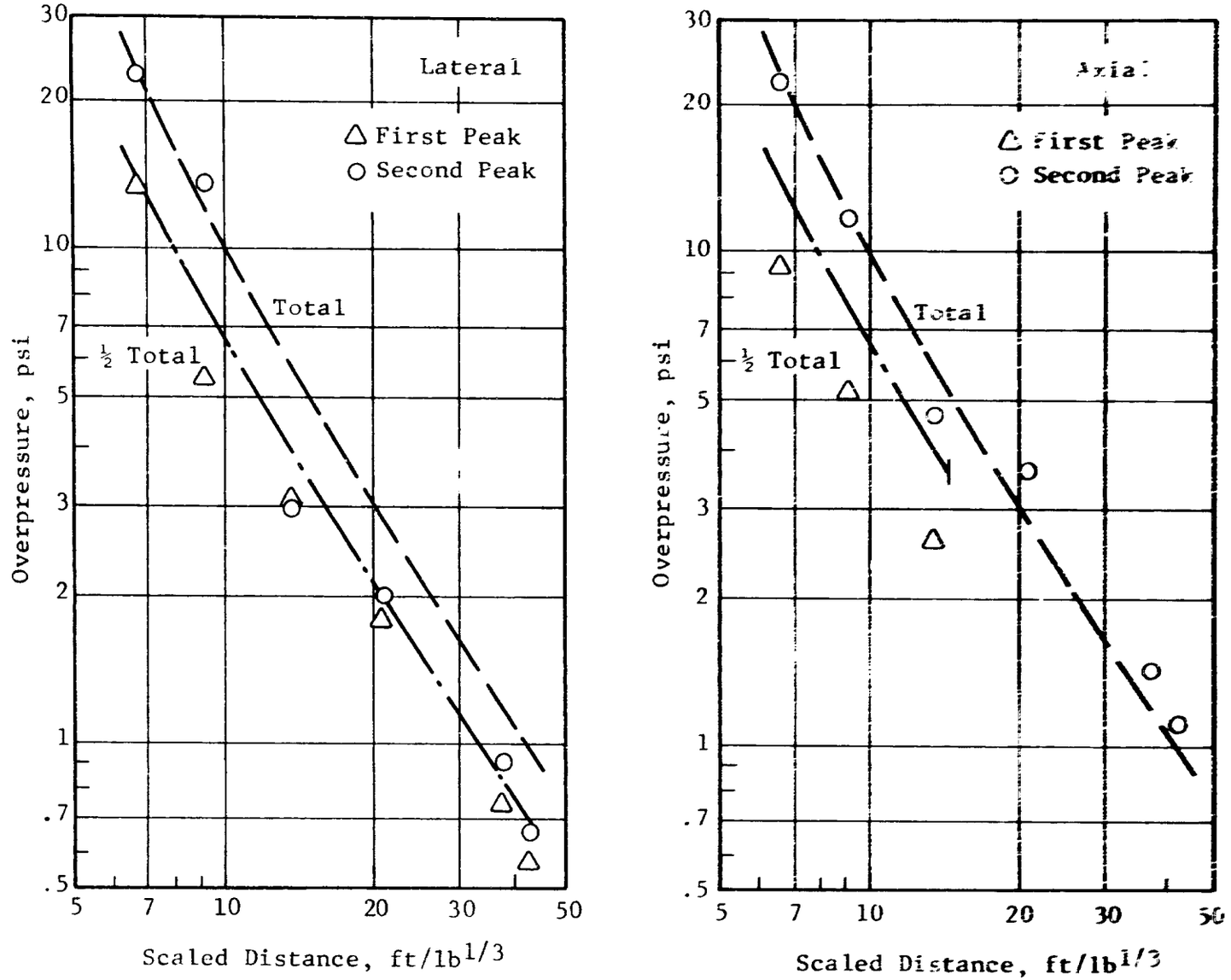

Figure 44 Pressures, Shot No. 9, Charge Weight Ratio 1:1, Time Delay 2.59 ms/lb$^{1/3}$

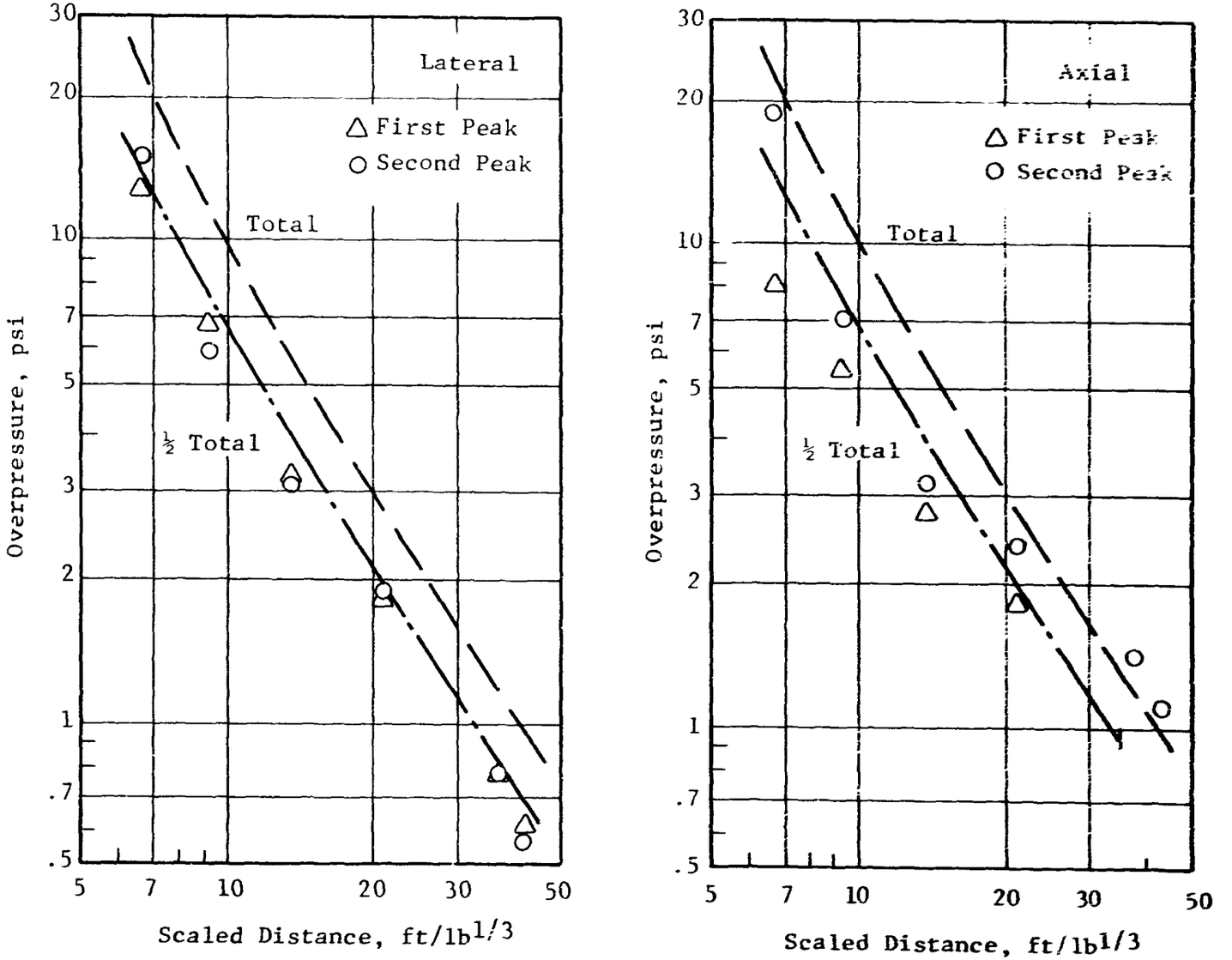

Figure 45 Pressures, Shot No. 14, Charge Weight Ratio 1:1, Time Delay 3.17 ms/lb$^{1/3}$

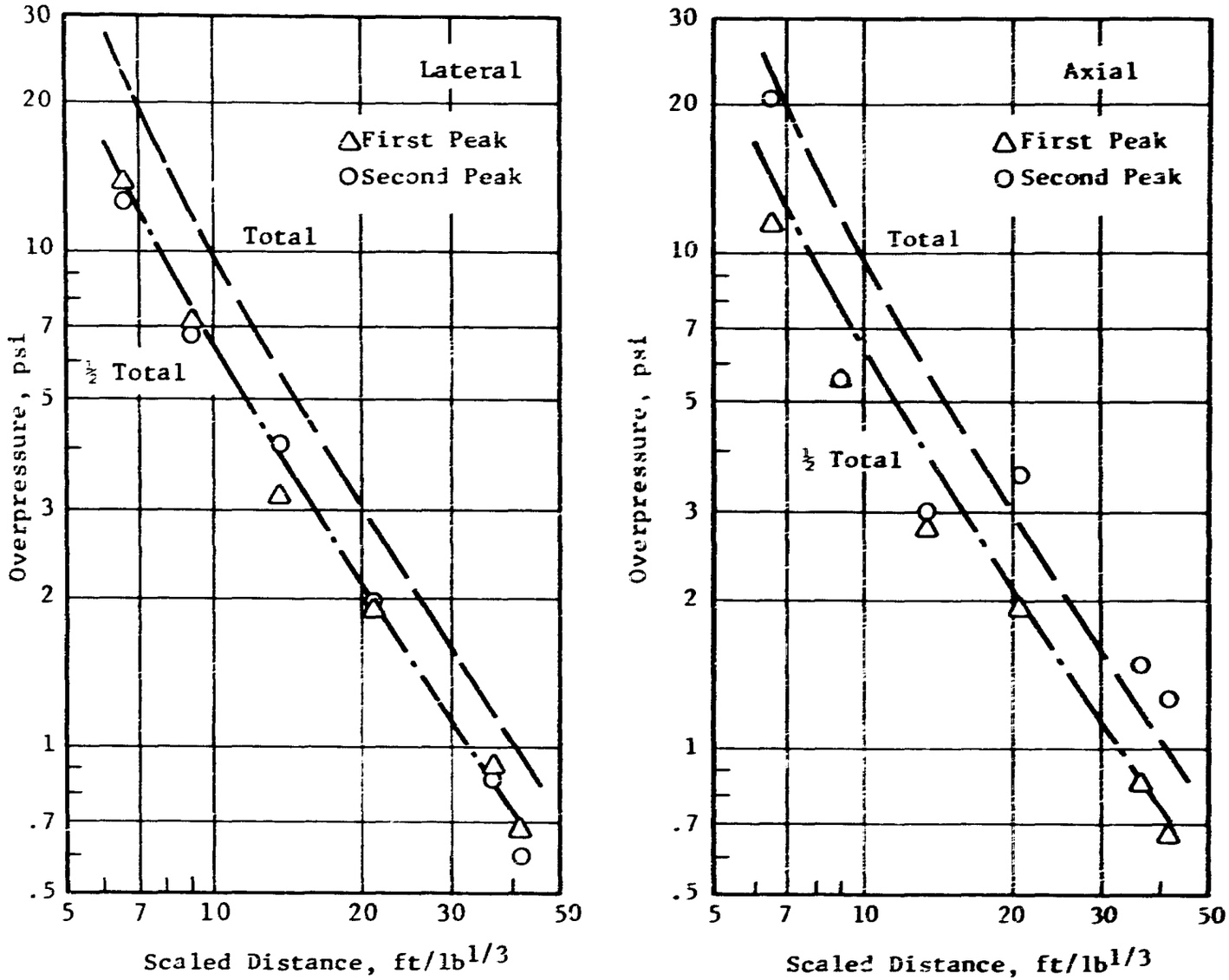

Figure 46 Pressures, Shot No. 15, Charge Weight Ratio 1:1, Time Delay 3.65 ms/lb$^{1/3}$

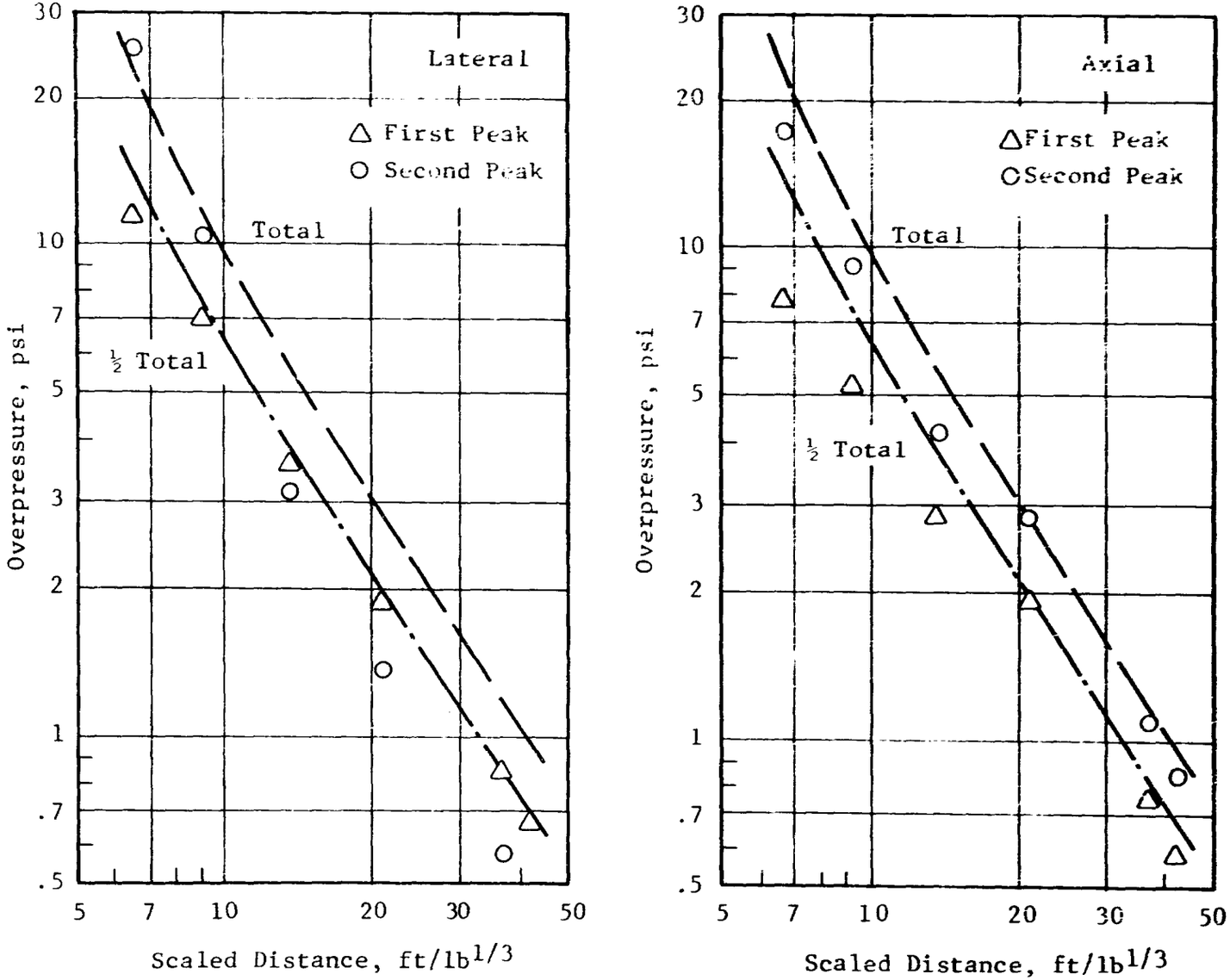

Figure 47 Pressures, Shot No. 20, Charge Weight Ratio 1:1, Time Delay 4.11 ms/lb$^{1/3}$

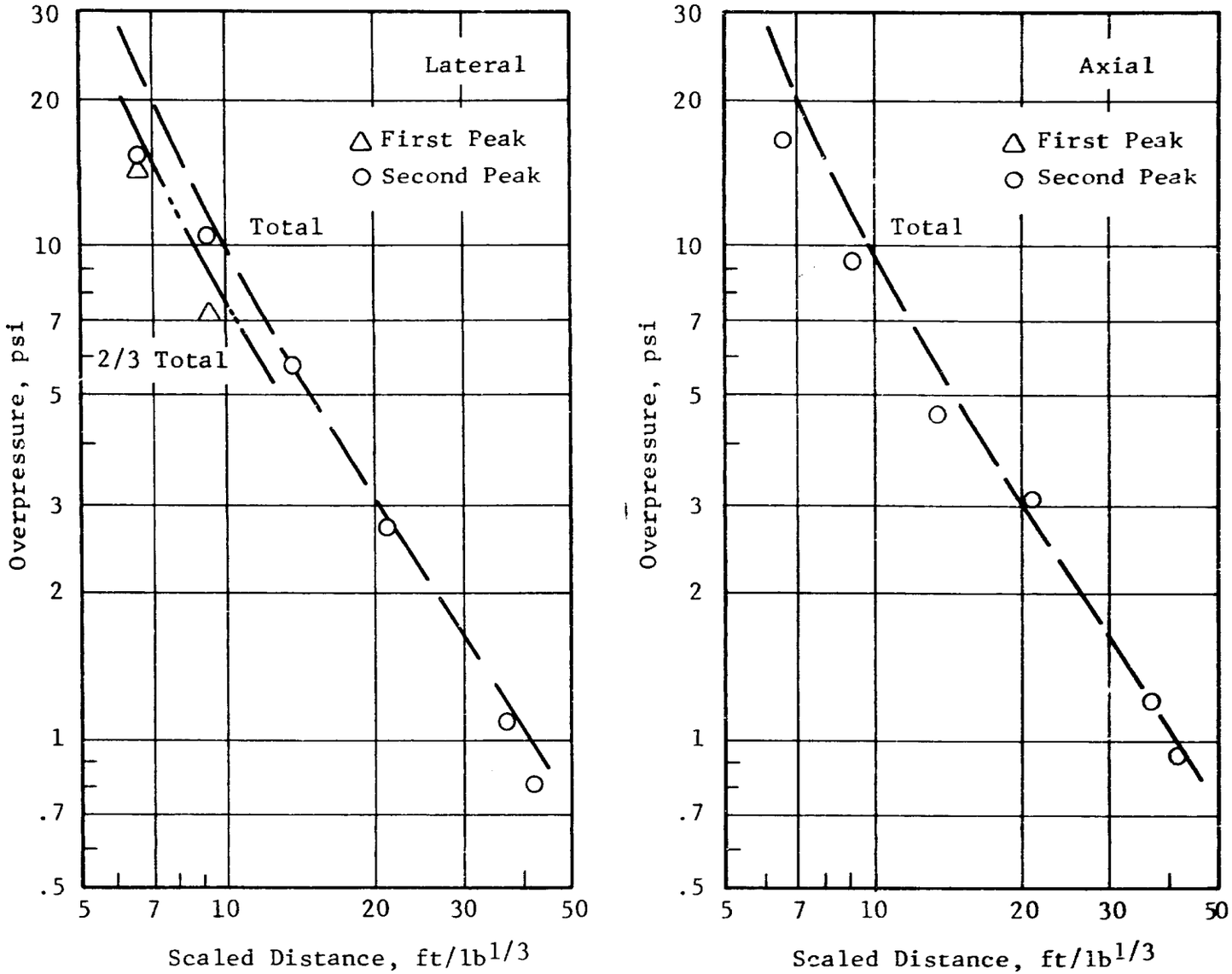

Figure 48 Pressures, Shot No. 17, Charge Weight Ratio 2:1, Time Delay 0.58 ms/$lb^{1/3}$

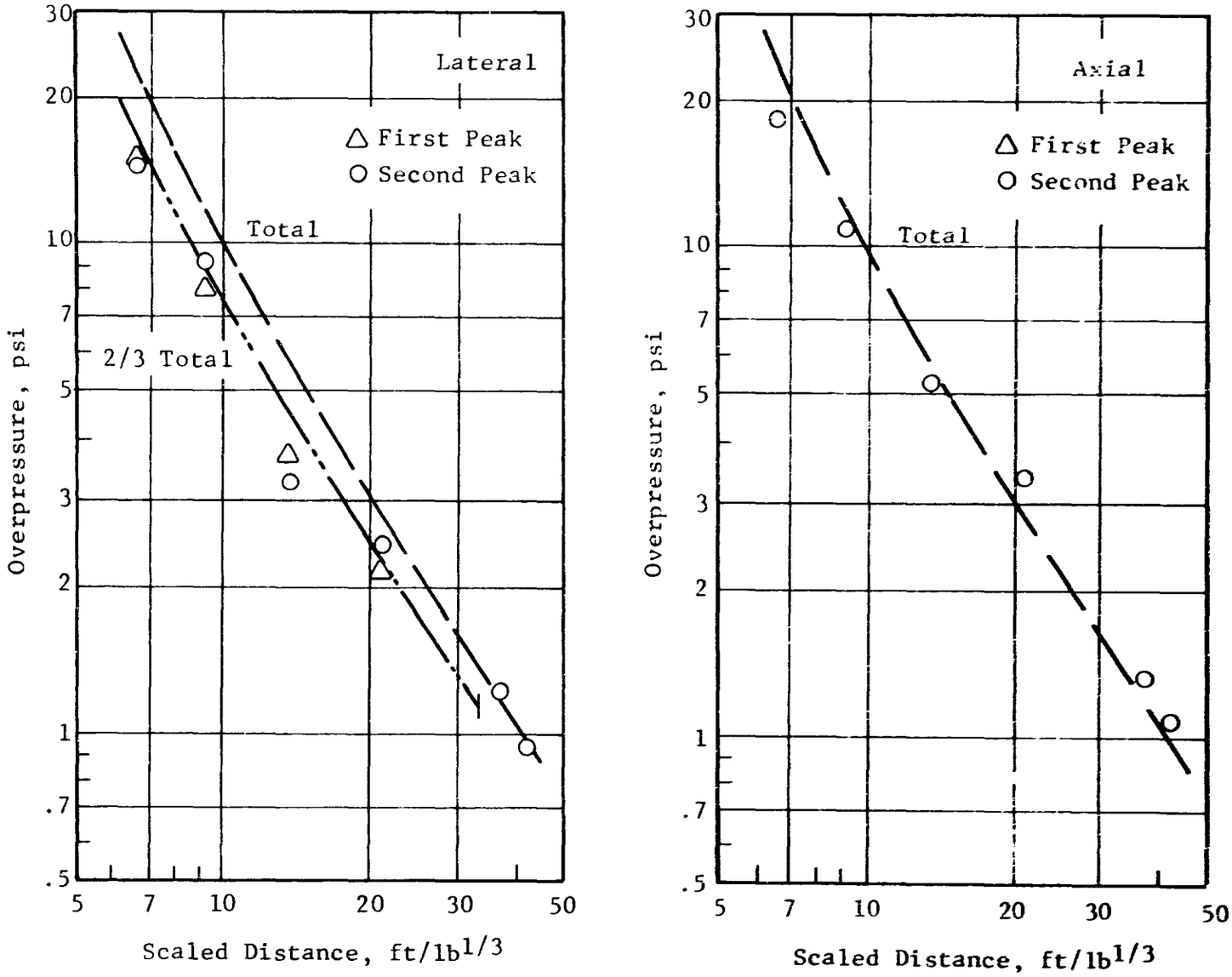

Figure 49 Pressures, Shot No. 16, Charge Weight Ratio 2:1, Time Delay 1.16 ms/lb$^{1/3}$

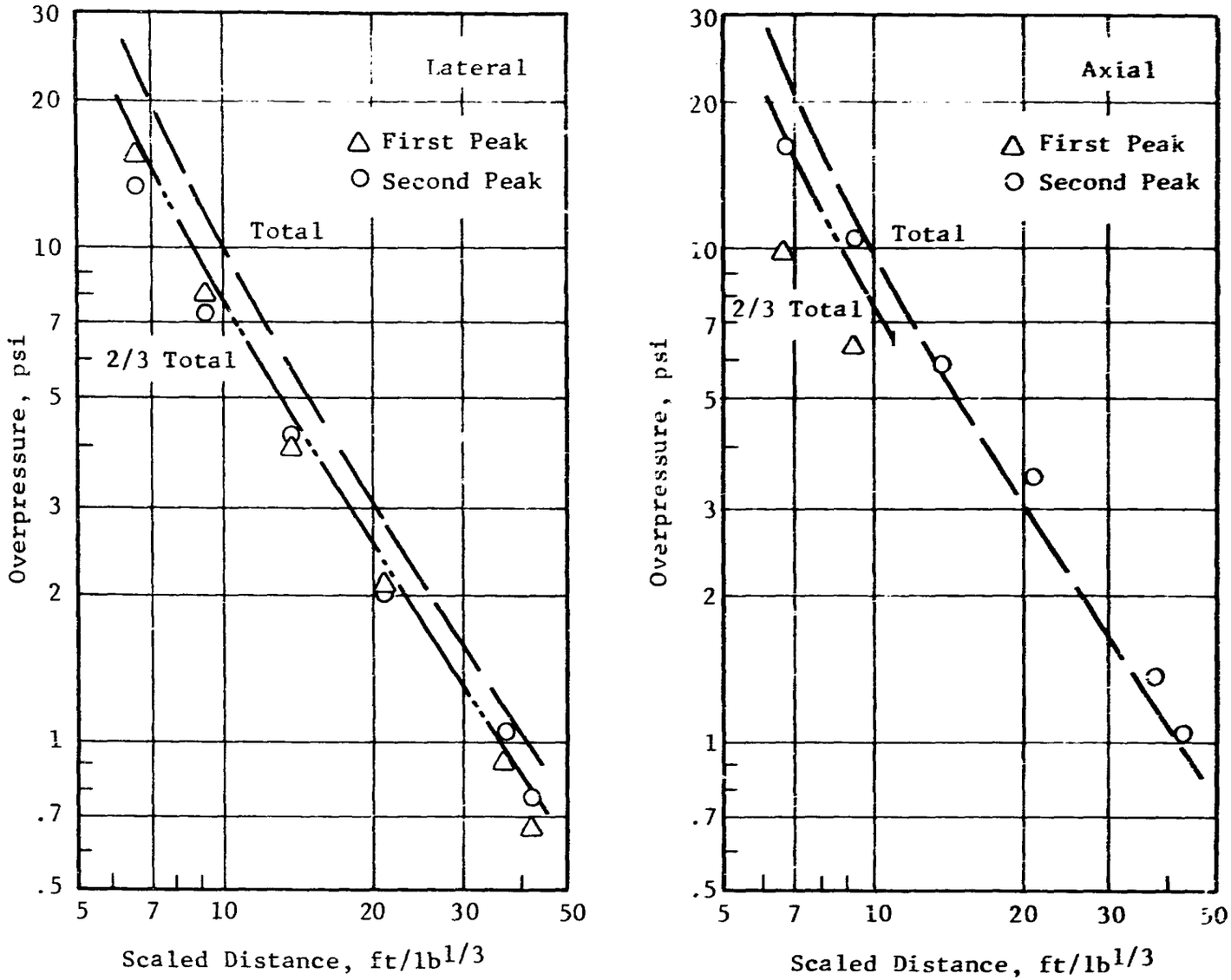

Figure 50 Pressures, Shot No. 18, Charge Weight Ratio 2:1, Time Delay 1.62 ms/lb$^{1/3}$

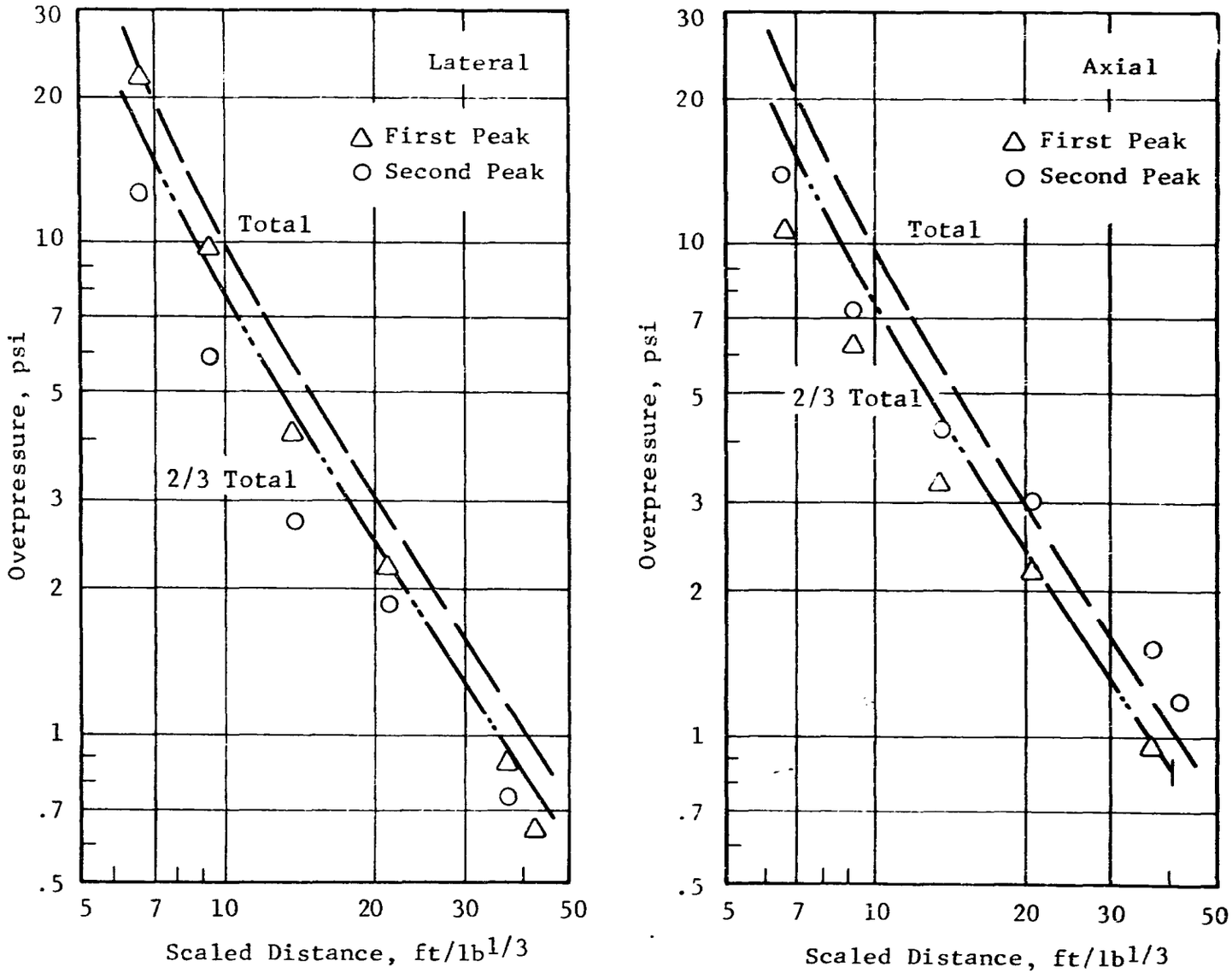

Figure 51 Pressures, Shot No. 19, Charge Weight Ratio 2:1, Time Delay 2.57 ms/lb$^{1/3}$

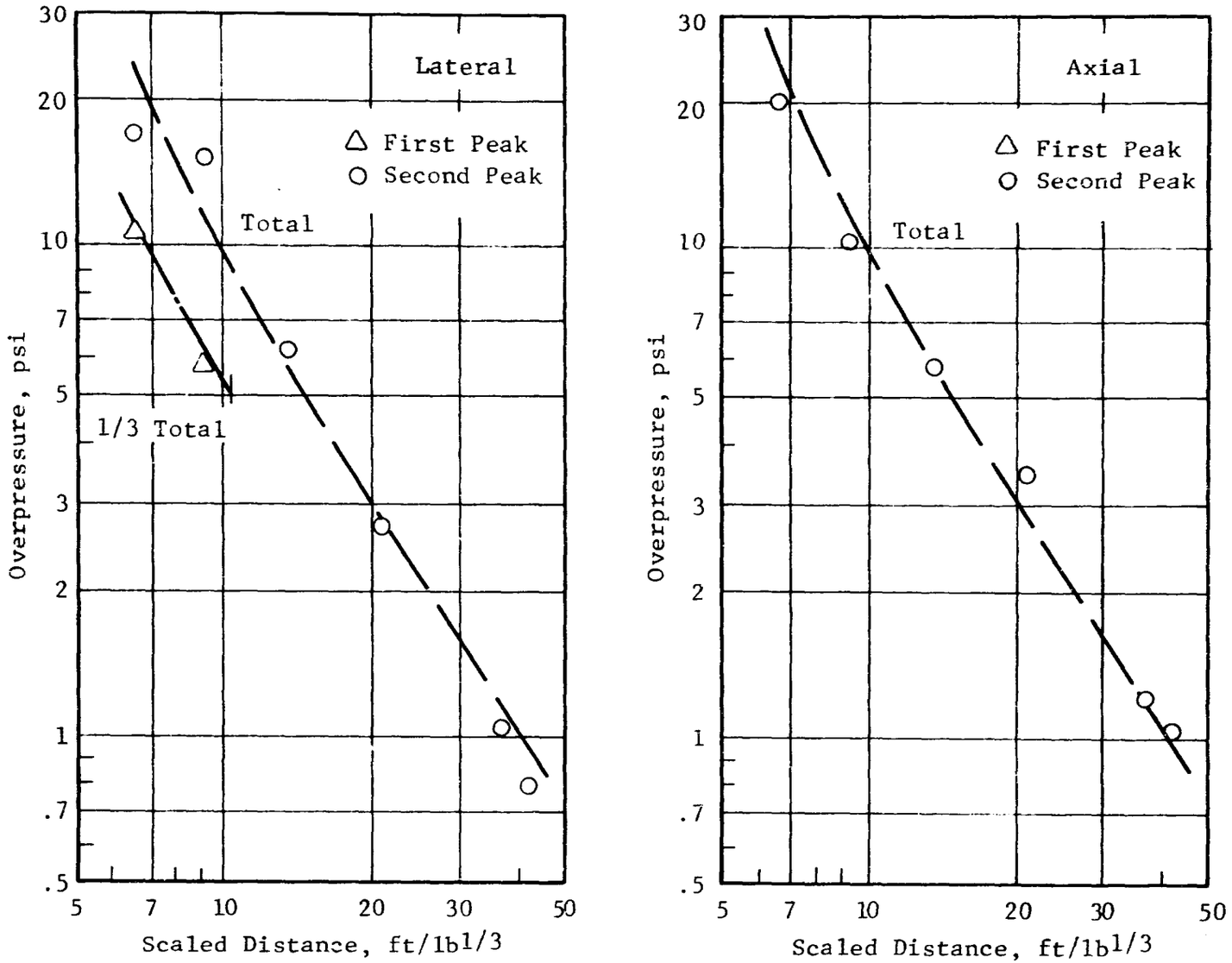

Figure 52 Pressure, Shot No. 24, Charge Weight Ratio 1:2, Time Delay 1.10 ms/lb$^{1/3}$

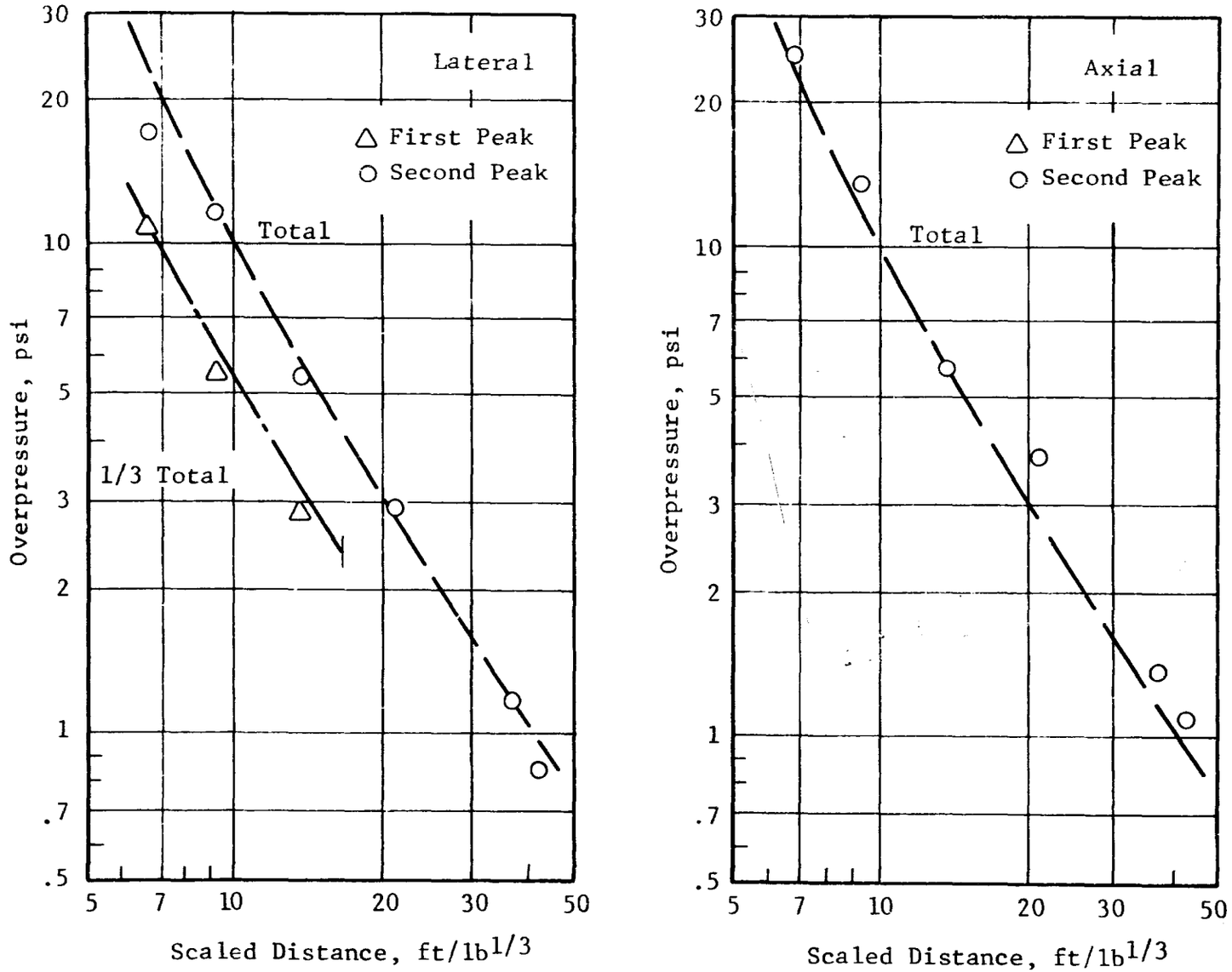

Figure 53 Pressures, Shot No. 22, Charge Weight Ratio 1:2, Time Delay 1.64 ms/$lb^{1/3}$

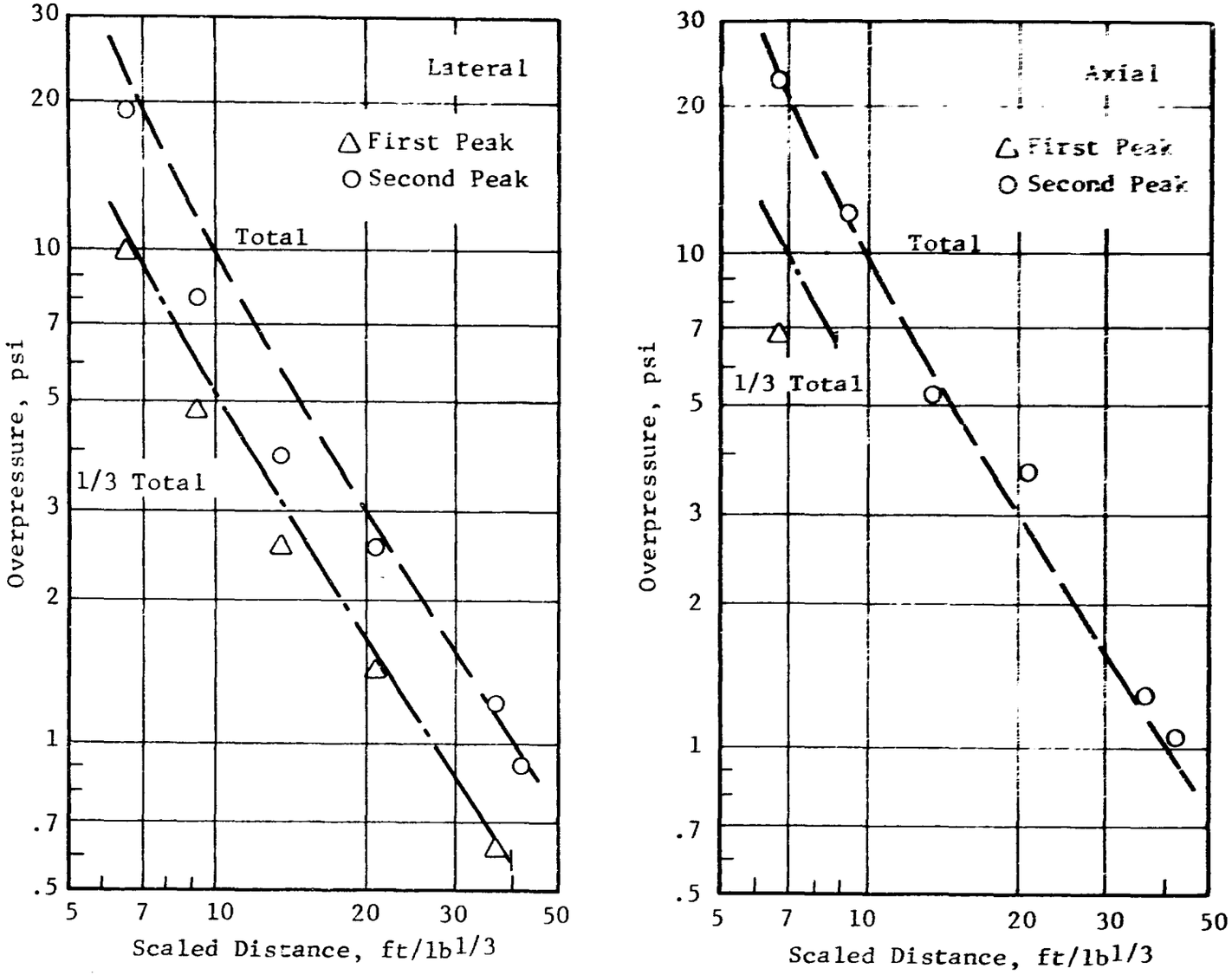

Figure 54 Pressures, Shot No. 23, Charge Weight Ratio 1:2, Time Delay 2.14 ms/lb$^{1/3}$

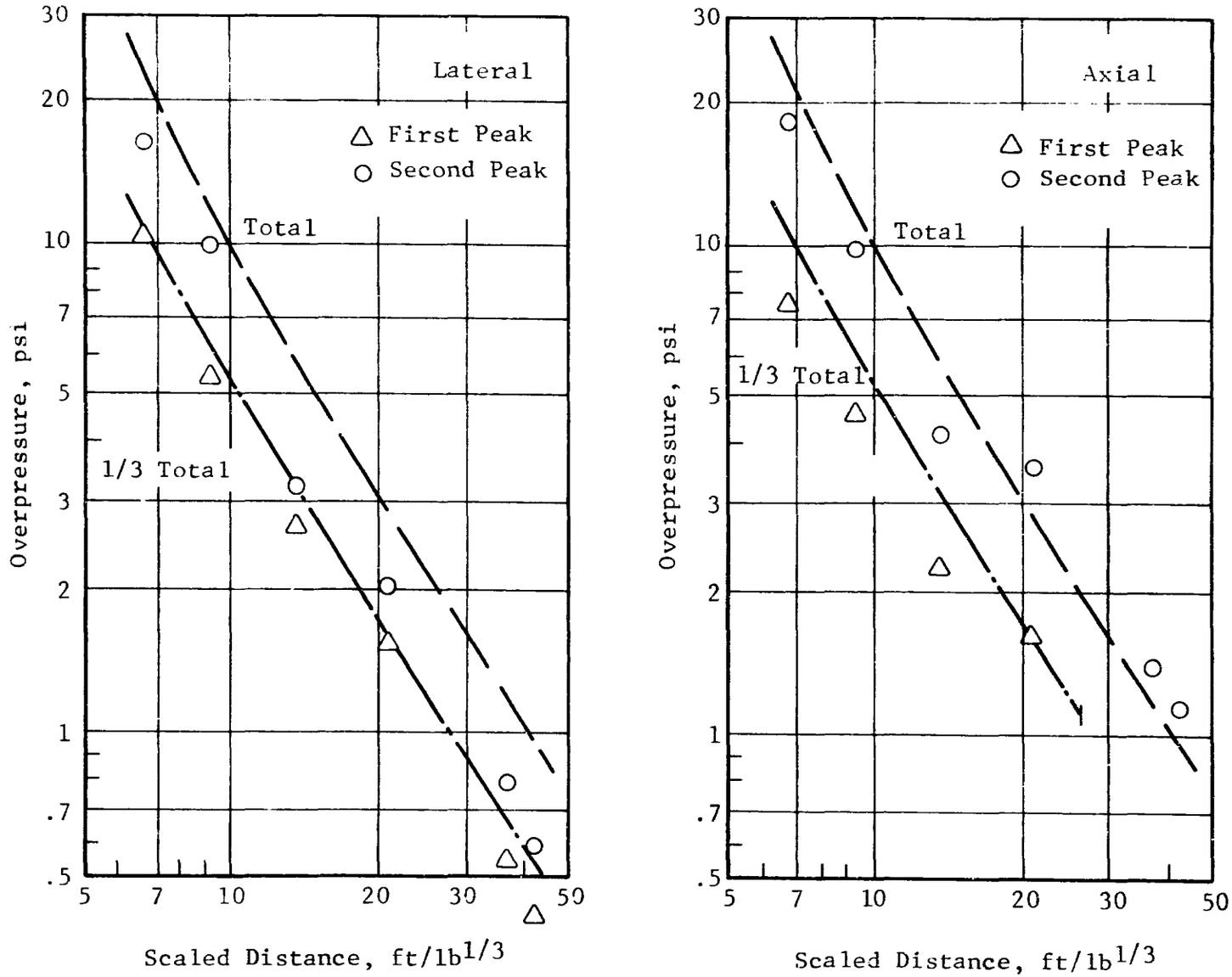

Figure 55 Pressures, Shot No. 25, Charge Weight Ratio 1:2, Time Delay 3.22 ms/lb$^{1/3}$

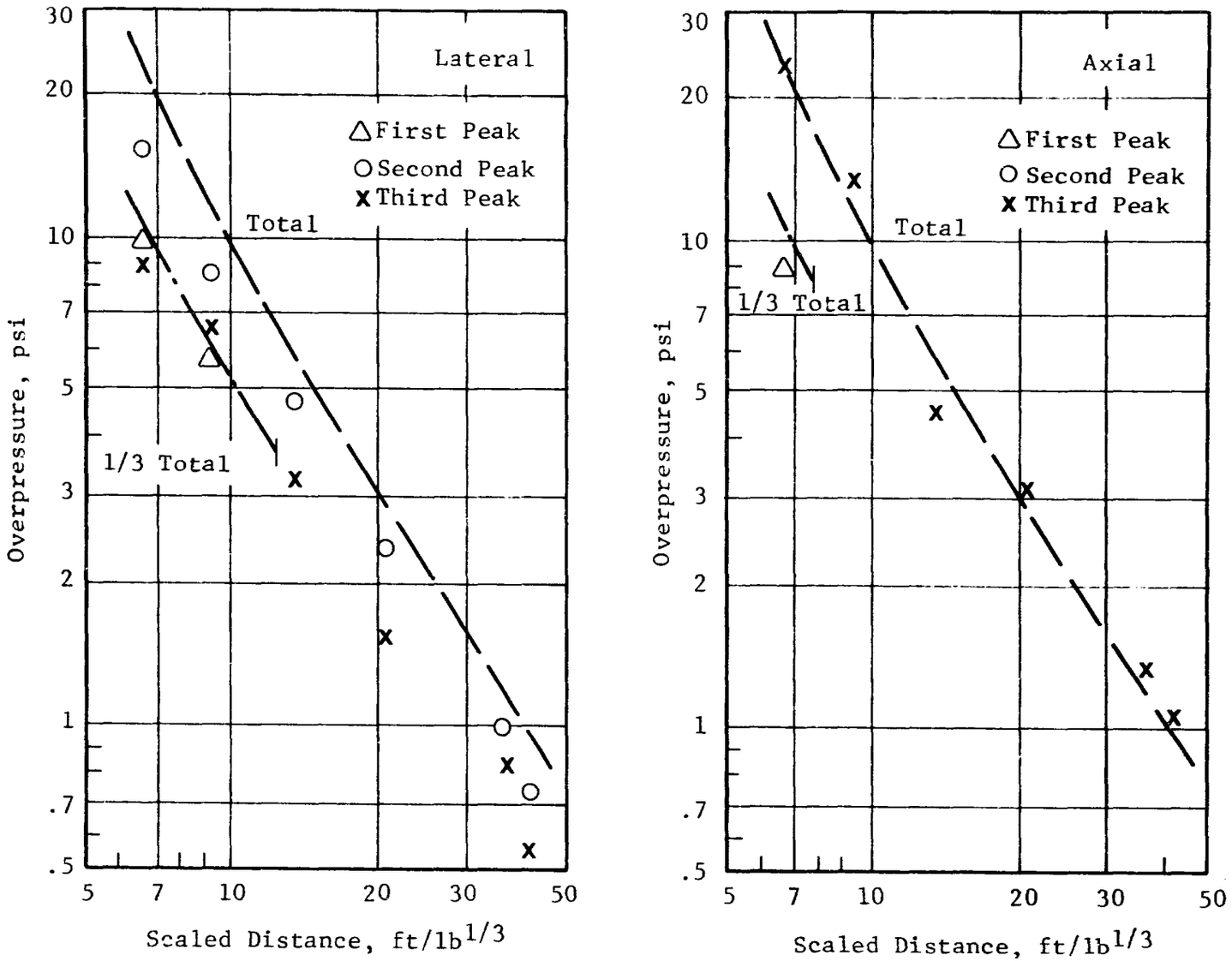

Figure 56 Pressures, Shot No. 28, Charge Weight Ratio 1:1:1, Time Delay 1.10 ms/lb$^{1/3}$

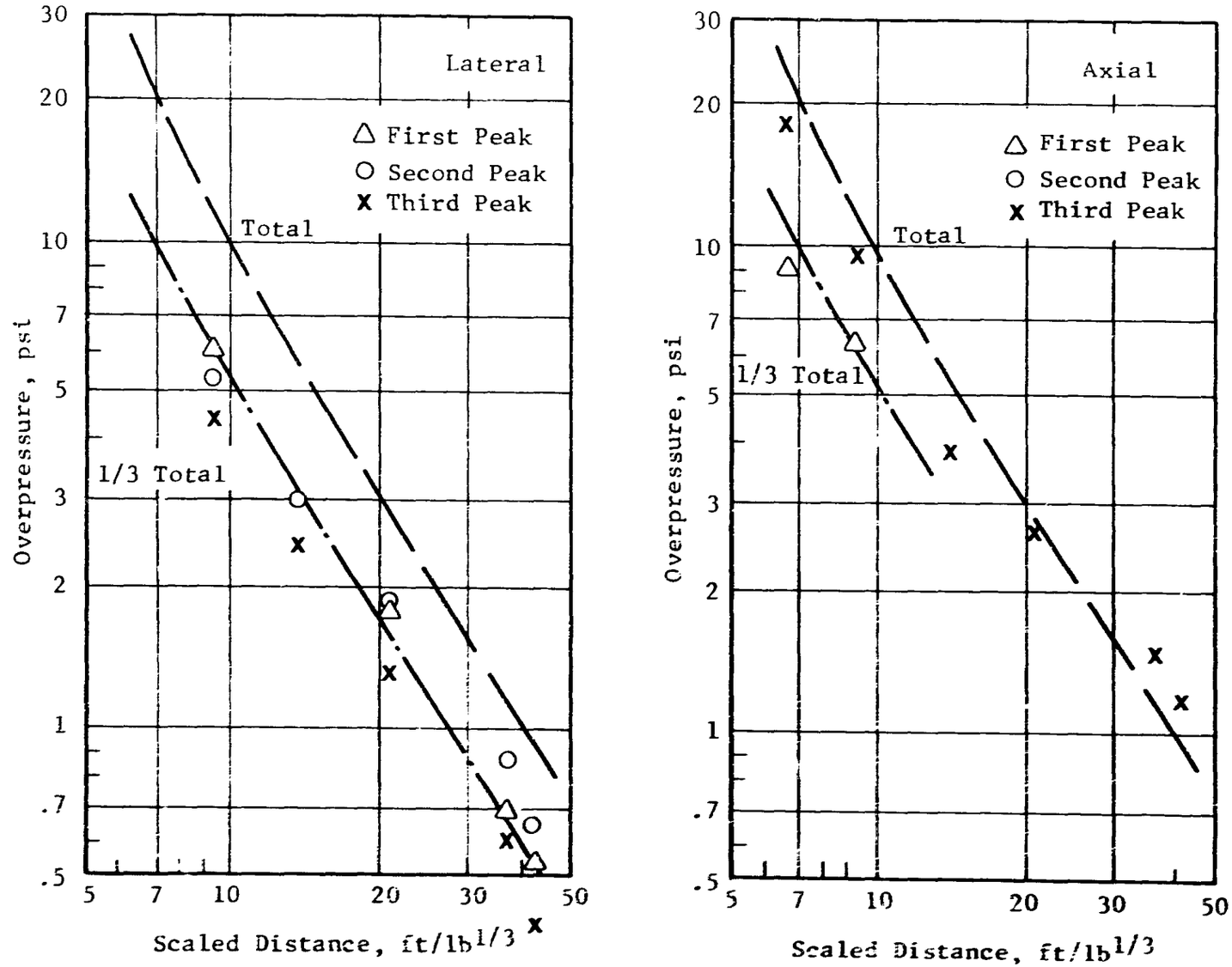

Figure 57 Pressures, Shot No. 29, Charge Weight Ratio 1:1:1, Time Delay 1.66 ms/lb$^{1/3}$

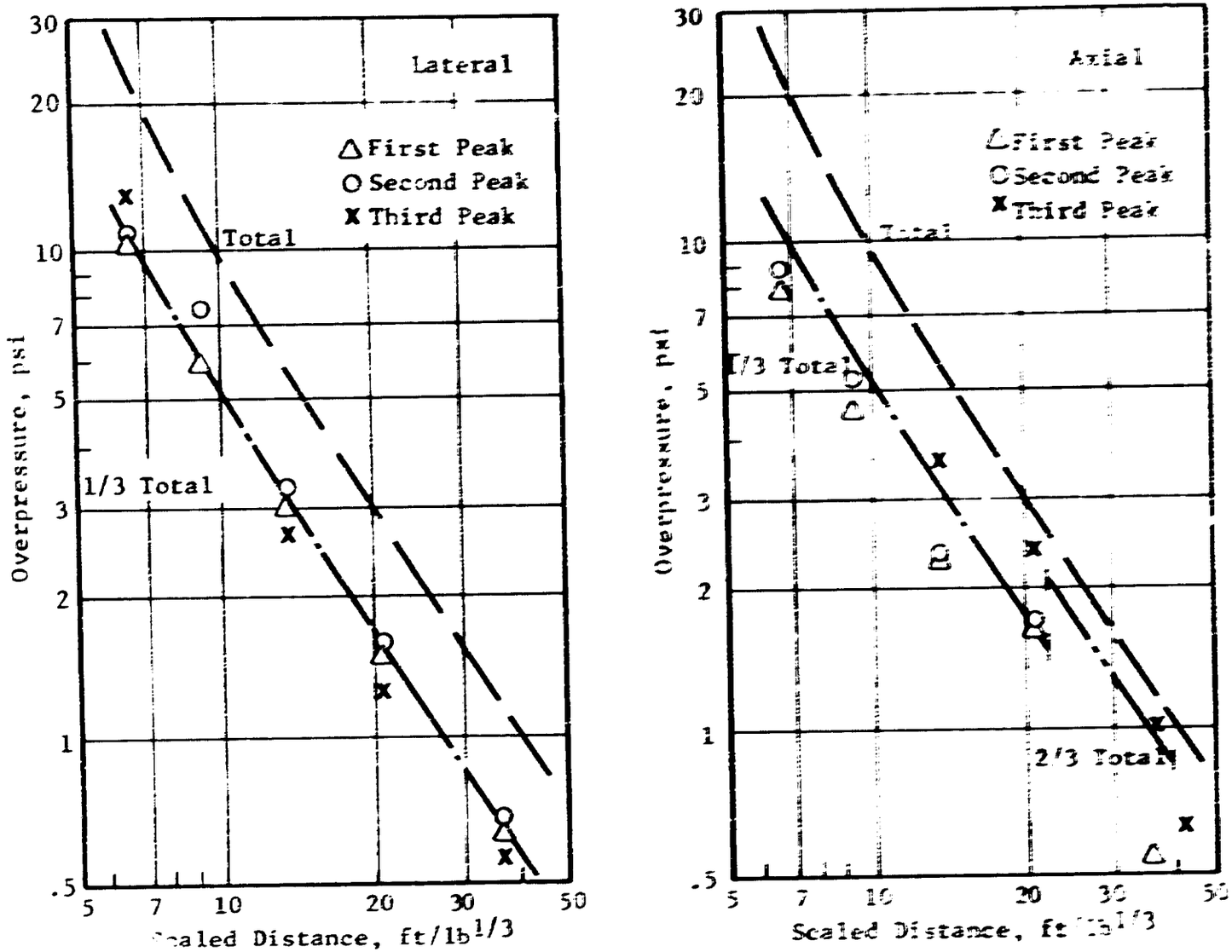

Figure 55 Pressures, Shot No. 30, Charge Weight Ratio 1:1:1, Time Delay 2.67 ms/lb^1/3

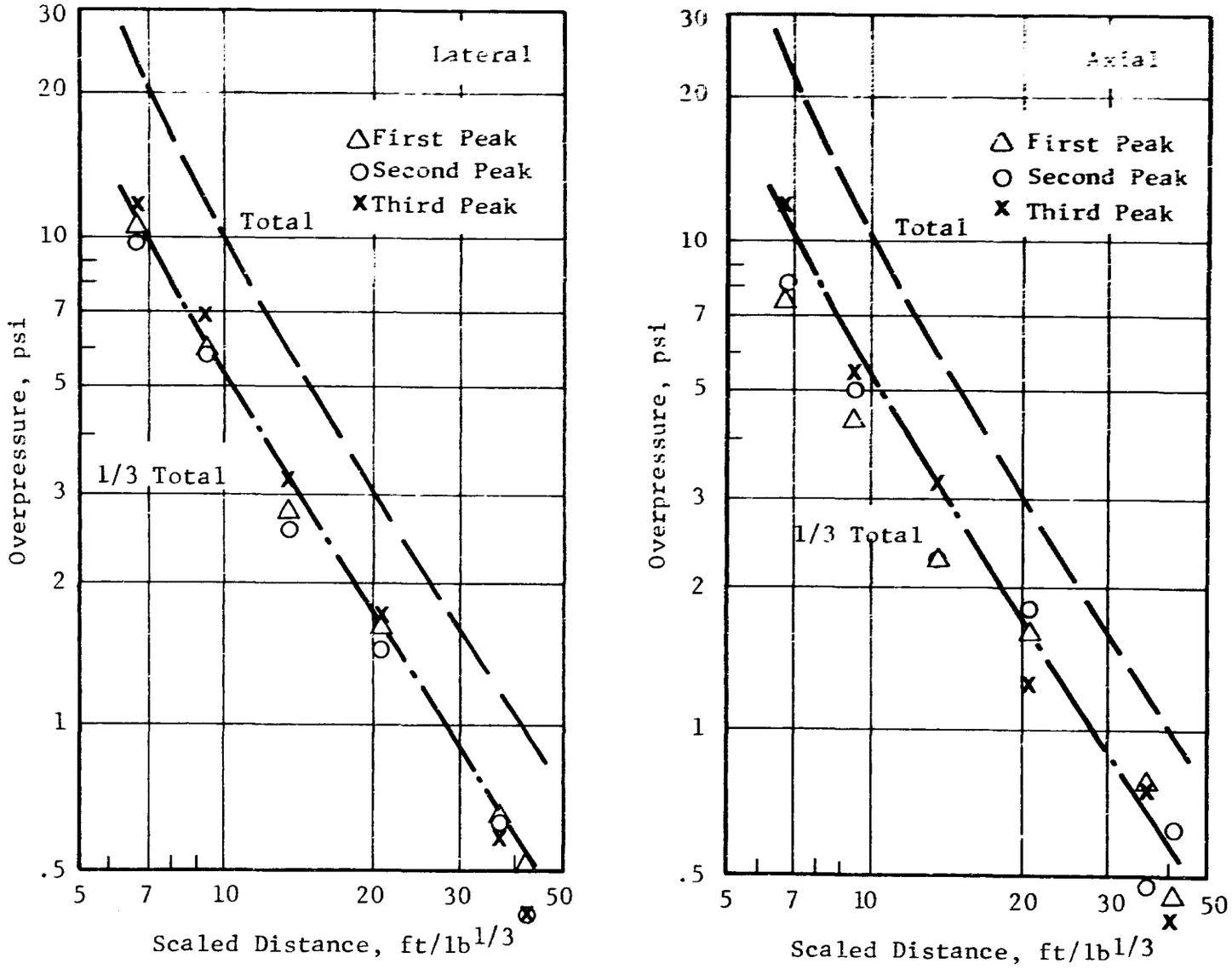

Figure 59 Pressures, Shot No. 31, Charge Weight Ratio 1:1:1, Time Delay 3.17 ms/lb$^{1/3}$

6. CONCLUSIONS AND RECOMMENDATIONS

Scale model experiments and analysis of air blast from sequential explosions yield a fairly complete understanding of blast pulse coalescence phenomena, and provide a basis for supplementing current regulations governing the siting of explosive storage and processing facilities.

6.1 Conclusions

- The results we have obtained agree quite well with data from similar studies with widely different explosive weights (ranging from 1/4 to 5000 times the quantity of explosive in our experiments). Thus blast coalescence phenomena can be investigated quite adequately with scale model experiments.

- When coalescence of successive blasts occurs, the resulting shock pressure is substantially the same as that from simultaneous explosion of the total weight of explosive in the event.

- There is no tendency for the pulse from a second explosion to overtake the first when the scaled time delay is greater than

  3.2 msec/lb$^{1/3}$ for a charge weight ratio of 1:1
  2.6 msec/lb$^{1/3}$ for a charge weight ratio of 2:1
  3.7 msec/lb$^{1/3}$ for a charge weight ratio of 1:2

  where the time delay is referenced to the total weight of explosive in the event.

- There is a considerable directional effect in evidence when the line of observation is axial to the line of centers of the charges. The enhancement of coalescence, relative to positions lateral to the line of centers, is equivalent to a reduction of the scaled explosion time delay by 1.3 msec/lb$^{1/3}$.

- When three successive explosions take place separated by two equal time intervals, the third shock tends to overtake the second well before the second overtakes the first. Thus this type of event may be treated (conservatively) as a two-explosion event with a charge weight ratio of 1:2.

6.2 Recommendations

- Existing explosive storage and facilities design regulations are unconservative with regard to the treatment of sequential explosions. In siting adjacent structures, the design basis accident should be taken as the total explosive weight in adjacent bays, unless it can be assured that propagation between the two (equal) stores will be delayed by more than 3.2 msec/$lb^{1/3}$ for lateral target positions, or by more than 4.5 msec/$lb^{1/3}$ for axial target positions. For scaled time delays greater than these, the shocks from two successively detonated charges of equal weight will not coalesce in the lateral and axial directions, respectively, at any distance of importance in the siting of adjacent structures (i.e., to 80 ft/$lb^{1/3}$). For example, the shock waves from two successively detonated 5000-lb charges will not coalesce in the lateral direction provided the time delay between explosions is greater than $3.2 \cdot (10{,}000)^{1/3} = 69$ msec. For unequal explosive stores, these time delay criteria may be strengthened or relaxed in accordance with the rules given in Section 6.1.

- The directional effect we have found at observation stations axial to the line of centers of the charges should be determined as a function of orientation of the observation line relative to the line of centers. If the effect decreases rapidly away from the axial direction, the time delay criteria recommended above may be unnecessarily stringent.

- The effect of initial charge spacing should be studied to determine whether there is any significant influence on coalescence criteria for realistic initial separation distances. No simple analytical model appears to exist which adequately represents widely separated explosions; this problem should be approached by means of model tests.

- The computer code developed in this work should be optimized with regard to computation time and flexibility, to provide a standard analytical tool for general use by explosion hazards analysts and facilities designers. In particular, it may be possible to devise a hybrid numerical method combining the desirable features of the natural-grid and fixed-time characteristic methods to improve stability, accuracy, and computation time.

REFERENCES

1. DoD Contractors' Safety Manual for Ammunition Explosives, and Related Dangerous Materials, DoD 4145.26M (October 1968).
2. K. Kaplan, "The Meaning of Simultaneity of Detonation with Respect to the Application of Quantity-Distance Regulations," Minutes, Ninth ASESB Seminar, 273-287, San Diego, California (August 1967).
3. URS Research Company, "Evaluation of Explosives Simultaneity Tests," NWC TP 4720, Naval Weapons Center (May 1969).
4. D. R. Hartree, "Some Practical Methods of Using Characteristics in the Calculation of Nonsteady Compressible Flow," Report No. AECU-2713, U. S. Atomic Energy Commission (September 1953).
5. R. C. Makino and R. E. Shear, "Unsteady Spherical Flow behind a Known Shock Line," BRL Report No. 1154 (November 1961).
6. P. C. Chou, R. R. Karpp, and S. L. Huang, "Numerical Calculation of Blast Waves by the Method of Characteristics," AIAA Journal 5, 618-623 (1967).
7. W. A. Walker and H. M. Sternberg, "The Chapman-Jouguet Isentrope and the Underwater Shockwave Performance of Pentolite," Proceedings, Fourth Symposium on Detonation, Vol. 1, B156-B169, NOL (October 1965).
8. F. J. Berry and M. Holt, "The Initial Propagation of Spherical Blast from Certain Explosives," Proc. Roy. Soc. A224, 236-251 (1954).
9. H. L. Brode, "A Calculation of the Blast Wave from a Spherical Charge of TNT," RM-1965, The Rand Corporation (August 1957).
10. L. I. Sedov, "Similarity and Dimensional Methods in Mechanics," Ch. 4, Academic Press, Inc., New York (1959).
11. P. C. Chou and S. L. Huang, "Late-Stage Equivalence in Spherical Blasts as Calculated by the Method of Characteristics," J. Appl. Phys. 40, 752-759 (1969).
12. C. N. Kingery and B. F. Pannill, "Peak Overpressure vs Scaled Distance for TNT Surface Bursts (Hemispherical Charges)," BRL Memorandum Report No. 1518 (April 1964).
13. LRL Explosives Chemistry Section, "Properties of Chemical Explosives, " Report No. UCRL-14592, Lawrence Radiation Laboratory (December 1965).

Appendix

COMPUTER CODE LISTINGS

Program BLOWUP computes air blast fields from two or three sequential explosions. It is written in FORTRAN IV user-oriented source language and has been executed on a CDC 6600, a large scientific computer. The program is based on a uniform gas bubble model of the explosion-product sphere and a constant-time numerical scheme for computing the shock propagation using the method of characteristics.

Computations are made at the shock wave discontinuities, at the bubble boundary, and at numerous interior points between these discontinuities in the air. The interior points are of three basic types: ordinary interior points, points adjacent to the shock waves, and points engulfed by the shock waves. The program consists of a main program and eleven subroutines corresponding to the type of point or discontinuity.

Program Elements

Main Program - program logic to direct the flow of control; initializations, scaling, and miscellaneous computations; input/output activity.

ITS - solution for initial time step
ISP - solution for initial interior shock
CSD - coalescence of shock discontinuities; impedance mismatch
BSD - solution at bubble boundary
OIP - solution at an ordinary interior point
SFD - solution at leading shock
SFA - solution at point adjacent to leading shock
NEP - solution at shock engulfed new point
SWD - solution at interior shock
SWA - solution at point adjacent to interior shock
IEP - solution at shock engulfed interior point

Input Data

FORMAT (3I5, 5F6.3, 2E8.1)

Columns	Variable	Description
1-5	NTS	number of time steps
6-10	NOUT	number of time steps per full output
11-15	NREZON	maximum number of interior points
16-21	W1	first charge (lb pentolite)
22-27	W2	second charge (lb pentolite)
28-33	W3	third charge (lb pentolite)
34-39	TSE	time of second explosion (msec)
40-46	TTE	time of third explosion (msec)
47-54	RMAX	maximum shock radius (ft)
55-62	DT	initial time step

The number of time steps computed is limited by both NTS and RMAX. The rezoning of the interior points is controlled by NREZON. Two modes of output are provided for in the program. The full output gives values of all variables as functions of radius, and is generated every NOUT time steps. An abbreviated output is otherwise generated which describes the bubble and the interior and leading shock waves only.

A portion of the abbreviated output for two 2-lb spheres of pentolite, detonated in free air 2.2 msec apart, appears at the end of the program listing given on succeeding pages. By symmetry, the results are the same as for two 1-lb hemispheres of pentolite detonated on a rigid ground surface. The output times and distances are scaled by the TNT equivalent of the total charge weight (2.55 lb) in the surface explosion problem represented in this way.

```
      PROGRAM BLOWUP (INPUT,OUTPUT,TAPE5=INPUT,TAPE6=OUTPUT)

      COMMON /MISCV/ A1,A2,A3,DELTAP,DELTAU,DT,DTH,DTHNU,G,GM1,GP1,
     1               ITERAT(500),ITERI,ITERSF,ITERSW,J,JP,NU,D0,P0
     2       /FIELD/ C(500,2),D(500,2),E(500,2),P(500,2),R(500,2),
     2               U(500,2)
     3       /RUVAR/ CBUBLE,DBUBLE,EBUBLE,PBUBLE,RBUBLE,UBUBLE,WBUBLE
     4       /SFVAR/ CSF(2),DSF(2),ESF(2),PSF(2),RSF(2),USF(2),USSF(2)
     5       /SWVAR/ CSW(2,2),DSW(2,2),ESW(2,2),PSW(2,2),RSW(2),
     6               USW(2,2),USSW(2)
     7       /SCVAR/ DTX,RSX,CSX1,CSX2,CSX3,CSX4,DSX1,DSX2,DSX3,DSX4,
     8               ESX1,ESX2,ESX3,ESX4,PSX1,PSX2,PSX3,PSX4,USX1,USX2,
     9               USX3,USX4,USSX1,USSX2,USSX4
      REAL NU
      LOGICAL LW2,LW3,LCHG2,LCHG3,LSS,LSC,LIMM,LOUT
      DATA A1          /0.35/,      CSC        /0.990/,      G  /1.4/,
     1     A2    /1.52342E-4/,      DELTAP     /1.E-4/,      NU /2.0/,
     2     A3    /2.32381E-5/,      DELTAU     /1.E-4/,      P0 /1.0/,
     3     PSTAR /1.01325E-6/,      DCHARG /1.650E+2/,       D0 /1.0/,
     4     DSTAR /1.22560E-3/,      ECHARG /5.866E-2/
      READ (5,10) NTS,NOUT,NREZON,W1,W2,W3,TSE,TTE,RMAX,DT
10    FORMAT (3I5,5F6.3,2E8.1)
      LW2=.FALSE. $ LCHG2=.FALSE. $ LSS=.FALSE. $ LIMM=.FALSE.
      LW3=.FALSE. $ LCHG3=.FALSE. $ LSC=.FALSE. $ LOUT=.FALSE.
      IF (W2 .GE. .0001)   LW2=.TRUE.
      IF (W3 .GE. .0001)   LW3=.TRUE.
      WSTAR=26.608*W1
      CRT=1./3. $ ESTAR=PSTAR/DSTAR          $ DC=DCHARG/DSTAR
      GM1=G-1.  $ VSTAR=SQRT(ESTAR)          $ EC=ECHARG/ESTAR
      GP1=G+1.  $ RSTAR=(WSTAR/PSTAR)**CRT $ TSTAR=RSTAR/VSTAR
      RC1=1./(4.1887902*DC*EC)**CRT
      RC2=RC1*(W2/W1)**CRT $ T2=1.E+3*TSE/TSTAR
      RC3=RC1*(W3/W1)**CRT $ T3=1.E+3*TTE/TSTAR
```

```
      WBAR=.5*1.402*(W1+W2+W3)/1.1 $ VBAR=32.808*VSTAR $ PBAR=14.7
      TBAR=1.E-3*TSTAR/WBAR**CRT    $ UBAR=DSTAR $ RMAX=RMAX/WBAR**CRT
      RBAR=.032808*RSTAR/WBAR**CRT $ EBAR=100.*EST AR/4.186
      RBUBLE=RC1 $ DBUBLE=DC
      WBUBLE=1.0 $ EBUBLE=EC
      PBUBLE=(A1+A2*DBUBLE)*DBUBLE*EBUBLE+A3*DBUBLE**3
      UBUBLE=SQRT(2.*(PBUBLE-P0)**2/(D0*(GP1*PBUBLE+GM1*P0)))
      CBUBLE=SQRT((A1+2.*A2*DBUBLE)*EBUBLE+3.*A3*DBUBLE**2*(A1+A2*
     1DBUBLE)*PBUBLE/DBUBLE)
      RSF(1)=RBUBLE + USF(1)=UBUBLE $ PSF(1)=PBUBLE
      DSF(1)=D0*(GP1*PSF(1)+GM1*P0)/(GM1*PSF(1)+GP1*P0)
      ESF(1)=PSF(1)/(GM1*DSF(1))
      CSF(1)=SQRT(GP1*PSF(1)/DSF(1))
      USSF(1)=USF(1)*DSF(1)/(DSF(1)-D0)
      R(1,1)=RSF(1) + P(1,1)=PSF(1) $ C(1,1)=CSF(1)
      U(1,1)=USF(1) + D(1,1)=DSF(1) $ E(1,1)=ESF(1)
      WRITE (6,11)
11    FORMAT (1H1)
      WRITE (6,12) W1
12    FORMAT (1H1,59X12H F L O W U P///41X49H SHOCK WAVE PROPAGATION FOR
     1 SEQUENTIAL EXPLOSIONS//26X79H CHARACTERISTIC SOLUTION FOR THE SHO
     2CK ENGULFED FIELD WITH A UNIFORM GAS BUBBLE///49X13H FIRST CHARGE,
     3F8.3,14H LBS-PENTOLITE)
      IF (L.EQ.2)   WRITE (6,13) W2,TSE
13    FORMAT (1H0,47X14H SECOND CHARGE,F8.3,14H LBS-PENTOLITE/51X11H TIM
     1E DELAY,F8.2,5H MSEC)
      IF (L.EQ.3)   WRITE (6,14) W3,TTE
14    FORMAT (1H0,48X 13H THIRD CHARGE,F8.3,14H LBS-PENTOLITE/51X11H TIM
     1E DELAY,F8.2,5H MSEC)
      WRITE (6,15)
15    FORMAT (1H0///51X30H * UNITS OF OUTPUT VARIABLES *///41X50H TIME
     1   MSEC/(LB-TNT)**1/3      PRESSURE    PSIG/41X50H RADIUS      FT/(
     2LB-TNT)**1/3      DENSITY    GM/CC/41X50H VELOCITY             FT/M
     3SEC      ENERGY   KCAL/GM//37X58H (NOTE- YIELD SCALING IS TNT AND
     4SURFACE BURST EQUIVALENT))
```

```
      WRITE (6,16)
16    FORMAT (1H0///10X30H INITIATION OF FIRST EXPLOSION//87X20H SONIC
     1     PARTICLE/34X73H RADIUS       PRESSURE       DENSITY       ENERGY
     2      VELOCITY      VELOCITY)
      ROUT=RBAR*RBUBLE        $ DOUT=DBAR*DBUBLE $ COUT=VBAR*CBUBLE
      POUT=PBAR*(PBUBLE-1.) $ EOUT=EBAR*EBUBLE $ UOUT=VBAR*UBUBLE
      WRITE (6,17) ROUT,POUT,DOUT,EOUT,COUT,UOUT
17    FORMAT (1H0,10X19H INTERIOR GAS BUBBLE,6E13.4)
      ROUT=RBAR*RSF(1)        $ DOUT=DBAR*DSF(1) $ COUT=VBAR*CSF(1)
      POUT=PBAR*(PSF(1)-1.) $ EOUT=EBAR*ESF(1) $ UOUT=VBAR*USF(1)
      WRITE (6,18) ROUT,POUT,DOUT,EOUT,COUT,UOUT
18    FORMAT (14X16H AIR SHOCK FRONT,6E13.4)
      T=DT $ DTH=DT/2. $ DTHNU=DTH*NU
      CALL ITS
      TT=CSC*(RSF(2)-R(1,2))/AMAX1(CSF(2),C(1,2))
      DRNP=DSF(1)*(RSF(2)-RSF(1)) $ RNPA=RSF(2)
      LT=1 $ J=1  $ KI=1 $ KO=2  $ KOUNT=NOUT
      LC=2 $ JP=2 $ KZ=1 $ KO1=3 $ ASSIGN 65 TO JJ $ GO TO 46
19    DTH=DT/2.       $ K=J  $ LT=LC
      DTHNU=DTH*NU    $ J=JP $ LC=LC+1
      T=T+DT          $ JP=K
      IF (.NOT. LSS)    GO TO 32
      IF (KI .GT. 1     GO TO 22
      CALL OUTP (3)
      RSW(JP)=RSW(J)+DT*USSW(J)
      IF (RSW(JP) .LT. R(3,JP))    GO TO 20
      TSAV=T-DT
      DT=DT*(R(3,J)-RSW(J))/(RSW(JP)-RSW(J)-R(3,JP)+R(3,J))
      DTH=DT/2. $ DTHNU=DTH*NU $ T=TSAV+DT
20    CALL ISP
      KI=2 $ KO=3 $ KO1=4
      X1=((RSW(JP)-RSW(J))/DT-.5*(U(2,J)+USW(1,J)))/(USW(1,JP)-USW(1,J))
      X2=(R(2,J)-RSW(J))/(DTH*(USW(1,JP)-USW(1,J)))
      R(2,J)=RSW(J)+(RSW(JP)-RSW(J))*(X1+SQRT(X1**2-X2))
      IF (USW(1,JP) .LT. USW(1,J))    GO TO 21
      R(2,J)=RSW(J)+(RSW(JP)-RSW(J))*(X1-SQRT(X1**2-X2))
```

```
21    CALL IFP (KI)
      GO TO 31
22    CALL BSD (KI)
      IF (LIMP)   GO TO 23
      CALL SWD (KI,K ,RP)
      GO TO 24
23    DTR=DT/(TX-T+D1)
      USW(2,JP)=USW(2,J)+DTR*(USX2-USW(2,J))
      CSW(2,JP)=CSW(2,J)+DTR*(CSX2-CSW(2,J))
      PSW(2,JP)=PSW(2,J)+DTR*(PSX2-PSW(2,J))
      DSW(2,JP)=DSW(2,J)+DTR*(DSX2-USW(2,J))
      ESW(2,JP)=ESW(2,J)+DTR*(ESX2-ESW(2,J))
      USW(1,JP)=USW(1,J)+DTR*(USX1-USW(1,J))
      CSW(1,JP)=CSW(1,J)+DTR*(CSX1-CSW(1,J))
      PSW(1,JP)=PSW(1,J)+DTR*(PSX1-PSW(1,J))
      DSW(1,JP)=DSW(1,J)+DTR*(DSX1-USW(1,J))
      ESW(1,JP)=ESW(1,J)+DTR*(ESX1-ESW(1,J))
      USF(JP)=USF(J)+DTR*(USX1-USF(J))
      CSF(JP)=CSF(J)+DTR*(CSX1-CSF(J))
      PSF(JP)=PSF(J)+DTR*(PSX1-PSF(J))
      DSF(JP)=DSF(J)+DTR*(DSX1-DSF(J))
      ESF(JP)=ESF(J)+DTR*(ESX1-ESF(J))
      RSW(JP)=RSW(J)+DTR*(RSX-RSW(J))
      RSF(JP)=RSF(J)+DTR*(RSX-RSF(J))
      USSW(JP)=USSW(J)+DTR*(USSX2-USSW(J))
      USSF(JP)=USSF(J)+DTR*(USSX1-USSF(J))
      ITERSW=ITERSF=0
24    IF (KI .EQ. 2)   GO TO 26
      KK=KI-1
      DO 25   K=2,KK
25    CALL DIP (K)
26    CALL SWA (KI)
```

```
      IF (.NOT. ISC)   GO TO 29
      RKI=R(KI,JP)     $ UKI=U(KI,JP)    $ PKI=P(KI,JP)    $ DKI=D(KI,JP)
      KI1=KI-1         $ D1=(D(KI1,JP)+DKI)*(RKI-R(KI1,JP))
      DR1=RS*(JP)-RKI  $ DR2=R(KI,JP)-RKI $ DET=(DR2*DR1*(DR2-DR1)
      XU=DR1*(U(KI1,JP)-UKI) $ YU=DR2*(US*(2,JP)-UKI)
      XP=DR1*(P(KI1,JP)-PKI) $ YP=DR2*(PS*(2,JP)-PKI)
      XD=DR1*(D(KI1,JP)-DKI) $ YD=DR2*(DS*(2,JP)-DKI)
      AU=(DR2*YU-DR1*XU)/DET $ BU=(XU-YU)/DET
      AP=(DR2*YP-DR1*XP)/DET $ BP=(XP-YP)/DET
      AD=(DR2*YD-DR1*XD)/DET $ BD=(XD-YD)/DET
27    KI1=KI   $ I=0
      KI=KI+1  $ R(KI,JP)=R(KI,JP)
28    L=L+1
      R(KI,JP)=R(KI1,JP)+DM/(D(KI1,JP)+D(KI,JP)) $ D=E(KI,JP)-RKI
      D(KI,JP)=DKI+D*(AD+DR*D) $ IF (L .LT. 3)   GO TO 28
      U(KI,JP)=UKI+D*(AU+DR*U)
      P(KI,JP)=PKI+D*(AP+DR*P)
      E(KI,JP)=P(KI,JP)/(GM1*D(KI,JP))
      C(KI,JP)=SQRT(GM*P(KI,JP)/D(KI,JP))
      IF (R(KI,JP) .LT. RS*(JP))   GO TO 27
      KI=KI-1
29    IF (LIM2)   GO TO 42
      IF (RP .LE. R(KO,J))   GO TO 31
      KI=KI+1
      X1=((RS*(JP)-R(KO,J))/DT-.5*(U(KO,J)+US*(1,J)))/(US*(1,JP)-
     1US*(1,J))
      X2=(R(KO,J)-RS*(J))/(DT+.5*(US*(1,JP)-US*(1,J)))
      R(KI,J)=RS*(J)+(RS*(JP)-RS*(J))*(X1+SQRT(X1**2-X2))
      IF (US*(1,JP) .LT. US*(1,J))   GO TO 30
      R(KI,J)=RS*(J)+(RS*(JP)-RS*(J))*(X1-SQRT(X1**2-X2))
30    KO=KO+1 $ KOI=KO+1
      CALL IEP (KI)
31    KOM1=KO-1          $ R(KOM1,J)=US*(1,J) $ P(KOM1,J)=PS*(1,J)
      R(KOM1,J)=-S*(J) $ U(KOM1,J)=CS*(1,J) $ D(KOM1,J)=DS*(1,J)
```

```
32    IF (.NOT. LSS)   CALL RSU (KZ)
      CALL SFD (KZ)
      IF (KZ-2)   36,35,33
33    KK=KZ-1
      DO 34   K=2,KK
34    CALL UIP (K)
35    CALL SFA (KZ)
36    IF (RNPA .GE. RSF(JP))   GO TO 37
      IF (RNPA .LT. RSF(JP))   RNPA=RSF(JP)
      KZ=KZ+1 $ R(KZ-1)=RNPA
      CALL NEP (KZ)
      RNP=DRNP/D(KZ,JP) $ RNPZ=R(KZ,JP)*RNP
37    IF (KI .EQ. 2 .OR. KZ .LT. NNEZON)   GO TO 40
      IF (.NOT. LSS)   GO TO 39
      N=1
      DO 38   K=3,KI,2 $ N=N+1
      U(N,JP)=U(K,JP) $ P(N,JP)=P(K,JP) $ R(N,JP)=R(K,JP)
      C(N,JP)=C(K,JP) $ D(N,JP)=D(K,JP) $ E(N,JP)=E(K,JP)
38    CONTINUE $ KI=N $ KO=KI+1 $ KOI=KO-1
39    KI1=KI+1 $ KZ=(KZ+1)/2     $ K=2*KI-3
      DO 40   N=KI1,KZ $ K=K+2
      U(N,JP)=U(K,JP) $ P(N,JP)=P(K,JP) $ R(N,JP)=R(K,JP)
      C(N,JP)=C(K,JP) $ D(N,JP)=D(K,JP) $ E(N,JP)=E(K,JP)
40    CONTINUE
      RNPA=RNPA+DNP $ DRNP=2.*DRNP
41    IF (KZ .GE. KO+2 .OR. .NOT. LSS)   GO TO 42
      LIMM=.TRUE. $ ASSIGN 44 TO JJ
42    TT=CSC*(R(2,JP)-R(1,JP))/AMAX1(C(1,JP),C(2,JP))
      IF (KI .EQ. 2 .OR. .NOT. LSS)   GO TO 44
      DO 43   K=3,KI $ M=K-1
43    TT=AMIN1(TT,CSC*(R(K,JP)-R(M,JP))/AMAX1(C(K,JP),C(M,JP)))
      IF (LIMM)   GO TO 44
44    IF (KZ .LT. 3)   GO TO 46
      DO 45   K=KO1,KZ $ M=K-1
45    TT=AMIN1(TT,CSC*(R(K,JP)-R(M,JP))/AMAX1(C(K,JP),C(M,JP)))
```

```
46    IF (LT .NE. KOUNT)   GO TO 58
      KOUNT=KOUNT+NOUT $ LOUT=.FALSE.
      TOUT=TBAR*T $  TOUT=TBAR*OUT
      WRITE (*,47) T,OUT,DTOUT,LT
47    FORMAT (1H1,4X3H TI E,E22.4/8X4HSTEP SIZE,E1 .6/8X11HSTEP NUMBER,
     1113//87X20H SO IC       PARTICLE/26X93H N      RADIUS       PRESSURE
     2      DENSITY       ENERGY       VELOCITY      VELOCITY     ITERATIONS)
      ROUT=RBAR*RBUBBLE       $ DOUT=DBAR*DBUBBLE $ COUT=VBAR*CBUBBLE
      POUT=PBAR*(PBUBBLE-1.) $ EOUT=EBAR*EBUBBLE $ UOUT=VBAR*UBUBBLE
      WRITE (6,48) ROUT,POUT,DOUT,EOUT,COUT,UOUT,ITERI
48    FORMAT (1H0,7X19H UNIFORM GAS BUBBLE,E16.4,5E13.4,I9)
      ROUT=RBAR*R(1,JP)       $ DOUT=DBAR*D(1,JP) $ COUT=VBAR*C(1,JP)
      POUT=PBAR*(P(1,JP)-1.) $ EOUT=EBAR*E(1,JP) $ UOUT=VBAR*U(1,JP)
      WRITE (6,49) ROUT,POUT,DOUT,EOUT,COUT,UOUT,ITERI
49    FORMAT (1H0,6X23H AIR CONTACT SURFACE  1P6E13.4,I9)
      IF (.NOT. LSS)   GO TO 54
      DO 50   K=2,NI
      ROUT=RBAR*R(K,JP)       $ DOUT=DBAR*D(K,JP) $ COUT=VBAR*C(K,JP)
      POUT=PBAR*(P(K,JP)-1.) $ EOUT=EBAR*E(K,JP) $ UOUT=VBAR*U(K,JP)
50    WRITE (6,51) K,ROUT,POUT,DOUT,EOUT,COUT,UOUT,ITERAT(K)
51    FORMAT (I3,6E13.4,I9)
      ROUT=RBAR*RSW(JP)          $ DOUT=DBAR*DSW(2,JP)
      UOUT=VBAR*USW(2,JP)        $ COUT=VBAR*CSW(2,JP)
      POUT=PBAR*(PSW(2,JP)-1.) $ EOUT=EBAR*ESW(2,JP)
      WRITE (6,52) ROUT,POUT,DOUT,EOUT,COUT,UOUT,ITERS
52    FORMAT (1H0,6X24H INTERIOR SHOCK WAVE,E16.4,5E13.4,I9)
      ROUT=RBAR*RSW(JP)          $ DOUT=DBAR*DSW(1,JP)
      UOUT=VBAR*USW(1,JP)        $ COUT=VBAR*CSW(1,JP)
      POUT=PBAR*(PSW(1,JP)-1.) $ EOUT=EBAR*ESW(1,JP)
      WRITE (6,53) ROUT,POUT,DOUT,EOUT,COUT,UOUT,ITERS
53    FORMAT (1H0,29X,6E13.4,I9)
54    IF (KZ .EQ. 1)   GO TO 56
      DO 55   K=KO,KZ
      ROUT=RBAR*R(K,JP)       $ DOUT=DBAR*D(K,JP) $ COUT=VBAR*C(K,JP)
      POUT=PBAR*(P(K,JP)-1.) $ EOUT=EBAR*E(K,JP) $ UOUT=VBAR*U(K,JP)
55    WRITE (6,51) K,ROUT,POUT,DOUT,EOUT,COUT,UOUT,ITERAT(K)
```

```
56    ROUT=RBAR*RSF(JP)       $ DOUT=DBAR*DSF(JP) $ COUT=VBAR*CSF(JP)
      POUT=PBAR*(PSF(JP)-1.) $ EOUT=EBAR*ESF(JP) $ UOUT=VBAR*USF(JP)
      WRITE (6,57) ROUT,POUT,DOUT,EOUT,COUT,UOUT,ITERSF
57    FORMAT (1H ,10X16H AIR SHOCK FRONT,E16.4,5E13.4,I9)
      GO TO JJ,(65,66)
58    IF (LOUT)   GO TO 60
      LOUT=.TRUE.
      WRITE (6,59)
59    FORMAT (1H1,31X15H TIME       STEP,62X6H POINT/19X29H TIME
     1STEP      NUMBER,24X43H RADIUS       PRESSURE      VELOCITY     INDEX)
60    TOUT=TBAR*T $ DTOUT=TBAR*DT $ ROUT=RBAR*RBUBBLE
      POUT=PBAR*(PBUBBLE-1.)        $ UOUT=VBAR*UBUBBLE
      WRITE (6,61) TOUT,DTOUT,LT,ROUT,POUT,UOUT
61    FORMAT (1H0,E28.4,E13.4,I7,3X19H UNIFORM GAS BUBBLE,E12.4,2E13.4)
      IF (.NOT. LSS)   GO TO 63
      ROUT=RBAR*RSW(JP) $ POUT=PBAR*(PS*(2,JP)-1.) $ UOUT=VBAR*USSW(JP)
      WRITE (6,62) ROUT,POUT,UOUT,KI
62    FORMAT (49X20H INTERIOR SHOCK WAVE,E12.4,2E13.4,I7)
63    KF=KZ $ IF (KZ .EQ. 1 .AND. LCHG2)   KF=0
      ROUT=RBAR*RSF(JP) $ POUT=PBAR*(PSF(JP)-1.) $ UOUT=VBAR*USSF(JP)
      WRITE (6,64) ROUT,POUT,UOUT,KF
64    FORMAT (53X16H AIR SHOCK FRONT,E12.4,2E13.4,I7)
      GO TO JJ,(65,66)
65    IF (RBAR*RSF(JP) .GE. RMAX .OR. LT .GE. NTS)   STOP
      DT=TT $ IF (.NOT. L*2)   GO TO 19
      IF (T .LT. T2 .OR. LSS)   GO TO 19
      IF (LCHG2)   GO TO 66
      T2=T $ LCHG2=.TRUE. $ LSS=.TRUE.
      WBUBLE=WBUBLE+W2/W1
      DBUBLE=DC*(RC1**3+RC2**3)/RBUBLE**3
      GO TO 67
66    IF (.NOT. L*3)   GO TO 19
      IF (T .LT. T3 .OR. LSS)   GO TO 19
      IF (LCHG3)   GO TO 19
      T3=T $ LCHG3=.TRUE. $ LSS=.TRUE.
      WBUBLE=WBUBLE+W3/W1
      DBUBLE=DC*(RC1**3+RC2**3+RC3**3)/RBUBLE**3
```

```
67    EBUBLE=WBUBLE/(4.188790*DBUBLE*RBUBLE**3)
      PBUBLE=(A1+A2*DBUBLE)*DBUBLE*EBUBLE+A3*DBUBLE**3
      CBUBLE=SQRT((A1+2.*A2*DBUBLE)*EBUBLE+3.*A3*DBUBLE**2+(A1+A2*
     1DBUBLE)*PBUBLE/DBUBLE)
      PSW(1,JP)=P(1,JP) $ USW(1,JP)=U(1,JP) $ RSW(1,JP)=R(1,JP)
      DSW(1,JP)=D(1,JP) $ CSW(1,JP)=C(1,JP) $ ESW(1,JP)=E(1,JP)
      PSW(2,JP)=PBUBLE
      DSW(2,JP)=DSW(1,JP)*(GP1*PSW(2,JP)+GM1*PSW(1,JP))/(GM1*PSW(2,JP)+
     1GP1*PSW(1,JP))
      ESW(2,JP)=PSW(2,JP)/(GM1*DSW(2,JP))
      CSW(2,JP)=SQRT(G*PSW(2,JP)/DSW(2,JP))
      USW(2,JP)=USW(1,JP)+SQRT((PSW(2,JP)-PSW(1,JP))*(1./DSW(1,JP)-1./
     1DSW(2,JP)))
      USSW(JP)=(DSW(2,JP)*USW(2,JP)-DSW(1,JP)*USW(1,JP))/(DSW(2,JP)-
     1DSW(1,JP))
      P(1,JP)=PSW(2,JP) $ U(1,JP)=USW(2,JP) $ E(1,JP)=ESW(2,JP)
      D(1,JP)=DSW(2,JP) $ C(1,JP)=CSW(2,JP) $ UBUBLE=USW(2,JP)
      GO TO 19
68    IF (KO .EQ. 0)   GO TO 69
      KO=0 $ KZ=1
      CALL CSD (KI)
      TX=T+DTX
69    IF (LSC)   GO TO 71
      IF (T+TT .LT. TX)   GO TO 70
      TT=TX-T $ LSC=.TRUE.
70    DT=TT   $ GO TO 19
71    USF(JP)=USX4 $ PSF(JP)=PSX4 $ ESF(JP)=ESX4 $ USSF(JP)=USSX4
      CSF(JP)=CSX4 $ DSF(JP)=DSX4 $ RSF(JP)=RSX  $ LOUT=.FALSE.
      POUT=PBAR*(PSX1-1.) $ EOUT=EBAR*ESX1 $ UOUT=VBAR*USX1
      DOUT=DBAR*DSX1      $ COUT=VBAR*CSX1 $ USOUT=VBAR*USSX1
      WRITE (6,72) POUT,DOUT,EOUT,COUT,UOUT,USOUT
72    FORMAT (1H0////42X48HIMPEDANCE MISMATCH AT POINT OF SHOCK COALESCE
     1NCE//80X32H SONIC      PARTICLE       SHOCK/40X74H PRESSURE      D
     2ENSITY      ENERGY      VELOCITY     VELOCITY     VELOCITY/17X5H (
     3T=)/22X16H AIR SHOCK FRONT,E12.4,5E13.4)
```

```
      POUT=PBAR*(PSX2-1.) $ EOUT=EBAR*ESX2 $ UOUT=VBAR*USX2
      DOUT=DBAR*DSX2      $ COUT=VBAR*CSX2 $ USOUT=VBAR*USSX2
      WRITE (6,73) POUT,DOUT,EOUT,COUT,UOUT,USOUT
   73 FORMAT (18X20H INTERIOR SHOCK WAVE,E12.4,5E13.4)
      POUT=PBAR*(PSX3-1.) $ EOUT=EBAR*ESX3 $ UOUT=VBAR*USX3
      DOUT=DBAR*DSX3      $ COUT=VBAR*CSX3
      WRITE (6,74) POUT,DOUT,EOUT,COUT,UOUT
   74 FORMAT (17X5H (T*)/21X17H RAREFACTION WAVE,E12.4,4E13.4)
      POUT=PBAR*(PSX4-1.) $ EOUT=EBAR*ESX4 $ UOUT=VBAR*USX4
      DOUT=DBAR*DSX4      $ COUT=VBAR*CSX4 $ USOUT=VBAR*USSX4
      WRITE (6,75) POUT,DOUT,EOUT,COUT,UOUT,USOUT
   75 FORMAT (22X16H AIR SHOCK FRONT,E12.4,5E13.4)
      DRNP=.5*DM*DSF(JP)/D0
      RNPA=RSF(JP)+.2*(DM-(D(KI,JP)+DSF(JP))*(RSF(JP)-R(KI,JP)))/D0
      KZ=KI $ KO=2  $ LSS=.FALSE. $ LIMM=.FALSE.
      KI=1  $ KO1=3 $ LSC=.FALSE. $ ASSIGN 65 TO J1 $ GO TO 65
      END
```

```
      SUBROUTINE ITS
      COMMON /MISCV/ A1,A2,A3,DELTAP,DELTAU,DT,DTH,DTHNU,G,GM1,GP1,
     1               ITERAT(500),ITERI,ITERSF,ITERSW,J,JP,NU,PO
     2      /FIELD/ C(500,2),D(500,2),E(500,2),P(500,2),R(500,2),
     2               U(500,2)
     3      /RUVAR/ CBUBLE,DBUBLE,EBUBLE,PBUBLE,RBUBLE,UBUBLE,WBUBLE
     4      /SFVAR/ CSF(2),DSF(2),ESF(2),PSF(2),RSF(2),USF(2),USSF(2)
      REAL NU
      PSF(2)=PSF(1) $ CSF(2)=CSF(1) $ USSF(2)=USSF(1)
      DSF(2)=DSF(1) $ USF(2)=USF(1)
      P(1,2)=P(1,1) $ C(1,2)=C(1,1) $ U(1,2)=U(1,1)
      D(1,2)=D(1,1) $ E(1,2)=E(1,1)
      UA=UB=U(1,1) $ PSAVI=PSAVSF=0. $ DBUB=DBUBLE
      CA=CB=C(1,1) $ USAVI=USAVSF=0. $ ITERI=0
100   ITERI=ITERI+1 $ IF (ITERI .GT. 200)    STOP
      RSF(2)=RSF(1)+DTH*(USSF(1)+USSF(2))
      DRSF=RSF(2)-RSF(1) $ DTHRB=DTH/DRSF $ APSF=(PSF(2)-PSF(1))/DRSF
      AUSF=(USF(2)-USF(1))/DRSF                $ ADSF=(DSF(2)-DSF(1))/DRSF
      R(1,2)=R(1,1)+DTH*(U(1,1)+U(1,2))
      Y=DTRB*(U(1,2)-C(1,2)+UB-CB) $ RB=(R(1,2)-Y*RSF(2))/(1.-Y)
      DTHNUB=DTRB*(RSF(2)-RB)*NU    $ DRB=RB-RSF(1)
      PB=PSF(1)+DRB*APSF $ UB=USF(1)+DRB*AUSF
      DB=DSF(1)+DRB*ADSF $ CB=SQRT(G*PB/DB)
      DBUBLE=DBUB*(R(1,1)/R(1,2))**3 $ Y1=(A1+A2*DBUBLE)*DBUBLE
      Y2=.5*Y1*(1./DBUBLE-1./DBUB)    $ Y3=A3*DBUBLE**3
      P(1,2)=(Y1*EBUBLE-Y2*P(1,1)+Y3)/(1.+Y2)
      D(1,2)=D(1,1)*(GP1*P(1,2)+GM1*P(1,1))/(GM1*P(1,2)+GP1*P(1,1))
      E(1,2)=P(1,2)/(GM1*D(1,2))
      C(1,2)=SQRT(G*P(1,2)/D(1,2))
      U(1,2)=UB+.5*(P(1,2)-PB)*(1./(D(1,2)*C(1,2))+1./(DB*CB))+
     1DTHNUB*(C(1,2)*U(1,2)/R(1,2)+CB*UB/RB)
```

```
      DRI=R(1,2)-R(1,1)          $ API=(P(1,2)-P(1,1))/DRI
      AUI=(U(1,2)-U(1,1))/DRI $ AUI=(U(1,2)-U(1,1))/DRI $ DTRA=DTH/DRI
      Y=DTRA*(USF(2)+CSF(2)+UA*CA) $ RA=(RSF(2)-Y*R(1,2))/(1.-Y)
      DTHNDA=DTRA*(R(1,2)-RA)*NU    $ DRA=RA-R(1,1)
      PA=P(1,1)+DRA*API $ UA=U(1,1)+DRA*AUI
      DA=D(1,1)+DRA*DRI $ CA=SQRT(G*PA/DA)
      X1=1./D0-1./DSF(2)          $ X2=1./(DSF(2)*CSF(2))+1./(DA*CA)
      X3=1.+DTHNDA*CSF(2)/RSF(2) $ X4=X3/X2 $ X5=X1*X4**2
      X6=X5+PA+2.*(UA-DTHNDA*CA*UA/RA)/X2
      PSF(2)=X5+X6-2.*X4*SQRT(X1*(X6-P0))
      DSF(2)=D0*((GP1*PSF(2)+GM1*P0)/(GM1*PSF(2)+GP1*P0)
      ESF(2)=PSF(2)/(GM1*DSF(2))
      CSF(2)=SQRT(G*PSF(2)/DSF(2))
      X1=1./D0-1./DSF(2)
      USF(2)=SQRT(X1*(PSF(2)-P0))
      USSF(2)=USF(2)/(D0*X1)
      IF (ABS(1.-PSA1/P(1,2)) .LT. DELTAP .AND. ABS(1.-PSAVSF/PSF(2))
     1.LT. DELTAP .AND. ABS(1.-USAV1/U(1,2)) .LT. DELTAU .AND. ABS(1.-
     2USAVSF/USF(2)) .LT. DELTAU)   GO TO 101
      PSAVSF=PSF(2) $ PSAV1=P(1,2)
      USAVSF=USF(2) $ USAV1=U(1,2) $ GO TO 100
  101 RBUBLE=R(1,2) $ PBUBLE=P(1,2)
      UBUBLE=U(1,2) $ EBUBLE=(PBUBLE-Y3)/Y1
      CBUBLE=SQRT((A1+2.*A2*UBUBLE)*EBUBLE+3.*A3*UBUBLE**2+(A1+A2*
     1UBUBLE)*PBUBLE/DBUBLE)
      ABUBLE=4.18879 2*DBUBLE*EBUBLE*RBUBLE**3
      ITERSF=ITER1
      U(2,2)=USF(2) $ P(2,2)=PSF(2) $ R(2,2)=RSF(2)
      C(2,2)=CSF(2) $ D(2,2)=DSF(2) $ E(2,2)=ESF(2)
      RETURN
      END
```

```
      SUBROUTINE ISP

      COMMON /MISCV/ A1,A2,A3,DELTAP,DELTAU,DT,DTH,DTHNU,G,GM1,GP1,
     1               ITERAT(500),ITERI,ITERSF,ITERSW,J,JP,NU,P0,P0
     2      /FIELD/ C(500,2),D(500,2),E(500,2),P(500,2),R(500,2),
     2               U(500,2)
     3      /RUVAR/ CRUBLE,DRUBLE,ERUBLE,PRUBLE,RRUBLE,URUBLE,WRUBLE
     4      /SWVAR/ CSW(2,2),DSW(2,2),ESW(2,2),PSW(2,2),RSW(2),
     5               USW(2,2),USSW(2)
      REAL NU
      P(1,JP)=P(1,J) $ U(1,JP)=U(1,J) $ RSW(2,JP)=RSW(2,J)
      D(1,JP)=D(1,J) $ C(1,JP)=C(1,J) $ USSW(JP)=USSW(J)
      K0=2  $ USW(1,JP)=USW(1,J) $ UP=U(2,J)
      K01=3 $ CSW(1,JP)=CSW(1,J) $ UAP=USW(1,J) $ UBP=U(3,J)
      K02=4 $ DSW(1,JP)=DSW(1,J) $ CAP=CSW(1,J) $ CBP=C(3,J)
      UA=UB=U(1,J) $ PSAVI=PSAVSW=0. $ DRUB=DBUBLE
      CA=CB=C(1,J) $ USAVI=USAVSW=0. $ ITERI=0
      DR1=R(K01,J)-R(K0,J) $ DR2=RSW(J)-R(K0,J) $  ET=DR2*DR1*(DR2-DR1)
      XU=DR1*(USW(1,J)-U(K0,J)) $ YU=DR2*(U(K01,J)-U(K0,J))
      XP=DR1*(PSW(1,J)-P(K0,J)) $ YP=DR2*(P(K01,J)-P(K0,J))
      XD=DR1*(DSW(1,J)-D(K0,J)) $ YD=DR2*(D(K01,J)-D(K0,J))
      AU1=(DR2*YU-DR1*XU)/DET $ BU1=(XU-YU)/DET
      AP1=(DR2*YP-DR1*XP)/DET $ BP1=(XP-YP)/DET
      AD1=(DR2*YD-DR1*XD)/DET $ BD1=(XD-YD)/DET
      DR1=R(K02,J)-R(K01,J) $ DR2=R(K0,J)-R(K01,J)
      DET=DR2*DR1*(DR2-DR1)
      XU=DR1*(U(K0,J)-U(K01,J)) $ YU=DR2*(U(K02,J)-U(K01,J))
      XP=DR1*(P(K0,J)-P(K01,J)) $ YP=DR2*(P(K02,J)-P(K01,J))
      XD=DR1*(D(K0,J)-D(K01,J)) $ YD=DR2*(D(K02,J)-D(K01,J))
      AU2=(DR2*YU-DR1*XU)/DET $ BU2=(XU-YU)/DET
      AP2=(DR2*YP-DR1*XP)/DET $ BP2=(XP-YP)/DET
      AD2=(DR2*YD-DR1*XD)/DET $ BD2=(XD-YD)/DET
```

```
200   ITERI=ITERI+1 $ IF (ITERI .GT. 200)   STOP
      RSW(JP)=RSW(J)+DTH*(USSW(J)+USSW(JP))
      PSAVP=USAVP=0.
201   RP=RSW(JP)-DTH*(US*(1,JP)+UP) $ DRP=RP-R(KO,J)
      PP=P(KO,J)+DRP*(AP1+DRP*BP1) $ UP=U(KO,J)+DR*(AU1+DRP*BU1)
      DP=D(KO,J)+DRP*(AD1+DRP*BD1) $ CP=SQRT(G*PP/DP)
      RAP=RSW(JP)-DTH*(US*(1,JP)+CSW(1,JP)+UAP+CAP) $ DRAP=RAP-R(KO,J)
      PAP=P(KO,J)+DRAP*(AP1+DRAP*BP1) $ UAP=U(KO,J)+DRAP*(AU1+DRAP*BU1)
      DAP=D(KO,J)+DRAP*(AD1+DRAP*BD1) $ CAP=SQRT(G*PAP/DAP)
      RBP=RSW(JP)-DTH*(US*(1,JP)-CSW(1,JP)+UBP-CBP)
      IF (RBP .GT. R(KO1,J))   GO TO 202
      DRBP=RBP-R(KO,J)
      PBP=P(KO,J)+DRBP*(AP1+DRBP*BP1) $ UBP=U(KO,J)+DRBP*(AU1+DRBP*BU1)
      DBP=D(KO,J)+DRBP*(AD1+DRBP*BD1) $ CBP=SQRT(G*PBP/DBP) $ GO TO 203
202   DRBP=RBP-R(KO1,J)
      PBP=P(KO1,J)+DRBP*(AP2+DRBP*BP2) $UBP=U(KO1,J)+DRBP*(AU2+DRBP*BU2)
      DBP=D(KO1,J)+DRBP*(AD2+DRBP*BD2) $CBP=SQRT(G*PBP/DBP)
203   Z1=1./(DSW(1,JP)*CSW(1,JP)) $ Z2=CSW(1,JP)*USW(1,JP)/RSW(JP)
      Z1A=.5*(Z1+1./(DAP*CAP))     $ Z2A=Z2+CAP*UAP/RAP
      Z1B=.5*(Z1+1./(DBP*CBP))     $ Z2B=Z2+CBP*UBP/RBP
      ZA=UAP+PAP*Z1A-DTHNU*Z2A
      PSW(1,JP)=(ZA-UBP+PBP*Z1B-DTHNU*Z2P)/(Z1A+Z1B)
      USW(1,JP)=ZA-PSW(1,JP)*Z1A
      DSW(1,JP)=DP*(GP1*PSW(1,JP)+GM1*PP)/(GM1*PSW(1,JP)+GP1*PP)
      CSW(1,JP)=SQRT(G*PSW(1,JP)/DSW(1,JP))
      IF (ABS(1.-PSAVP/PSW(1,JP)) .LT. DELTAP .AND. ABS(1.-USAVP/
     1USW(1,JP)) .LT. DELTAU)   GO TO 204
      PSAVP=PSW(1,JP) $ USAVP=USW(1,JP) $ GO TO 201
204   IF (ITERI .GT. 1)   GO TO 205
      DSW(2,JP)=DSW(1,JP)*(GP1*PSW(2,JP)+GM1*PSW(1,JP))/(GM1*PSW(2,JP)+
     1GP1*PSW(1,JP))
      USW(2,JP)=USW(1,JP)+SQRT((PSW(2,JP)-PSW(1,JP))*(1./DSW(1,JP)-1./
     1DSW(2,JP)))
      CSW(2,JP)=SQRT(G*PSW(2,JP)/DSW(2,JP))
205   DRSW=RSW(JP)-RSW(J)                $ APSW=(PSW(2,JP)-PSW(2,J))/DRSW
      AUSW=(USW(2,JP)-USW(2,J))/DRSW $ ADSW=(DSW(2,JP)-DSW(2,J))/DRSW
```

```
R(1,JP)=R(1,J)+DTH*(U(1,J)+U(1,JP)) $ DTRB=DTH/DBSW
Y=DTRB*(U(1,JP)-C(1,JP)+UB-CB) $ RB=(R(1,JP)-Y*RSW(JP))/(1.-Y)
DTHNUB=DTRB*(RSW(JP)-RB)*NU $ DRB=RB-RSW(J)
PB=PSW(2,J)+DRB*APSW $ UB=USW(2,J)+DRB*AUSW
DB=DSW(2,J)+DRB*ADSW $ CB=SQRT(G*PB/DB)
DBUBLE=DBUB*(R(1,J)/R(1,JP))**3 $ Y1=(A1+A2*BUBLE)*DBUBLE
Y2=.5*Y1*(1./DBUBLE-1./DBUB) $ Y3=A3*DBUBLE**3
P(1,JP)=(Y1*EBUBLE-Y2*P(1,J)+Y3)/(1.+Y2)
D(1,JP)=D(1,J)*(GP1*P(1,JP)+GM1*P(1,J))/(GM1*P(1,JP)+GP1*P(1,J))
E(1,JP)=P(1,JP)/(GM1*D(1,JP))
C(1,JP)=SQRT(G*P(1,JP)/D(1,JP))
U(1,JP)=UB+.5*(P(1,JP)-PB)*(1./(D(1,JP)*C(1,JP))+1./(DB*CB))+
1DTHNUB*(C(1,JP)*U(1,JP)/R(1,JP)+CB*UB/RB)
DRI=R(1,JP)-R(1,J) $ API=(P(1,JP)-P(1,J))/DRI
AUI=(U(1,JP)-U(1,J))/DRI $ ADI=(D(1,JP)-D(1,J))/DRI $ DTRA=DTH/DRI
Y=DTRA*(USW(2,JP)+CSW(2,JP)+UA+CA) $ RA=(RSW(JP)-Y*R(1,JP))/(1.-Y)
DTHNUA=DTRA*(R(1,JP)-RA)*NU $ DRA=RA-R(1,J)
PA=P(1,J)+DRA*API $ UA=U(1,J)+DRA*AUI
DA=D(1,J)+DRA*ADI $ CA=SQRT(G*PA/DA)
X1=1./DSW(1,JP)-1./DSW(2,JP)
X2=1./(DSW(2,JP)*CSW(2,JP))+1./(DA*CA)
X3=1.+DTHNUA*CSW(2,JP)/RSW(JP) $ X4=X3/X2 $ X5=X1*X4**2
X6=X5+PA+2.*(UA-USW(1,JP)-DTHNUA*(CSW(2,JP)*USW(1,JP)/RSW(JP)+
1CA*UA/RA))/X2
PSW(2,JP)=X5+X6-2.*X4*SQRT(X1*(X6-PSW(1,JP)))
DSW(2,JP)=DSW(1,JP)*(GP1*PSW(2,JP)+GM1*PSW(1,JP))/(GM1*PSW(2,JP)+
1GP1*PSW(1,JP))
CSW(2,JP)=SQRT(G*PSW(2,JP)/DSW(2,JP))
USW(2,JP)=USW(1,JP)+SQRT((PSW(2,JP)-PSW(1,JP))*(1./DSW(1,JP)-1./
1DSW(2,JP)))
USSW(JP)=(DSW(2,JP)*USW(2,JP)-DSW(1,JP)*USW(1,JP))/(DSW(2,JP)-
1DSW(1,JP))
```

```
      IF (ABS(1.-PSAVI/P(1,JP)) .LT. DELTAP .AND. ABS(1.-PSAVSW/
     1PSW(2,JP)) .LT. DELTAP .AND. ABS(1.-USAVI/U(1,JP)) .LT. DELTAU
     2 .AND. ABS(1.-USAVSW/USW(2,JP)) .LT. DELTAU)   GO TO 206
      PSAVSW=PSW(2,JP) $ PSAVI=P(1,JP)
      USAVSW=USW(2,JP) $ USAVI=U(1,JP) $ GO TO 200
  206 RBUBLE=R(1,JP) $ PBUBLE=P(1,JP)
      UBUBLE=U(1,JP) $ EBUBLE=(PBUBLE-Y3)/Y1
      CBUBLE=SQRT((A1+2.*A2*UBUBLE)*EBUBLE+3.*A3*UBUBLE**2+(A1+A2*
     1DBUBLE)*PBUBLE/DBUBLE)
      WBUBLE=4.1A879-2*DBUBLE*EBUBLE*RBUBLE**3
      ESW(1,JP)=PSW(1,JP)/(GM1*DSW(1,JP))
      ESW(2,JP)=PSW(2,JP)/(GM1*DSW(2,JP))
      ITERSW=ITER1
      RETURN
      END
```

```
      SUBROUTINE CSD (KI)

      COMMON /MISCV/ A1,A2,A3,DELTAP,DELTAU,DT,DTH,DTHNU,G,GM1,GP1,
     1               ITERAT(500),ITER1,ITERSF,ITERSW,J,JP,NU,P0,R0
     2      /FIELD/ C(500,2),D(500,2),E(500,2),P(500,2),R(500,2),
     2               U(500,2)
     3      /SFVAR/ CSF(2),DSF(2),ESF(2),PSF(2),RSF(2),USF(2),USSF(2)
     4      /SWVAR/ CSW(2,2),DSW(2,2),ESW(2,2),PSW(2,2),RSW(2),
     5               USW(2,2),USSW(2)
     6      /SCVAR/ DTX,RSX,CSX1,CSX2,CSX3,CSX4,DSX1,DSX2,DSX3,DSX4,
     7               ESX1,ESX2,ESX3,ESX4,PSX1,PSX2,PSX3,PSX4,USX1,USX2,
     8               USX3,USX4,USSX1,USSX2,USSX4
      REAL NU
      USX1=USF(JP) $ UA=U(KI,JP)     $ UB=USW(1,JP)    $ PSAVX2=0.
      CSX1=CSF(JP) $ CA=C(KI,JP)     $ CB=CSW(1,JP)    $ USAVX2=0.
      DSX1=DSF(JP) $ USSX1=USSF(JP) $ USSX2=USSW(JP) $ ITERX=0
      DRS=RSF(JP)-RSW(JP)            $ APS=(PSF(JP)-PSW(1,JP))/DRS
      AUS=(USF(JP)-USW(1,JP))/DRS    $ AUS=(USF(JP)-USW(1,JP))/DRS
300   ITERX=ITERX+1 $ IF (ITERX .GT. 200)   STOP
      PSAVX1=USAVX1=0.
301   DTX=2.*DRS/(USSW(JP)+USSX2-USSF(JP)-USSX1)
      DTHX=DTX/2. $ DTHNUX=DTHX*NU
      RSX=RSF(JP)+DTHX*(USSF(JP)+USSX1)
      RHS=RSX-DTHX*(USX1+CSX1+UB+CB) $ DRH=RHS-RSW(JP)
      PB=PSW(1,JP)+DRH*APS $ UB=USW(1,JP)+DRH*AUS
      DB=DSW(1,JP)+DRH*AUS $ CB=SQRT(G*PB/DB)
      X1=1./D0-1./DSX1       $ X2=1./(DSX1*CSX1)+1./(UP+CB)
      X3=1.+DTHNUX*CSX1/RSX $ X4=X3/X2 $ X5=X1*X4**2
      X6=X5+PP+2.*(UA-DTHNUX*CB*UP/RH)/X2
      PSX1=X5+X6-2.**X4*SQRT(X1*(X6-P0))
      DSX1=D0*(GP1*PSX1+GM1*P0)/(GM1*PSX1+GP1*P0)
      ESX1=PSX1/(GM1*DSX1)
      CSX1=SQRT(G*PSX1/DSX1)
      USX1=SQRT((PSX1-P0)*(1./D0-1./DSX1))
      USSX1=USX1*DSX1/(DSX1-D0)
```

```
      IF (ABS(1.-PSAVX1/PSA1) .LT. DELTAP .AND. ABS(1.-USAVX1/USA1) .
     1DELTAU)   GO TO 302
      PSAVX1=PSX1 $ USAVX1=USX1 $ GO TO 301
  302 IF (ITERX .GT. 1)   GO TO 303
      PSX2=PSW(2,JP)
      DSX2=USX1*(GP1*PSX2+GM1*PSX1)/(GM1*PSX2+GP1*PSX1)
      USX2=USX1+SQRT((PSX2-PSX1)*(1./DSX1-1./DSX2))
      CSX2=SQRT(G*PSX2/DSX2)
  303 RA=RSX-DTHX*(USX2+CSX2+UA+CA) $ K=KI+1
  304 K=K-1   $ IF (R(K,JP) .GT. RA)   GO TO 304
      K1=K+1 $ IF (K .EQ. KI)   GO TO 305
      DRA=(RA-R(K,JP))/(R(K1,JP)-R(K,JP))
      PA=P(K,JP)+DRA*(P(K1,JP)-P(K,JP))
      UA=U(K,JP)+DRA*(U(K1,JP)-U(K,JP))
      DA=D(K,JP)+DRA*(D(K1,JP)-D(K,JP)) $ GO TO 306
  305 DRA=(RA-R(K,JP))/(RSW(JP)-R(K,JP))
      PA=P(K,JP)+DRA*(PSW(2,JP)-P(K,JP))
      UA=U(K,JP)+DRA*(USW(2,JP)-U(K,JP))
      DA=D(K,JP)+DRA*(DSW(2,JP)-D(K,JP))
  306 CA=SQRT(G*PA/DA)
      X1=1./DSX1-1./DSX2     $ X2=1./(DSX2*CSX2)+1./(DA*CA)
      X3=1.+DTHNUX*CSX2/RSX $ X4=X3/X2 $ X5=X1*X4**2
      X6=X5+PA+2.*(UA-USX1-DTHNUX*(CSX2*USX1/RSX+CA*UA/RA))/X2
      PSX2=X5+X6-2.*X4*SQRT(X1*(X6-PSX1))
      DSX2=DSX1*(GP1*PSX2+GM1*PSX1)/(GM1*PSX2+GP1*PSX1)
      ESX2=PSX2/(GM1*DSX2)
      CSX2=SQRT(G*PSX2/DSX2)
      USX2=USX1+SQRT((PSX2-PSX1)*(1./DSX1-1./DSX2))
      USSX2=(DSX2*USX2-DSX1*USX1)/(DSX2-DSX1)
```

```
      IF (ABS(1.-PSAVX2/PSX2) .LT. DELTAP .AND. ABS(1.-USAVX2/USX2) .LT.
     1DELTAU)   GO TO 307
      PSAVX2=PSX2 $ USAVX2=USX2 $ GO TO 300
  307 PSAV=0. $ Y1=2.*CSX2/G-1 $ USX3=USX2
      USAV=0. $ Y2=G-1/(2.*G)
  308 X1=D0*USX3**2
      PSX3=P0*GP1*X1/4.+SQRT(X1*(G*P0+X1*GP1**2/16.))
      USX3=.5*(USX3+USX2+Y1*(1.-(PSX3/PSX2)**Y2))
      IF (ABS(1.-PSAV/PSX3) .LT. DELTAP .AND. ABS(1.-USAV/USX3) .LT.
     1DELTAU)   GO TO 309
      PSAV=PSX3 $ USAV=USX3 $ GO TO 308
  309 PSX4=PSX3 $ USX4=USX3
      DSX3=DSX2*(PSX3/PSX2)**(1./G)
      DSX4=D0*(GP1*PSX4+GM1*P0)/(GM1*PSX4+GP1*P0)
      ESX3=PSX3/(GM1*DSX3)
      ESX4=PSX4/(GM1*DSX4)
      CSX3=SQRT(G*PSX3/DSX3)
      CSX4=SQRT(G*PSX4/DSX4)
      USSX4=USX4*DSX4/(DSX4-D0)
      RETURN
      END
```

```
      SUBROUTINE RSD (K1)

      COMMON /MISCV/ A1,A2,A3,DELTAP,DELTAU,DT,DTH,DTHRO,G,GM1,GP1,
     1               ITERAT(500),ITERI,ITERSF,ITERSW,J,JP,NU,DO,PO
     2       /FIELD/ C(500,2),D(500,2),E(500,2),P(500,2),R(500,2),
     2               U(500,2)
     3       /RUVAR/ CDOUBLE,DRDOUBLE,EDOUBLE,PDOUBLE,RDOUBLE,UDOUBLE,WDOUBLE
      REAL NU
      U(1,JP)=U(1,J) $ UB=U(2,J) $ PSAV=0.
      C(1,JP)=C(1,J) $ CB=C(2,J) $ USAV=0.
      D(1,JP)=D(1,J) $ DRDUB=DRDUBLE
      IF (K1 .GT. 2)   GO TO 400
      DR=R(1,J)-R(2,J)
      AU=(U(1,J)-U(2,J))/DR $ BU=0.
      AP=(P(1,J)-P(2,J))/DR $ BP=0.
      AD=(D(1,J)-D(2,J))/DR $ BD=0. $ GO TO 401
400   DR1=R(3,J)-R(2,J) $ DR2=R(1,J)-R(2,J) $ DET=DR2*DR1*(DR2-DR1)
      XU=DR1*(U(1,J)-U(2,J)) $ YU=DR2*(U(3,J)-U(2,J))
      XP=DR1*(P(1,J)-P(2,J)) $ YP=DR2*(P(3,J)-P(2,J))
      XD=DR1*(D(1,J)-D(2,J)) $ YD=DR2*(D(3,J)-D(2,J))
      AU=(DR2*YU-DR1*XU)/DET $ BU=(XU-YU)/DET
      AP=(DR2*YP-DR1*XP)/DET $ BP=(XP-YP)/DET
      AD=(DR2*YD-DR1*XD)/DET $ BD=(XD-YD)/DET
401   ITERI=0
402   ITERI=ITERI+1 $ IF (ITERI .GT. 200)   STOP
      R(1,JP)=R(1,J)+DTH*(U(1,J)+U(1,JP))
      RB=R(1,JP)-DTH*(U(1,JP)-C(1,JP)+UB-CB) $ DRB=RB-R(2,J)
      PB=P(2,J)+DRB*(AP+DRB*BP) $ DB=D(2,J)+DRB*(AD+DRB*BD)
      UB=U(2,J)+DRB*(AU+DRB*BU) $ CB=SQRT(G*PB/DB)
```

```
      DBUBLE=DBUB*(R(1,J)/R(1,JP))**3 $ Y1=(A1+A2*DBUBLE)*DBUBLE
      Y2=.5*Y1*(1./DBUBLE-1./DBUB)     $ Y3=A3*DBUBLE**2
      P(1,JP)=(Y1*EBUBLE-Y2*P(1,J)+Y3)/(1.+Y2)
      D(1,JP)=D(1,J)*(GP1*P(1,JP)+GM1*P(1,J))/(GM1*P(1,JP)+GP1*P(1,J))
      E(1,JP)=P(1,JP)/(GM1*D(1,JP))
      C(1,JP)=SQRT(G*P(1,JP)/D(1,JP))
      U(1,JP)=UB+.5*(P(1,JP)-PB)*(1./(D(1,JP)*C(1,JP))+1./(DB*CB))+
     1DTHNU*(C(1,JP)*U(1,JP)/R(1,JP)+CB*UB/RB)
      IF (ABS(1.-PSAV/P(1,JP)) .LT. DELTAP .AND. ABS(1.-USAV/U(1,JP))
     1.LT. DELTAU)    GO TO 403
      PSAV=P(1,JP)    $ USAV=U(1,JP)    $ GO TO 402
  403 PBUBLE=P(1,JP) $ UBUBLE=U(1,JP) $ RBUBLE=R(1,JP)
      EBUBLE=(P(1,JP)-Y3)/Y1
      CBUBLE=SQRT((A1+2.*A2*DBUBLE)*EBUBLE+3.*A3*DBUBLE**2+(A1+A2*
     1DBUBLE)*PBUBLE/DBUBLE)
      WBUBLE=4.188792*DBUBLE*EBUBLE*RBUBLE**3
      RETURN
      END
```

```
      SUBROUTINE DIP (K)

      COMMON /MISCV/ A1,A2,A4,DELTAP,DELTAU,DT,DTH,DTHMU,G,GM1,GP1,
     1               ITERAT(500),ITER1,ITERSF,ITERSW,J,JP,MU,P0,P0
     2      /FIELD/ C(500,2),D(500,2),E(500,2),P(500,2),R(500,2),
     3               U(500,2)
     3      /SWVAR/ CSW(2,2),DSW(2,2),ESW(2,2),PSW(2,2),RSW(2),
     4               USW(2,2),USSW(2)
      REAL MU
      KM1=K-1 $ UA=U(KM1,J) $ U(K,JP)=U(K,J)
      KP1=K+1 $ CA=C(KM1,J) $ C(K,JP)=C(K,J)
      PSAV=0. $ DB=U(KP1,J) $ D(K,JP)=D(K,J)
      USAV=0. $ CB=C(KP1,J)
      DR1=R(KP1,J)-R(K,J) $ DR2=R(KM1,J)-R(K,J) $ DET=DR2*DR1*(DR2-DR1)
      XU=DR1*(U(KM1,J)-U(K,J)) $ YU=DR2*(U(KP1,J)-U(K,J))
      XP=DR1*(P(KM1,J)-P(K,J)) $ YP=DR2*(P(KP1,J)-P(K,J))
      XD=DR1*(D(KM1,J)-D(K,J)) $ YD=DR2*(D(KP1,J)-D(K,J))
      AU=(DR2*YU-DR1*XU)/DET $ BU=(XU-YU)/DET
      AP=(DR2*YP-DR1*XP)/DET $ BP=(XP-YP)/DET
      AD=(DR2*YD-DR1*XD)/DET $ BD=(XD-YD)/DET
      ITERAT(K)=
500   ITERAT(K)=ITERAT(K)+1 $ IF (ITERAT(K) .GT. 200)   STOP
      R(K,JP)=R(K,J)+DTH*(U(K,JP)+U(K,J))
      RA=R(K,JP)-DTH*(U(K,JP)+C(K,JP)+UA+CA) $ DRA=RA-R(K,J)
      RB=R(K,JP)-DTH*(U(K,JP)-C(K,JP)+UB-CB) $ DRB=RB-R(K,J)
      UA=U(K,J)+DRA*(AU+DRA*BU) $ UB=U(K,J)+DRB*(AU+DRB*BU)
      PA=P(K,J)+DRA*(AP+DRA*BP) $ PB=P(K,J)+DRB*(AP+DRB*BP)
      DA=D(K,J)+DRA*(AD+DRA*BD) $ DB=D(K,J)+DRB*(AD+DRB*BD)
      CA=SQRT(G*PA/DA)          $ CB=SQRT(G*PB/DB)
```

```
Z1=1./(D(K,JP)*C(K,JP)) $ Z2=C(K,JP)*U(K,JP)/R(K,JP)
Z1A=.5*(Z1+1./(DA*CA))  $ Z2A=Z2+CA*UA/RA
Z1B=.5*(Z1+1./(DB*CB))  $ Z2B=Z2+CB*UB/RB
ZA=UA+PA*Z1A-DTHNU*Z2A
P(K,JP)=(ZA-UB+PB*Z1B-DTHNU*Z2B)/(Z1A+Z1B)
U(K,JP)=ZA-P(K,JP)*Z1A
D(K,JP)=D(K,J)*(GP1*P(K,JP)+GM1*P(K,J))/(GM1*P(K,JP)+GP1*P(K,J))
E(K,JP)=P(K,JP)/(GM1*D(K,JP))
C(K,JP)=SQRT(G*P(K,JP)/D(K,JP))
IF (ABS(1.-PSAV/P(K,JP)) .LT. DELTAP .AND. ABS(1.-USAV/
1U(K,JP)) .LT. DELTAU)   RETURN
PSAV=P(K,JP) $ USAV=U(K,JP) $ GO TO 500
END
```

```
      SUBROUTINE SFD (KF)

      COMMON /MISCV/ A1,A2,A3,DELTAP,DELTAU,DT,DTH,DTHNU,G,G1,G2,
     1               ITERAT(500),ITER1,ITERSF,ITERSW,J,JP,NU,ND,PD
     2       /FIELD/ U(500,2),D(500,2),E(500,2),P(500,2),R(500,2),
     2               V(500,2)
     3       /SFVAR/ USF(2),VSF(2),ESF(2),PSF(2),RSF(2),USF(2),USSF(2)
      REAL NU
      PSAV=0. $ PA=P(KF,J) $ USF(JP)=USF(J) $ VSF(JP)=VSF(J) $ KF1=KF-1
      USAV=0. $ CA=C(KF,J) $ CSF(JP)=CSF(J) $ USSF(JP)=USSF(J)
      IF (KF .GT. 1)   GO TO 600
      DR=RSF(J)-R(1,J)
      AU=(USF(J)-U(1,J))/DR $ BU=0.
      AP=(PSF(J)-P(1,J))/DR $ BP=0.
      AD=(DSF(J)-D(1,J))/DR $ BD=0. $ GO TO 601
600   DR1=RSF(J)-R(KF,J) $ DR2=R(KF1,J)-R(KF,J) $ DET=DR2*DR1*(DR2-DR1)
      XU=DR1*(U(KF1,J)-U(KF,J)) $ YU=DR2*(USF(J)-U(KF,J))
      XP=DR1*(P(KF1,J)-P(KF,J)) $ YP=DR2*(PSF(J)-P(KF,J))
      XD=DR1*(D(KF1,J)-D(KF,J)) $ YD=DR2*(DSF(J)-D(KF,J))
      AU=(DR2*YU-DR1*XU)/DET $ BU=(XU-YU)/DET
      AP=(DR2*YP-DR1*XP)/DET $ BP=(XP-YP)/DET
      AD=(DR2*YD-DR1*XD)/DET $ BD=(XD-YD)/DET
601   ITERSF=0
602   ITERSF=ITERSF+1 $ IF (ITERSF .GT. 200)   STOP
      RSF(JP)=RSF(J)+DTH*(USSF(JP)+USSF(J))
      RA=RSF(JP)-DTH*(USF(JP)+CSF(JP)+UA+CA) $ DRA=RA-R(KF,J)
      PA=P(KF,J)+DRA*(AP+DRA*BP) $ DA=D(KF,J)+DRA*(AD+DRA*BD)
      UA=U(KF,J)+DRA*(AU+DRA*BU) $ CA=SQRT(G*PA/DA)
```

```
      X1=1./D0-1./DSF(JP)              $ X2=1./(DSF(JP)*CSF(JP))+1./(DA*CA)
      X3=1.+DTHNU*CSF(JP)/RSF(JP) $ X4=X3/X2 $ X5=X1*X4**2
      X6=X5+PA+2.*(UR-DTHNU*CA*UA/RA)/X2
      PSF(JP)=X5*X6-.5*X4*SQRT(X1*(X6-P0))
      DSF(JP)=D0*(GP1*PSF(JP)+GM1*P0)/(GM1*PSF(JP)+GP1*P0)
      ESF(JP)=PSF(JP)/(GM1*DSF(JP))
      CSF(JP)=SQRT(G*PSF(JP)/DSF(JP))
      USF(JP)=SQRT((PSF(JP)-P0)*(1./D0-1./DSF(JP)))
      USSF(JP)=USF(JP)*DSF(JP)/(DSF(JP)-D0)
      IF (ABS(1.-PSAV/PSF(JP)) .LT. DELTAP .AND. A S(1.-USAV/USF(JP))
     1.LT. DELTAU)    GO TO 603
      PSAV=PSF(JP) $ USAV=USF(JP) $ GO TO 602
  603 IF (KF .GT. 1)    RETURN
      U(2,JP)=USF(JP) $ P(2,JP)=PSF(JP) $ R(2,JP)=RSF(JP)
      C(2,JP)=CSF(JP) $ D(2,JP)=DSF(JP) $ E(2,JP)=ESF(JP)
      RETURN
      END
```

```
      SUBROUTINE SFA (KF)

      COMMON /MISCV/ A1,A2,A3,DELTAP,DELTAU,DT,DTH,DTHNU,G,GP1,GP1,
                     ITERAT(500),ITER1,ITERSF,ITERSW,J,JP,NU,DU,PU
     1       /FIELD/ C(500,2),D(500,2),E(500,2),P(500,2),R(500,2),
     2               U(500,2)
     3       /SFVAR/ CSF(2),DSF(2),ESF(2),PSF(2),RSF(2),USF(2),USSF(2)
      REAL NU
      U(KF,JP)=U(KF,J) $ KF1=KF-1 $ UA=U(KF1,J) $ UB=USF(J)
      C(KF,JP)=C(KF,J) $ PSAV=0.   $ CA=C(KF1,J) $ CB=CSF(J)
      D(KF,JP)=D(KF,J) $ USAV=0.
      DR1=RSF(J)-R(KF,J) $ DR2=R(KF1,J)-R(KF,J) $ DET=DR2*DR1*(DR2-DR1)
      XU=DR1*(U(KF1,J)-U(KF,J)) $ YU=DR2*(USF(J)-U(KF,J))
      XP=DR1*(P(KF1,J)-P(KF,J)) $ YP=DR2*(PSF(J)-P(KF,J))
      XD=DR1*(D(KF1,J)-D(KF,J)) $ YD=DR2*(DSF(J)-D(KF,J))
      AU=(DR2*YU-DR1*XU)/DET $ BU=(XU-YU)/DET
      AP=(DR2*YP-DR1*XP)/DET $ BP=(XP-YP)/DET
      AD=(DR2*YD-DR1*XD)/DET $ BD=(XD-YD)/DET
      DRSF=RSF(JP)-RSF(J) $ DTRB=DTHNU/DRSF $ AUSF=(USF(JP)-USF(J))/DRSF
      APSF=(PSF(JP)-PSF(J))/DRSF                $ ADSF=(DSF(JP)-DSF(J))/DRSF
      ITERAT(KF)=0
  700 ITERAT(KF)=ITERAT(KF)+1 $ IF (ITERAT(KF) .GT. 200)    STOP
      R(KF,JP)=R(KF,J)+DTH*(U(KF,JP)+U(KF,J))
      RA=R(KF,JP)-DTH*(U(KF,JP)+C(KF,JP)+UA+CA) $ DRA=RA-R(KF,J)
      PA=P(KF,J)+DRA*(AP+DRA*BP) $ DA=D(KF,J)+DRA*(AD+DRA*BD)
      UA=U(KF,J)+DRA*(AU+DRA*BU) $ CA=SQRT(G*PA/DA)
      Y1=U(KF,JP)-C(KF,JP)+UB-CB $ Y2=Y1*DTH/DRSF
      RB=(R(KF,JP)-Y2*RSF(JP))/(1.-Y2)
      IF (RB .LT. RSF(J))    GO TO 701
      DRB=RB-RSF(J)        $ DTHNUB=DTRB*(RSF(JP)-RB)
      PB=PSF(J)+DRB*APSF   $ DB=DSF(J)+DRB*ADSF
      UB=USF(J)+DRB*AUSF   $ GO TO 702
  701 RB=R(KF,JP)-DTH*Y1           $ DRB=RB-R(KF,J)
      PB=P(KF,J)+DRB*(AP+DRB*BP) $ DB=D(KF,J)+DRB*(AD+DRB*BD)
      UB=U(KF,J)+DRB*(AU+DRB*BU) $ DTHNUB=DTHNU
  702 CB=SQRT(G*PB/DB)
```

```
Z1=1./(D(KF,JP)*C(KF,JP))
Z2=C(KF,JP)*U(KF,JP)/R(KF,JP)
Z1A=.5*(Z1+1./(UA*CA)) $ Z2A=Z2+CA*UA/RA
Z1B=.5*(Z1+1./(UB*CB)) $ Z2B=Z2+CB*UB/RB
ZA=UA+PA*Z1A-DTHNU*Z2A
P(KF,JP)=(ZA-UB+PB*Z1B-DTHNUB*Z2B)/(Z1A+Z1B)
U(KF,JP)=ZA-P(KF,JP)*Z1A
D(KF,JP)=D(KF,J)*(GM1*P(KF,JP)+GM1*P(KF,J))/(GM1*P(KF,JP)+GP1*
1P(KF,J))
E(KF,JP)=P(KF,JP)/(GM1*D(KF,JP))
C(KF,JP)=SQRT(G*P(KF,JP)/D(KF,JP))
IF (ABS(1.-PSAV/P(KF,JP)) .LT. DELTAP .AND. ABS(1.-USAV/
1U(KF,JP)) .LT. DELTAU)   RETURN
PSAV=P(KF,JP) $ USAV=U(KF,JP) $ GO TO 700
END
```

```
      SUBROUTINE NEP (KF)

      COMMON /MISCV/ A1,A2,A3,DELTAP,DELTAU,DT,DTH,DTHNU,G,GM1,GP1,
     1               ITERAT(500),ITER1,ITERSF,ITERSW,J,JP,NU,D0,P0
     2      /FIELD/ C(500,2),D(500,2),E(500,2),P(500,2),R(500,2),
     2               U(500,2)
     3      /SFVAR/ CSF(2),DSF(2),ESF(2),PSF(2),RSF(2),USF(2),USSF(2)
      REAL NU
      KF1=KF-1 $ PSAV=0. $ UA=U(KF1,J) $ UB=USF(JP)
      KF2=KF-2 $ USAV=0. $ CA=C(KF1,J) $ CB=CSF(JP)
      IF (KF .GT. 2)   GO TO 800
      DR=RSF(J)-R(1,J)
      AU=(USF(J)-U(1,J))/DR $ BU=0.
      AP=(PSF(J)-P(1,J))/DR $ BP=0.
      AD=(DSF(J)-D(1,J))/DR $ BD=0. $ GO TO 801
800   DR1=RSF(J)-R(KF1,J) $ DR2=R(KF2,J)-R(KF1,J)
      DET=DR2*DR1*(DR2-DR1)
      XU=DR1*(U(KF2,J)-U(KF1,J)) $ YU=DR2*(USF(J)-U(KF1,J))
      XP=DR1*(P(KF2,J)-P(KF1,J)) $ YP=DR2*(PSF(J)-P(KF1,J))
      XD=DR1*(D(KF2,J)-D(KF1,J)) $ YD=DR2*(DSF(J)-D(KF1,J))
      AU=(DR2*YU-DR1*XU)/DET $ BU=(XU-YU)/DET
      AP=(DR2*YP-DR1*XP)/DET $ BP=(XP-YP)/DET
      AD=(DR2*YD-DR1*XD)/DET $ BD=(XD-YD)/DET
801   DRSF=RSF(JP)-RSF(J) $ DTRR=DTHNU/DRSF $ AUSF=(USF(JP)-USF(J))/DRSF
      APSF=(PSF(JP)-PSF(J))/DRSF                $ ADSF=(DSF(JP)-DSF(J))/DRSF
      DRN=R(KF,J)-RSF(J)        $ DTHN=DTH-DRN*DTRR/U
      P(KF,J)=PSF(J)+DRN*APSF $ D(KF,J)=DSF(J)+DRN*ADSF
      U(KF,J)=USF(J)+DRN*AUSF $ C(KF,J)=SQRT(G*P(KF,J)/D(KF,J))
      E(KF,J)=P(KF,J)/(GM1*D(KF,J))
      U(KF,JP)=U(KF,J) $ C(KF,JP)=C(KF,J) $ D(KF,JP)=D(KF,J)
```

```
      ITERAT(KF)=0
802   ITERAT(KF)=ITERAT(KF)+1 $ IF (ITERAT(KF) .GT. 200)   STOP
      R(KF,JP)=R(KF,J)+DTHN*(U(KF,JP)+U(KF,J))
      RA=R(KF,JP)-DTH*(U(KF,JP)+C(KF,JP)+UA+CA) $ DRA=RA-R(KF1,J)
      PA=P(KF1,J)+DRA*(AP+DRA*BP) $ UA=U(KF1,J)+DRA*(AU+DRA*BU) $ CA=SQRT(G*PA/DA)
      Y1=U(KF,JP)-C(KF,JP)+UB-CB  $ Y2=Y1*DTH/DRSF
      RB=(R(KF,JP)-Y2*RSF(JP))/(1.-Y2)
      DRR=RB-RSF(J)          $ DTHNU=DTRR*(RSF(JP)-RB)
      PB=PSF(J)+DRR*APSF  $ DB=DSF(J)+DRR*ADSF
      UB=USF(J)+DRR*AUSF  $ CB=SQRT(G*PB/DB)
      Z1=1./(D(KF,JP)*C(KF,JP))
      Z2=C(KF,JP)*U(KF,JP)/R(KF,JP)
      Z1A=.5*(Z1+1./(DA*CA)) $ Z2A=Z2+CA*UA/RA
      Z1B=.5*(Z1+1./(DB*CB)) $ Z2B=Z2+CB*UB/RB
      ZA=UA+PA*Z1A-DTHNU*Z2A
      P(KF,JP)=(ZA-UB+PB*Z1B-DTHNUB*Z2B)/(Z1A+Z1B)
      U(KF,JP)=ZA-P(KF,JP)*Z1A
      D(KF,JP)=D(KF,J)*(GM1*P(KF,JP)+GP1*P(KF,J))/(GM1*P(KF,JP)+GP1*
     1P(KF,J))
      E(KF,JP)=P(KF,JP)/(GM1*D(KF,JP))
      C(KF,JP)=SQRT(G*P(KF,JP)/D(KF,JP))
      IF (ABS(1.-PSAV/P(KF,JP)) .LT. DELTAP .AND. ABS(1.-USAV/
     1U(KF,JP)) .LT. DELTAU)   RETURN
      PSAV=P(KF,JP) $ USAV=U(KF,JP) $ GO TO 802
      END
```

```
      SUBROUTINE SWD (KI,KO,RP)

      COMMON /MISCV/ A1,A2,A3,DELTAP,DELTAU,DT,DTH,DTHNU,G,GM1,GP1,
     1               ITER1(500),ITER1,ITERSF,ITERSW,J,JP,NU,ND,PO
     2      /FIELD/ U(500,2),D(500,2),E(500,2),P(500,2),R(500,2),
     2               C(500,2)
     3      /SFVAR/ USF(2),VSF(2),ESF(2),PSF(2),RSF(2),USF(2),USSF(2)
     4      /SWVAR/ USW(2,2),DSW(2,2),ESW(2,2),PSW(2,2),RSW(2),
     5               DSW(2,2),USSW(2)
      REAL NU
      KI1=KI-1 $ USW(1,JP)=USW(1,J) $ UP=U(KO,J)
      KO1=KO+1 $ CSW(1,JP)=CSW(1,J) $ UAP=USW(1,J) $ UBP=U(KO1,J)
      KO2=KO+2 $ DSW(1,JP)=DSW(1,J) $ CAP=CSW(1,J) $ CBP=C(KO1,J)
      PSAV=0. $ UA=U(KI,J)
      USAV=0. $ CA=C(KI,J)
      USSW(JP)=AMIN1(USSW(J),(RSF(JP)-RSW(J))/DTH-USSW(J))
      DR1=RSW(J)-R(KI,J) $ DR2=R(KI1,J)-R(KI,J) $ DET=DR2*DR1*(DR2-DR1)
      XU=DR1*(U(KI1,J)-U(KI,J)) $ YU=DR2*(USW(2,J)-U(KI,J))
      XP=DR1*(P(KI1,J)-P(KI,J)) $ YP=DR2*(PSW(2,J)-P(KI,J))
      XD=DR1*(D(KI1,J)-D(KI,J)) $ YD=DR2*(DSW(2,J)-D(KI,J))
      AU=(DR2*YU-DR1*XU)/DET $ BU=(XU-YU)/DET
      AP=(DR2*YP-DR1*XP)/DET $ BP=(XP-YP)/DET
      AD=(DR2*YD-DR1*XD)/DET $ BD=(XD-YD)/DET
      DR1=R(KO1,J)-R(KO,J) $ DR2=RSW(J)-R(KO,J) $ DET=DR2*DR1*(DR2-DR1)
      XU=DR1*(USW(1,J)-U(KO,J)) $ YU=DR2*(U(KO1,J)-U(KO,J))
      XP=DR1*(PSW(1,J)-P(KO,J)) $ YP=DR2*(P(KO1,J)-P(KO,J))
      XD=DR1*(DSW(1,J)-D(KO,J)) $ YD=DR2*(D(KO1,J)-D(KO,J))
      AU1=(DR2*YU-DR1*XU)/DET $ BU1=(XU-YU)/DET
      AP1=(DR2*YP-DR1*XP)/DET $ BP1=(XP-YP)/DET
      AD1=(DR2*YD-DR1*XD)/DET $ BD1=(XD-YD)/DET
```

```
      DR1=R(K02,J)-R(K01,J) $ DR2=R(K0,J)-R(K01,J)
      DET=DR2*DR1*(DR2-DR1)
      XU=DR1*(U(K0,J)-U(K01,J)) $ YU=DR2*(U(K02,J)-U(K01,J))
      XP=DR1*(P(K0,J)-P(K01,J)) $ YP=DR2*(P(K02,J)-P(K01,J))
      XD=DR1*(D(K0,J)-D(K01,J)) $ YD=DR2*(D(K02,J)-D(K01,J))
      AU2=(DR2*YU-DR1*XU)/DET $ BU2=(XU-YU)/DET
      AP2=(DR2*YP-DR1*XP)/DET $ BP2=(XP-YP)/DET
      AD2=(DR2*YD-DR1*XD)/DET $ BD2=(XD-YD)/DET
      ITERSW=0
900   ITERSW=ITERSW+1 $ IF (ITERSW .GT. 200)    STOP
      RSW(JP)=RS(J)+DTH*(USSW(J)+USSW(JP))
      PSAVP=USAVP=0.
901   RP=RSW(JP)-DTH*(USW(1,JP)+UP) $ DRP=RP-R(K0,J)
      PP=P(K0,J)+DRP*(AP1+DRP*BP1) $ UP=U(K0,J)+DRP*(AU1+DRP*BU1)
      DP=D(K0,J)+DRP*(AD1+DRP*BD1) $ CP=SQRT(G*PP/DP)
      RAP=RSW(JP)-DTH*(USW(1,JP)+CSW(1,JP)+UAP+CAP) $ DRAP=RAP-R(K0,J)
      PAP=P(K0,J)+DRAP*(AP1+DRAP*BP1) $ UAP=U(K0,J)+DRAP*(AU1+DRAP*BU1)
      DAP=D(K0,J)+DRAP*(AD1+DRAP*BD1) $ CAP=SQRT(G*PAP/DAP)
      RBP=RSW(JP)-DTH*(USW(1,JP)-CSW(1,JP)+UBP-CBP)
      IF (RBP .GT. R(K01,J))    GO TO 902
      DRBP=RBP-R(K0,J)
      PBP=P(K0,J)+DRBP*(AP1+DRBP*BP1) $ UBP=U(K0,J)+DRBP*(AU1+DRBP*BU1)
      DBP=D(K0,J)+DRBP*(AD1+DRBP*BD1) $ CBP=SQRT(G*PBP/DBP) $ GO TO 903
902   DRBP=RBP-R(K01,J)
      PBP=P(K01,J)+DRBP*(AP2+DRBP*BP2) $UBP=U(K01,J)+DRBP*(AU2+DRBP*BU2)
      DBP=D(K01,J)+DRBP*(AD2+DRBP*BD2) $CBP=SQRT(G*PBP/DBP)
903   Z1=1./(DSW(1,JP)*CSW(1,JP)) $ Z2=CSW(1,JP)*USW(1,JP)/RSW(JP)
      Z1A=.5*(Z1+1./(UAP*CAP))      $ Z2A=Z2+CAP*UAP/RAP
      Z1B=.5*(Z1+1./(UBP*CBP))      $ Z2B=Z2+CBP*UBP/RBP
      ZA=UAP+PAP*Z1A-DTHNU*Z2A
      PSW(1,JP)=(ZA-UBP+PBP*Z1B-DTHNU*Z2B)/(Z1A+Z1B)
      USW(1,JP)=ZA-PSW(1,JP)*Z1A
      DSW(1,JP)=DP*(GP1*PSW(1,JP)+GM1*PP)/(GM1*PSW(1,JP)+GP1*PP)
      CSW(1,JP)=SQRT(G*PSW(1,JP)/DSW(1,JP))
```

```
      IF (ABS(1.-PSAVP/PSW(1,JP)) .LT. DELTAP .AND. ABS(1.-USAVP/
     1USW(1,JP)) .LT. DELTAU)   GO TO 904
      PSAVP=PSW(1,JP) $ USAVP=USW(1,JP) $ GO TO 901
  904 IF (ITERSW .GT. 1)   GO TO 905
      PSW(2,JP)=PSW(2,J)
      DSW(2,JP)=DSW(1,JP)*(GP1*PSW(2,JP)+GM1*PSW(1,JP))/(GM1*PSW(2,JP)+
     1GP1*PSW(1,JP))
      USW(2,JP)=USW(1,JP)+SQRT((PSW(2,JP)-PSW(1,JP))*(1./DSW(1,JP)-1./
     1DSW(2,JP)))
      CSW(2,JP)=SQRT(G*PSW(2,JP)/DSW(2,JP))
  905 RA=RSW(JP)-DTH*(USW(2,JP)+CSW(2,JP)+UA*CA) $ DRA=RA-R(KI,J)
      PA=P(KI,J)+DRA*(AP+DRA*BP) $ UA=U(KI,J)+DRA*(AU+DRA*BU)
      DA=D(KI,J)+DRA*(AD+DRA*BD) $ CA=SQRT(G*PA/DA)
      X1=1./DSW(1,JP)-1./DSW(2,JP)
      X2=1./(DSW(2,JP)*CSW(2,JP))+1./(DA*CA)
      X3=1.+DTHNU*CSW(2,JP)/RSW(JP) $ X4=X3/X2 $ X5=X1*X4**2
      X6=X5+PA+2.*(UA-USW(1,JP)-DTHNU*(CSW(2,JP)*USW(1,JP)/RSW(JP)+
     1CA*UA/PA))/X2
      PSW(2,JP)=X5+X4-2.*X4*SQRT(X1*(X6-PSW(1,JP)))
      DSW(2,JP)=DSW(1,JP)*(GP1*PSW(2,JP)+GM1*PSW(1,JP))/(GM1*PSW(2,JP)+
     1GP1*PSW(1,JP))
      CSW(2,JP)=SQRT(G*PSW(2,JP)/DSW(2,JP))
      USW(2,JP)=USW(1,JP)+SQRT((PSW(2,JP)-PSW(1,JP))*(1./DSW(1,JP)-1./
     1DSW(2,JP)))
      USSW(JP)=(DSW(2,JP)*USW(2,JP)-DSW(1,JP)*USW(1,JP))/(DSW(2,JP)-
     1DSW(1,JP))
      IF (ABS(1.-PSAV/PSW(2,JP)) .LT. DELTAP .OR. ABS(1.-USAV/USW(2,JP))
     1.LT. DELTAU)   GO TO 906
      PSAV=PSW(2,JP) $ USAV=USW(2,JP) $ GO TO 900
  906 ESW(1,JP)=PSW(1,JP)/(GM1*DSW(1,JP))
      ESW(2,JP)=PSW(2,JP)/(GM1*DSW(2,JP))
      RETURN
      END
```

```
      SUBROUTINE SWA (KI)

      COMMON /MISCV/ A1,A2,A3,DELTAP,DELTAU,DT,DTH,DTHNU,G,GM1,GP1,
     1               ITERAT(500),ITERI,ITERSF,ITERSW,J,JP,NU,D0,P0
     2       /FIELD/ C(500,2),D(500,2),E(500,2),P(500,2),R(500,2),
     2               U(500,2)
     3       /SWVAR/ CSW(2,2),DSW(2,2),ESW(2,2),PSW(2,2),RSW(2),
     4               USW(2,2),USSW(2)
      REAL NU
      U(KI,JP)=U(KI,J) $ KI1=KI-1 $ UA=U(KI1,J) $ UB=USW(2,J)
      C(KI,JP)=C(KI,J) $ PSAV=0.  $ CA=C(KI1,J) $ CB=CSW(2,J)
      D(KI,JP)=D(KI,J) $ USAV=0.
      DR1=RSW(J)-R(KI,J) $ DR2=R(KI1,J)-R(KI,J) $ E1=DR2*DR1*(DR2-DR1)
      XU=DR1*(U(KI1,J)-U(KI,J)) $ YU=DR2*(USW(2,J)-U(KI,J))
      XP=DR1*(P(KI1,J)-P(KI,J)) $ YP=DR2*(PSW(2,J)-P(KI,J))
      XD=DR1*(D(KI1,J)-D(KI,J)) $ YD=DR2*(DSW(2,J)-D(KI,J))
      AU=(DR2*YU-DR1*XU)/E1 $ BU=(XU-YU)/E1
      AP=(DR2*YP-DR1*XP)/E1 $ BP=(XP-YP)/E1
      AD=(DR2*YD-DR1*XD)/E1 $ BD=(XD-YD)/E1
      DRSW=RSW(JP)-RSW(J)                $ AUSW=(USW(2,JP)-USW(2,J))/DRSW
      APSW=(PSW(2,JP)-PSW(2,J))/DRSW $ AUSW=(DSW(2,JP)-USW(2,J))/DRSW
      DTRB=DTHNU/DRS  $ ITERAT(KI)=0
1000  ITERAT(KI)=ITERAT(KI)+1 $ IF (ITERAT(KI) .GT. 200)   STOP
      R(KI,JP)=R(KI,J)+DTH*(U(KI,JP)+U(KI,J))
      RA=R(KI,JP)-DTH*(U(KI,JP)+C(KI,JP)+UA+CA) $ DRA=RA-R(KI,J)
      PA=P(KI,J)+DRA*(AP+DRA*BP) $ DA=D(KI,J)+DRA*(AD+DRA*BD)
      UA=U(KI,J)+DRA*(AU+DRA*BU) $ CA=SQRT(G*PA/DA)
      Y1=U(KI,JP)-C(KI,JP)+UB-CB $ Y2=Y1*DTH/DRSW
      RB=(R(KI,JP)-Y2*RSW(JP))/(1.-Y2)
```

```
      IF (RB .LT. RS (J))   GO TO 1001
      DRB=RB-RSW(J)          $ DTHNUB=DTRB*(RSW(JP)-RR)
      PB=PSW(2,J)+DR**APS*   $ DB=DSW(2,J)+DRB*AUSW
      UB=USW(2,J)+DR**AUS*   $ GO TO 1002
1001  RB=R(KI,JP)-DT*Y1                $ DRB=RB-R(KI,J)
      PB=P(KI,J)+DRB*(AP+(BM1*P)  $ DB=D(KI,J)+DRB*(AD+(BM1*D)
      UB=U(KI,J)+DRB*(AU+(BM1*U)  $ DTHNUB=DTHNU
1002  CB=SQRT(G*P/D)
      Z1=1./(D(KI,JP)*C(KI,JP))
      Z2=C(KI,JP)*U(KI,JP)/R(KI,JP)
      Z1A=.5*(Z1+1./(DA*CA))  $ Z2A=Z2+CA*UA/RA
      Z1B=.5*(Z1+1./(DB*CB))  $ Z2B=Z2+CB*UB/RB
      ZA=UA+PA*Z1A-DTHNU*Z2A
      P(KI,JP)=(ZA-UB+PB*Z1B-DTHNUB*Z2B)/(Z1A+Z1B)
      U(KI,JP)=ZA-P(KI,JP)*Z1A
      D(KI,JP)=D(KI,J)*(GP1*P(KI,JP)+GM1*P(KI,J))/(GM1*P(KI,JP)+GP1*
     1P(KI,J))
      E(KI,JP)=P(KI,JP)/(GM1*D(KI,JP))
      C(KI,JP)=SQRT(G*P(KI,JP)/D(KI,JP))
      IF (ABS(1.-PSAV/P(KI,JP)) .LT. DELTAP .AND. ABS(1.-USAV/
     1U(KI,JP)) .LT. DELTAU)   RETURN
      PSAV=P(KI,JP)   $ USAV=U(KI,JP) $ GO TO 1000
      END
```

```
      SUBROUTINE IEP (KI)

      COMMON /MISCV/ A1,A2,A3,DELTAP,DELTAU,DT,DTH,DTHNU,G,GM1,GP1,
     1               ITERAT(500),ITERI,ITERSF,ITERSW,J,JP,NU,D0,P0
     2       /FIELD/ R(500,2),U(500,2),E(500,2),P(500,2),R(500,2),
     2               J(500,2)
     3       /SWVAR/ RSW(2,2),USW(2,2),ESW(2,2),PSW(2,2),CSW(2),
     4               DSW(2,2),USSW(2)
      REAL NU
      KI1=KI-1 $ PSAV=0. $ UA=U(KI1,J) $ UB=USW(2,JP)
      KI2=KI-2 $ USAV=0. $ CA=C(KI1,J) $ CB=CSW(2,JP)
      IF (KI .GT. 2)   GO TO 1100
      DRI=R(1,JP)-R(1,J)          $ DTRA=DTHNU/DRI
      API=(P(1,JP)-P(1,J))/DRI $ AUI=(U(1,JP)-U(1,J))/DRI
      ADI=(D(1,JP)-D(1,J))/DRI $ GO TO 1101
1100  DR1=RSW(J)-R(KI1,J) $ DR2=R(KI2,J)-R(KI1,J)
      DET=DR2*DR1*(DR2-DR1)
      XU=DR1*(U(KI2,J)-U(KI1,J)) $ YU=DR2*(USW(2,J)-U(KI1,J))
      XP=DR1*(P(KI2,J)-P(KI1,J)) $ YP=DR2*(PSW(2,J)-P(KI1,J))
      XD=DR1*(D(KI2,J)-D(KI1,J)) $ YD=DR2*(USW(2,J)-U(KI1,J))
      AU=(DR2*YU-DR1*XU)/DET $ BU=(XU-YU)/DET
      AP=(DR2*YP-DR1*XP)/DET $ BP=(XP-YP)/DET
      AD=(DR2*YD-DR1*XD)/DET $ BD=(XD-YD)/DET
1101  DRSW=RSW(JP)-RSW(J)                $ AUSW=(USW(2,JP)-USW(2,J))/DRSW
      APSW=(PSW(2,JP)-PSW(2,J))/DRSW $ ADSW=(DSW(2,JP)-DSW(2,J))/DRSW
      DTRB=DTHNU/DRSW $ DRN=R(KI,J)-RSW(J) $ DTHN=DTH-DRN*DTRB/NU
      P(KI,J)=PSW(2,J)+DRN*APSW $ D(KI,J)=DSW(2,J)+DRN*ADSW
      U(KI,J)=USW(2,J)+DRN*AUSW $ C(KI,J)=SQRT(G*P(KI,J)/D(KI,J))
      E(KI,J)=P(KI,J)/(GM1*D(KI,J))
      U(KI,JP)=U(KI,J) $ C(KI,JP)=C(KI,J) $ D(KI,JP)=D(KI,J)
```

```
      ITEMAT(KT)=0
1107  ITEMAT(KT)=ITE-T(KT)+1 $ IF (ITEMAT(KT) .GT. 200)   STOP
      R(KI,JP)=R(KI,J)+DTHR*(U(KI,JP)+U(KI,J))
      IF (KI .GT. 2)   GO TO 1105
      Y1=U(2,JP)+C(2,JP)*DA*CA    $ Y2=Y1*DTH/DR1
      RA=(R(2,JP)-Y2*R(1,JP))/(1.-Y2)
      DRA=DA-R(1,J)       $ DTHRDA=DTRA*(R(1,JP)-RA)
      PA=P(1,J)+RHO*.5*U1   $ UA=U(1,J)+DTHRA*C1
      DA=D(1,J)+DA*.5*U1    $ CA=SQRT(GPA/DA)  > GO TO 1104
1103  RA=R(KT,JP)-DT*(U(KI,JP)+U(KI,JP)+DA*CA)
      DRA=DA-R(KT,J)                $ DTHRDA=DTHRO
      PA=P(KT,J)+DRO*(AL+DA*PP)  $ UA=U(KT,J)+DTHRO*(AL+DA*PP)
      UA=U(KT,J)+DTHRO*(AL+DA*PP)  $ CA=SQRT(GPA/D )
1104  Y1=U(KT,JP)-C(KI,JP)*DT-CB   $ Y2=Y1*DTH/DRS
      RB=(R(KI,JP)-Y2*RS(JP))/(1.-Y2
      DRB=PB-RS(J)          $ DTHRDU=DTRB*(RS(JP)-PB
      PB=PS(2,J)+DTH*APS    $ DB=DS(2,J)+DRB*AUS
      UB=US(2,J)+DTH*AUS    $ CB=SQRT(GPB/DB)
      Z1=1./(U(KT,JP)+C(KT,JP))
      Z2=C(KT,JP)*U(KI,JP)/P(KI,JP)
      Z1A=.5*(Z1+1./(U*CA))  $ Z2A=Z2+CA*UA/RA
      Z1B=.5*(Z1+1./(UB*CB))  $ Z2B=Z2+CB*UB/RB
      ZA=UA+PA*Z1A-DTH*UA*Z2A
      P(KI,JP)=(ZA-UB+PB*Z1B-DTHRUB*Z2B)/(Z1A+Z1B)
      U(KI,JP)=ZA-P(KI,JP)*Z1A
      D(KI,JP)=D(KI,J)*(GP1*P(KI,JP)+GM1*P(KI,J))/(GM1*P(KI,JP)+GP1*
     1P(KI,J))
      E(KI,JP)=P(KI,JP)/(GM1*D(KI,JP))
      C(KI,JP)=SQRT(GP(KI,JP)/D(KI,JP))
      IF (ABS(1.-PSAV/P(KI,JP)) .LT. DELTAP .AND.  ABS(1.-USAV/
     1U(KI,JP)) .LT. DELTAU)   RETURN
      PSAV=P(KI,JP)  $ USAV=U(KI,JP) $ GO TO 1102
      END
```

B L O W - P

SHOCK W VE PROPAGATION FOR SEQUENTIAL EXPLOSIONS

CHARACTERISTIC SOLUTION FOR THE SHOCK ENGULFED FIELD WITH A UNIFORM GAS BUBBLE

FIRST CHARGE 2.000 LBS-PENTOLITE

SECOND CHARGE 2.000 LBS-PENTOLITE
TIME DELAY 2.2 MSEC

* UNITS OF OUTPUT VARIABLES *

TIME	MSEC/(LB-TNT)**1/3	PRESSURE	PSIG
RADIUS	FT/(LB-TNT)**1/3	DENSITY	GM/CC
VELOCITY	FT/MSEC	ENERGY	KCAL/GM

(NOTE- YIELD SCALING IS TNT AND SURFACE BURST EQUIVALENT)

TIME	TIME STEP	STEP NUMBER		RADIUS	PRESSURE
2.540E+00	3.4406E-03	601	UNIFORM GAS BUBBLE	2.6224E+00	9.7866E+00
			INTERIOR SHOCK WAVE	4.0379E+00	3.2174E+01
			AIR SHOCK FRONT	6.0038E+00	1.6984E+01
2.575E+00	3.4451E-03	602	UNIFORM GAS BUBBLE	2.6248E+00	9.6990E+00
			INTERIOR SHOCK WAVE	4.0458E+00	3.1993E+01
			AIR SHOCK FRONT	6.0092E+00	1.6953E+01
2.609E+00	3.4496E-03	603	UNIFORM GAS BUBBLE	2.6271E+00	9.6121E+00
			INTERIOR SHOCK WAVE	4.0539E+00	3.1816E+01
			AIR SHOCK FRONT	6.0147E+00	1.6923E+01
2.644E+00	3.4541E-03	604	UNIFORM GAS BUBBLE	2.6294E+00	9.5260E+00
			INTERIOR SHOCK WAVE	4.0617E+00	3.1641E+01
			AIR SHOCK FRONT	6.0201E+00	1.6892E+01
2.678E+00	3.4586E-03	605	UNIFORM GAS BUBBLE	2.6317E+00	9.4407E+00
			INTERIOR SHOCK WAVE	4.0696E+00	3.1467E+01
			AIR SHOCK FRONT	6.0255E+00	1.6861E+01
2.713E+00	3.4630E-03	606	UNIFORM GAS BUBBLE	2.6340E+00	9.3562E+00
			INTERIOR SHOCK WAVE	4.0774E+00	3.1296E+01
			AIR SHOCK FRONT	6.0310E+00	1.6831E+01
2.748E+00	3.4675E-03	607	UNIFORM GAS BUBBLE	2.6362E+00	9.2724E+00
			INTERIOR SHOCK WAVE	4.0853E+00	3.1127E+01
			AIR SHOCK FRONT	6.0364E+00	1.6800E+01

UNCLASSIFIED
Security Classification

DOCUMENT CONTROL DATA - R & D

(Security classification of title, body of abstract and indexing annotation must be entered when the overall report is classified)

1. ORIGINATING ACTIVITY (Corporate author)
IIT Research Institute
Chicago, Illinois 60616

2a. REPORT SECURITY CLASSIFICATION
Unclassified

2b. GROUP
N/A

3. REPORT TITLE
Blast Pressures from Sequential Explosions

4. DESCRIPTIVE NOTES (Type of report and inclusive dates)
Final Report, IITRI Project No. J6166

5. AUTHOR(S) (First name, middle initial, last name)
Thomas A. Zaker

6. REPORT DATE
October 1969

7a. TOTAL NO. OF PAGES
152

7b. NO. OF REFS
13

8a. CONTRACT OR GRANT NO
DAHC-04-69-C-0020

b. PROJECT NO.

c.

d.

9a. ORIGINATOR'S REPORT NUMBER(S)
J6166-Final Report

9b. OTHER REPORT NO(S) (Any other numbers that may be assigned this report)

10. DISTRIBUTION STATEMENT
Each transmittal of this document outside the agencies of the US Government must have prior approval of the Armed Services Explosives Safety Board, Washington, D.C. 20315.

11. SUPPLEMENTARY NOTES

12. SPONSORING MILITARY ACTIVITY
Armed Services Explosives Safety Board

13. ABSTRACT

This report describes a study of the air blast produced by sequentially detonated high explosive charges. Criteria are established relating the coalescence of successive blast waves to explosion time delay, charge weight, and distance from the explosion site. A finite-difference technique based on the method of characteristics was used to determine numerically the pressure fields produced by spherical charges with various time delays between successive detonations. Small-scale experiments were conducted with hemispherical explosive charges totaling 2 lb in weight detonated on a rigid surface. Transient pressures were observed at six stations on each of two gage lines. Comparisons are made between the peak pressures and pulse separations predicted numerically and those obtained experimentally. The results are useful in developing recommendations for siting of structures adjacent to multiple-unit explosive stores.

14. Key Words
Explosives Safety
Explosion Effects
Air Blast
Shock Waves
Method of Characteristics

DD FORM 1 NOV 65 1473

UNCLASSIFIED
Security Classification